HUNGARIAN AGRICULTURAL ENGINEERING

HUNGARIAN ACADEMY OF SCIENCES

Hungarian Agricultural Engineering

N° 43/2024

PERIODICAL OF THE COMMITTEE OF AGRICULTURAL AND BIOSYSTEM ENGINEERING OF THE HUNGARIAN ACADEMY OF SCIENCES

Published by
Hungarian University of Agriculture and Life Sciences
Institute of Technology
H-2103 Gödöllő, Páter K. u. 1.

HUNGARIAN UNIVERSITY OF AGRICULTURE AND LIFE SCIENCES
Institute of Technology

Gödöllő
2024

Published online: http://hae-journals.org
HU ISSN 0864-7410 (Print)
HU ISSN 2415-9751(Online)

PREFACE

In the name of the Committee of Agricultural and Biosystem Engineering of the Hungarian Academy of Sciences we would like to welcome everyone who is interested in reading our journal. The Hungarian Agricultural Engineering (HAE) journal was published 36 years ago for the very first time with an aim to introduce the most valuable and internationally recognized Hungarian studies about mechanisation in the field of agriculture and environmental protection.

In the year of 2014 the drafting committee decide to spread it also in electronic (on-line and DOI) edition and make it entirely international. From this year exclusively the Hungarian University of Agriculture and Life Science's Institute of Technology (former Szent István University's Faculty of Mechanical Engineering) took the responsibility to publish the paper twice a year in cooperation with the Hungarian Academy of Sciences.

Our goal is to occasionally report the most recent researches regarding mechanisation in agricultural sciences (agricultural and environmental technology and chemistry, livestock, crop production, feed and food processing, agricultural and environmental economics, energy production, engineering and management) with the help of several authors. The drafting committee has been established with the involvement of outstanding Hungarian and international researches who are recognised on international level as well. All papers are selected by our editorial board and a triple blind review process by prominent experts which process could give the highest guarantee for the best scientific quality.

We hope that our journal provides accurate information for the international scientific community and serves the aim of the Hungarian agricultural and environmental engineering research.

Gödöllő, 20.12.2024.

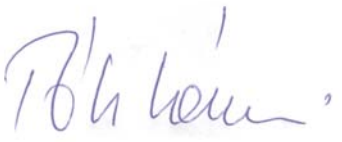

Dr. István SZABÓ
editor in chief

Dr. László TÓTH
editor in chief

HUNGARIAN AGRICULTURAL ENGINEERING
No 43/2024 5-17
Published online: http://hae-journals.org/
HU ISSN 0864-7410 (Print)
HU ISSN 2415-9751(Online)
DOI: 10.17676/HAE.2024.43.5
Received: 02.04.2024 - Accepted: 30.04.2024

PERIODICAL
OF THE COMMITTEE OF AGRICULTURAL AND BIOSYSTEM ENGINEERING OF THE HUNGARIAN ACADEMY OF SCIENCES
and
HUNGARIAN UNIVERSITY OF AGRICULTURE AND LIFE SCIENCES
INSTITUTE OF TECHNOLOGY

FINITE ELEMENT METHOD (CFX) INVESTIGATION OF THE FLUID FLOW DISTRIBUTION BEHAVIOR OF BOTH PARALLEL AND COUNTER TYPES OF HEAT EXCHANGERS

Author(s):
S. Hailemariam[1,2], J. Beke[1], I. Oldal[1], G. Kalácska[1]

Affiliation:
[1] Doctoral School of Mechanical Engineering – Hungarian University of Agriculture and Life Sciences, 2100 Gödöllő, Páter Károly u. 1., Hungary;
[2] Wollo University Kombolcha Institute of Technology School of Mechanical and Chemical Engineering Industrial Engineering Department, Wollo University, 1145 Dessie, Ethiopia

Email address:
shegawh@yahoo.com; beke.janos@uni-mate.hu; oldal.istvan@uni-mate.hu; kalacska.gabor@uni-mate.hu

Abstract: The thermal heat transfer behavior of hot and cold fluids within boundary conditions on both parallel and counter types of heat exchangers was investigated in this work using the computational fluid dynamics (CFD) approach in ANSYS Workbench (CFX). This technique helps us identify the precise values for the velocity, pressure, and temperature readings along and across the heat exchanger, in addition to determining how the three variables were distributed locally or globally. Cold water at 5 m/s and 20 °C, with a zero pressure at outlet or zero gauge pressure at outlet, was employed in this study, as was hot water at 4 m/s and 90 °C, with the zero pressure at outlet or zero gauge pressure at outlet. The results of any local or global temperature, pressure, and velocity values were represented along the length of both parallel and counter types of heat exchangers by color contours, where red indicated the largest value and blue the lowest. All of the global temperature, pressure, and velocity distributions were shown by charts positioned along the length of both parallel and counter-type heat exchangers. We came to the conclusion that when hot inlet fluid passes between the head and outer surface of cold fluid, there is a T-junction where high pressure and low velocity coexist. In comparison to parallel flow, the pressure and velocity distributions are lower in counter flow.

Keywords: ANYSY (CFX), CFD, heat transfer, pressure, temperature, thermal

1. Introduction

In many fields, efficient use of heat transfer is crucial, and because heat makes up a significant amount of final energy, it presents a significant barrier to the economic viability of many industrial processes [1–4]. The thermal engineering topic of study known as heat transfer is change, interchange, utilization, and formation of heat between bodies. Heat transport mechanisms include phase shift, conversion, radiation, and conduction. Heat exchangers are widely employed in industries [5–12]. Engineering applications in daily life and the industrial sector frequently use heat exchangers that are both parallel and counter [13–15]. Finding appropriate solutions is difficult since these heat exchangers are susceptible to thermal conduction, convection, radiation, and phase shifts in which energy is transmitted. To completely comprehend pressure distribution, temperature variation, and velocity variation in both parallel and counter-type heat exchangers from hot to cold is a significant phenomenon that necessitates substantial experimental investigation and numerical analysis. ANSYS CFX, a CFD modeling package, was used to evaluate the temperature variation and velocity on the flue, fin, and tube domains [16–18]. Complex phenomena such as thermal heat transfer between hot and cold fluids have been solved by modern technology. Researchers have used the commercial CFD code ANSYS to study the flue gas/water type parallel and counter heat exchangers [13–18]. Examining

the distribution and determine velocity, pressure, and velocity at any point within and across both parallel and counter types of heat exchangers is the goal of this work.

2. Materials and Methods

The distribution and calculation of pressure, temperature, velocity vector, streamlines, and velocity of both parallel and counter heat exchangers were all simulated with the use of the ANSYS Workbench software (CFX) and the computational fluid dynamics (CFD) method. Cold water was used at 5 m/s and 20 °C with the zero pressure at outlet or zero gauge pressure at outlet, while hot water was used at 4 m/s and 90 °C with zero pressure at outlet or zero gauge pressure at outlet. Fig. 1 depicts the steps of performing a general ANSYS workbench (CFX) and computational fluid dynamics while performing thermal heat transfer.

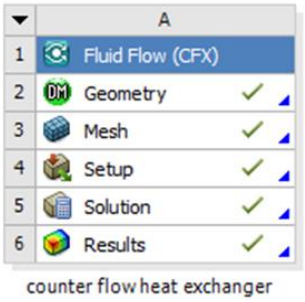

Figure 1. Steps in ANSYS CFX.

Assembly drawings generated by ANSYS Workbench Design Modular, along with the components for the hot and cold fluids within a 50-mm-diameter and 50-mm-high hot fluid cylinder in two different configurations, were used in the study. The dimensions of the hot fluid were two heads separated by 50 mm, and the cold fluid was 1000 mm long and 100 mm wide.

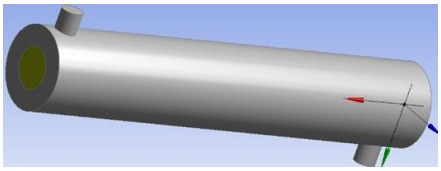

Figure 2. 3D model of cold fluid and hot fluid.

Numerous researchers employed loads and boundary conditions while using CFD and the FEM to simulate the characteristics of heat exchanger [9], and [19–32]. As seen in Fig. 3, giving names to both parallel fluid flow and counter fluid flow bodies cold fluid and their surfaces like cold fluid in face represented by letter A, cold fluid out face denoted by letter B, cold wall denoted by letter C and cold domain denoted by letter D.

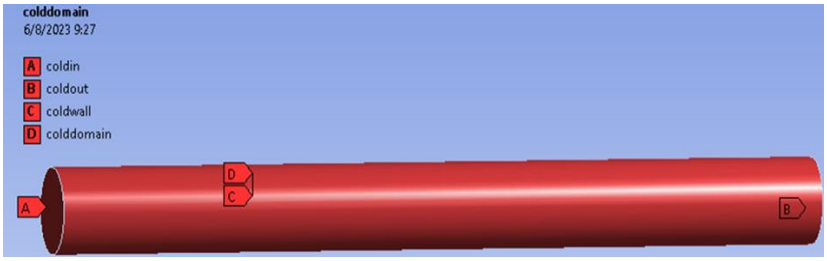

Figure 3. The naming of cold fluid.

As seen in Fig. 4, giving names to both parallel fluid flow and counter fluid flow bodies hot fluid and their surfaces like hot out fluid in face represented by letter A, hot fluid in face denoted by letter B, hot inner wall

denoted by letter C, hot outer walls denoted by letter D, hot faces represented by letter E and hot domain represented by letter F.

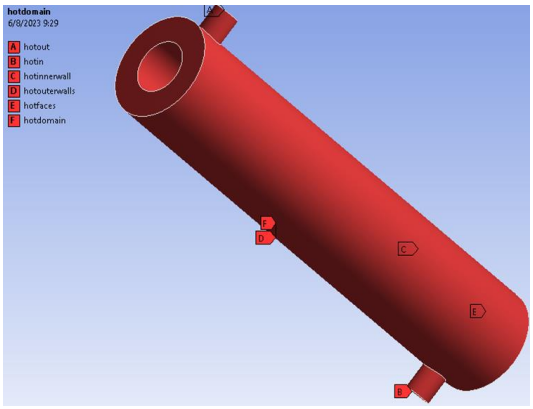

Figure 4. The naming of hot fluid.

The next stage in this research was to create contacts between the surfaces of the hot and cold fluids by connecting them. Fig. 5 in the below illustration illustrates how to create hot and cold fluid contact surfaces in the ANSYS workbench. As Fig. 5 makes evident, the target body is indicated by the blue colour, and the contact region is indicated by the red colour. You can also flip the setting.

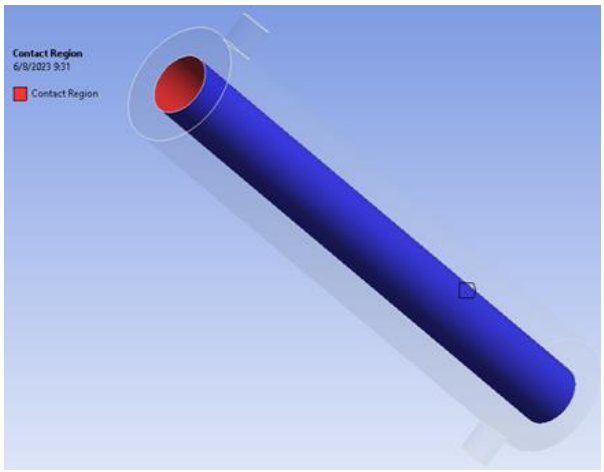

(a) Contact region and target body

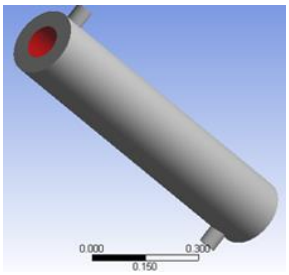

(b) Contact region

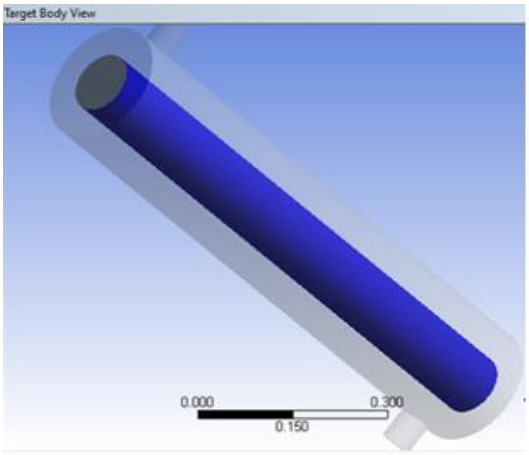

(c) Target body

Figure 5. Contact surfaces of cold fluid and hot fluid.

ANSYS geometry was used to define the computational fluid domain (CFD) was utilized to discretize the domain [33–39]. The discretization of the fluid model into a "mesh" composed of multiple elements is an essential precondition for the ANSYS CFX and CFD methodologies. The mesh size is influenced by numerous factors in the fluid model, such as density windows, surface curvatures, spacing between geometric entities, and field variable distribution [11], [12], [19], [22], [26] and [27]. The steps of inflation on the circumferential sides and the size of all edges are utilized as shown in Fig. 6.

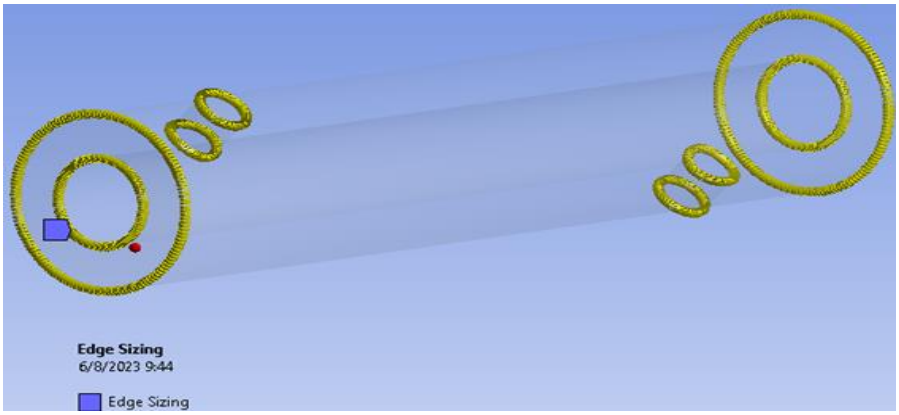

Figure 6. Edge meshing by division of numbers.

In three-dimensional numerical analysis, tetrahedrons, hexahedrons, and their combinations are commonly utilized. Highly efficient, easily implemented, flexible for creating adaptive meshes, and easily re-generable meshes are the advantages of tetrahedral element meshes. The automatic generation technology of tetrahedral element meshes is currently fully developed and finds widespread application in handling complex geometry. As demonstrated in Fig. 7, adaptive generation for the use and refining of tetrahedral meshes was also utilised in this work.

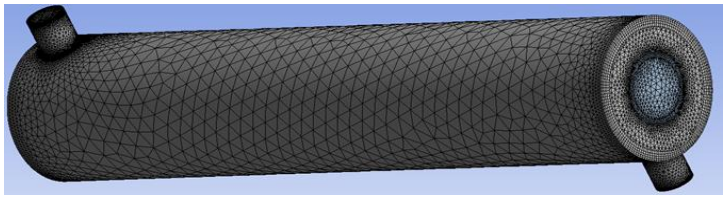

Figure 7. A mesh model of hot fluid and cold fluid.

Setup: Select water from the material library in this step. The fluid model was thermal energy. In the first case of parallel fluid flow, the hot and cold fluid assemblies would be subjected to all boundary conditions. Cold water was applied at the inlet at 5 m/s and 20 °C with zero length of cold fluid, and cold water was applied at the outlet at zero pressure and zero length of cold fluid. Furthermore, hot water was applied at the inlet at 4 m/s and 90 °C, 50 mm away from the edge of the hot fluid on the head, at 4 m/s and 90 °C.

Figure 8. Setup boundaries for parallel fluid flow.

The assemblies would then be subjected to all boundary conditions in the second case in a counter-fluid flow. Cold water was applied at the inlet at a 5 m/s and at a 20 °C with zero length of cold fluid, and zero pressure of cold water was applied at the outlet or end length of cold fluid. And also, hot water was applied at the input 4 m/s and 90 °C at 50 mm away from the edge of the hot fluid on the head on another side (950

mm away from the origin of the hot fluid) and at zero pressure of hot water at 50 mm away from the edge of the hot fluid flow on the heads. In addition, these applied wall boundary conditions to the two faces and the three outer sides of the hot fluid. Furthermore, the interface boundary between the cold outer face and the hot inner face was applied for heat transfer.

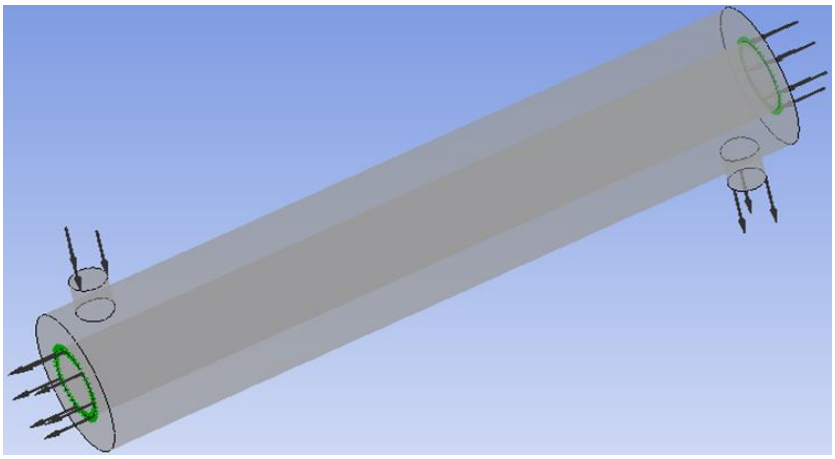

Figure 9. Setup of counter fluid flow.

3. Results

The simulation results below show the overall outcomes of both the parallel fluid flow and the counter-fluid flow, including streamlines of velocities, pressure distribution contours, pressure distribution charts, global velocity distribution contour plots, velocity vector distribution, global temperature distribution contour plots, and temperature distribution layouts. Fig. 10 shows below the streamline of velocities both (a) parallel fluid flow and (b) counter fluid flow using both inlets and outlets of cold and hot fluid flow; the red represents the maximum, and the blue denotes the minimum.

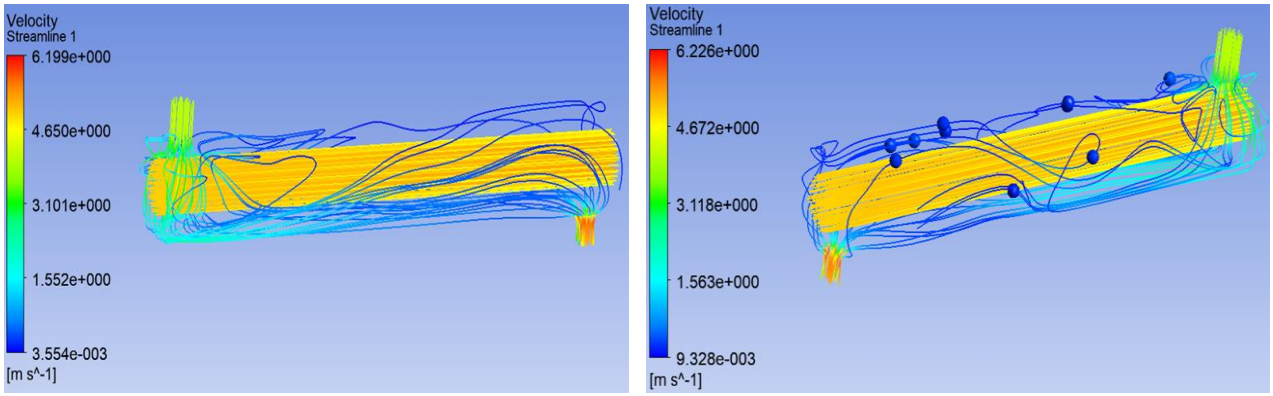

(a) Parallel fluid flow *(b)* Counter fluid flow

Figure 10. Shows streamlines of velocities.

Fig. 11 shows below the contour of the pressure distribution (global) of (a) parallel fluid flow and (b) counter fluid flow; the red shows high pressure and the blue represents low pressure. A T-junction is formed 50 mm away from the origin of the shell and tube when hot incoming fluid passes between the head and surface of the cool fluid as shown in Fig. 11 (a) parallel fluid flow. High pressure and low velocity coexist here. When hot inlet fluid flows through the head and makes contact with the cool fluid's contact surface, a T-junction forms 950 mm from the origin at the cold fluid's edge as shown in Fig. 11 (b) counter fluid flow. In this area, high pressure and low velocity coexist.

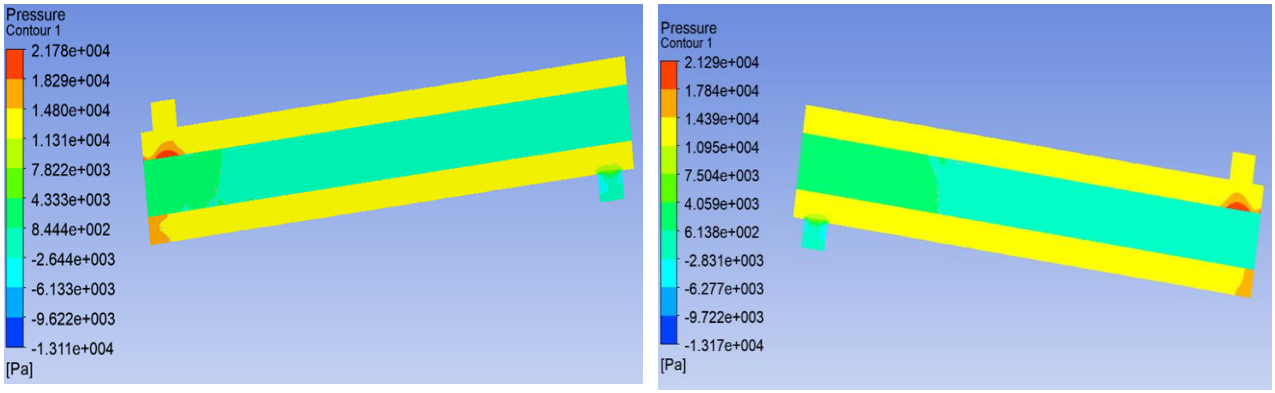

(a) Parallel fluid flow *(b)* Counter fluid flow

Figure 11. The contour of pressure distribution.

The pressure distribution charts for (a) parallel fluid flow and (b) counter fluid flow are displayed below in Fig. 12a and Fig. 12b. A chart of the pressure distribution (global) collected from 150 streamlines. Both the length and the pressure distribution are shown by the x and y axes, respectively. In case of (a) parallel fluid flow, when hot inlet fluid flows pass through the head and make contact with the cool fluid's contact surface, a T-junction forms 50 mm from the origin at the cold fluid's edge. In this region, high pressure and low velocity coexist. A T-junction is formed when hot fluid passes through the head and separates the surface of the cool fluid, 950 mm away from the origin of the cold fluid. In this region, low pressure and high velocity coexist. The reverse is true in case of (b) counter fluid flow case.

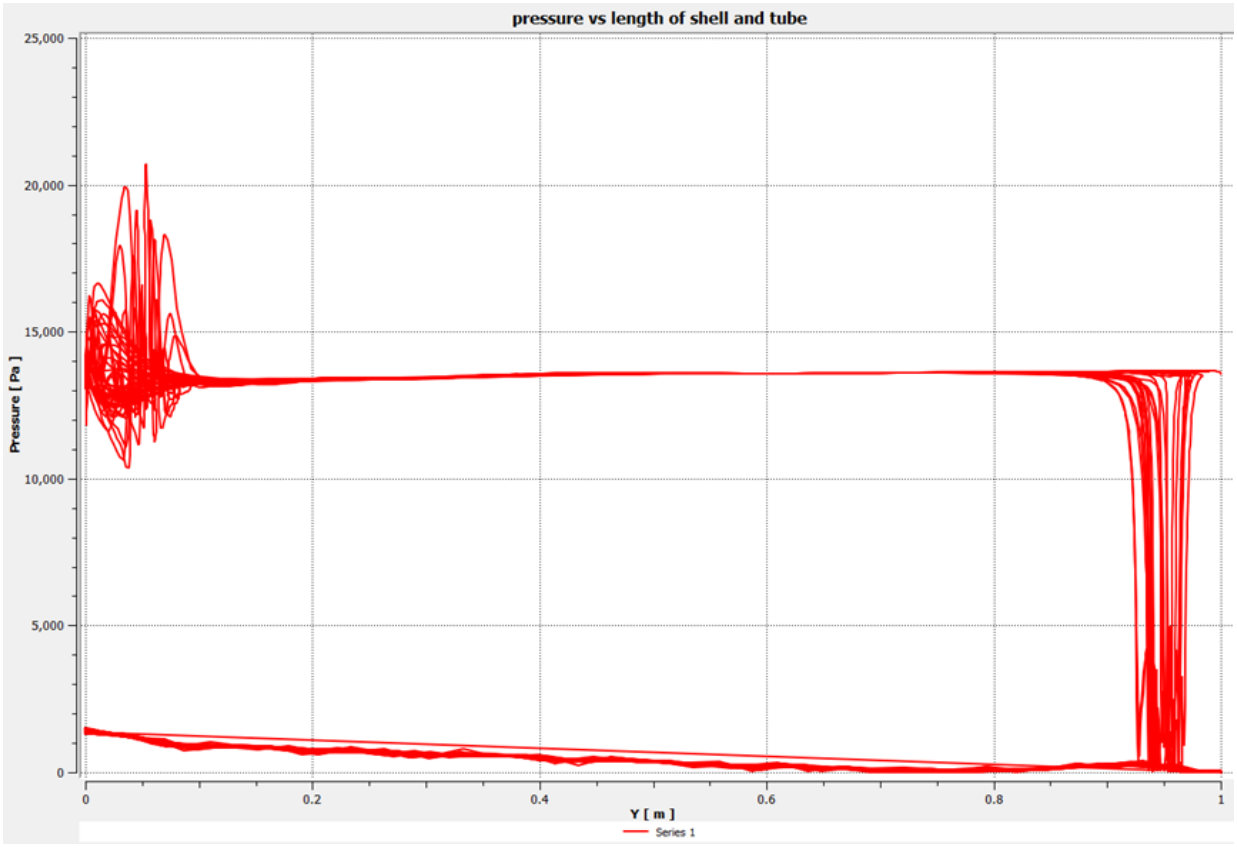

(a) Parallel fluid flow

Figure 12a. Pressure distribution graphs.

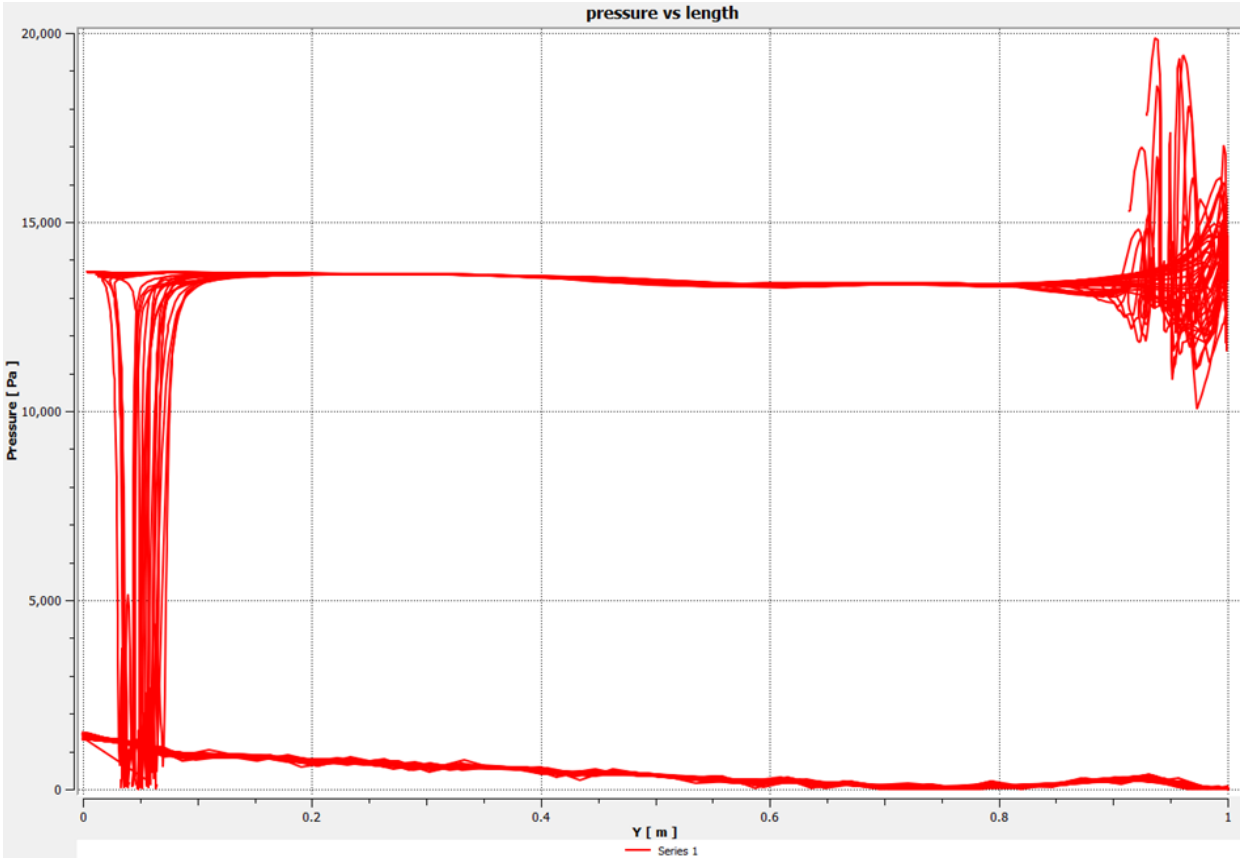

(b) Counter-fluid flow

Figure 12b. Pressure distribution graphs.

Fig. 13 shows the global velocity variation in both (a) parallel fluid flow and (b) counter fluid flow in the contour plot. The maximum velocity is shown in red, while the minimum velocity is shown in blue. In the pressure distribution charts for (a) parallel fluid flow and (b) counter fluid flow, as we elaborated before, the opposite is true. This implies that a certain region will have low velocity values when high pressure values occur.

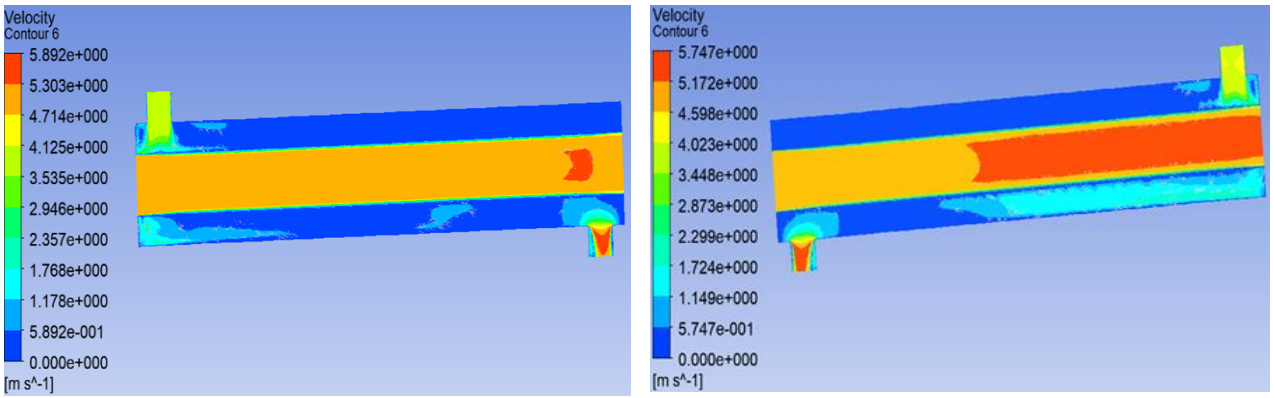

(a) Parallel fluid flow *(b)* Counter fluid flow

Figure 13. Global velocity distribution contour plot.

The velocity vector distribution for both (a) parallel fluid flow and (b) counter fluid flow is depicted below in Fig. 14. The highest velocity of the vector is denoted by the red arrow, while its minimum velocity is given by the blue arrow.

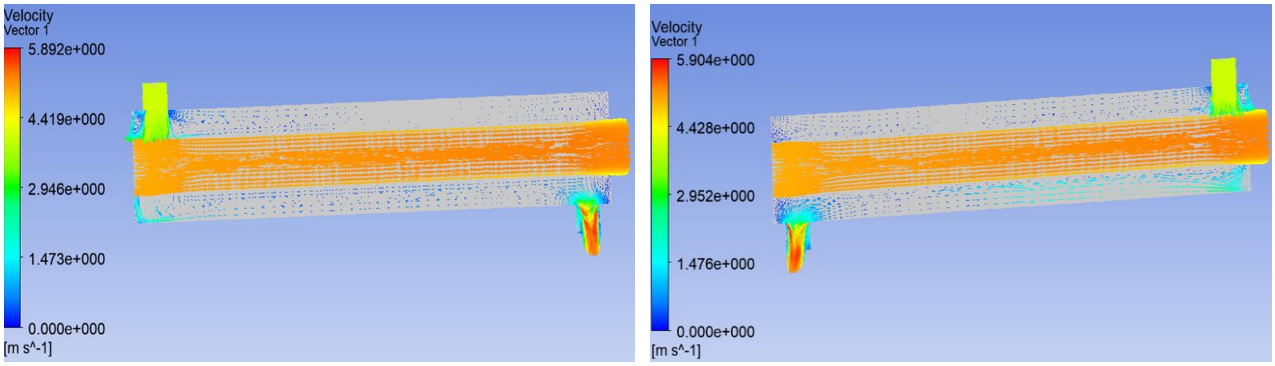

(a) Parallel fluid flow *(b)* Counter fluid flow

Figure 14. Velocity vector distribution.

Below are velocity distribution charts for (a) parallel fluid flow and (b) counter fluid flow, as shown in Fig. 15a and Fig. 15b. This represents the velocity variation on the y-axis and lengths on the x-axis. The chart of velocity distribution (global) obtained from the collection of 150 streamlines' dates. In (b) counter fluid flow Fig 15b, when hot inlet fluid flows through the head and makes contact with the cool fluid's contact surface, a T-junction forms 950 mm from the origin at the cold fluid's edge. In this area, high pressure and low velocity coexist. However, a T-junction is formed when hot fluid passes through the head and separates the surface of the cool fluid 50 mm away from the origin of the cold fluid. This region has both low pressure and high velocity. The reverse is true in case of (a) parallel fluid flow case. (Fig. 15a)

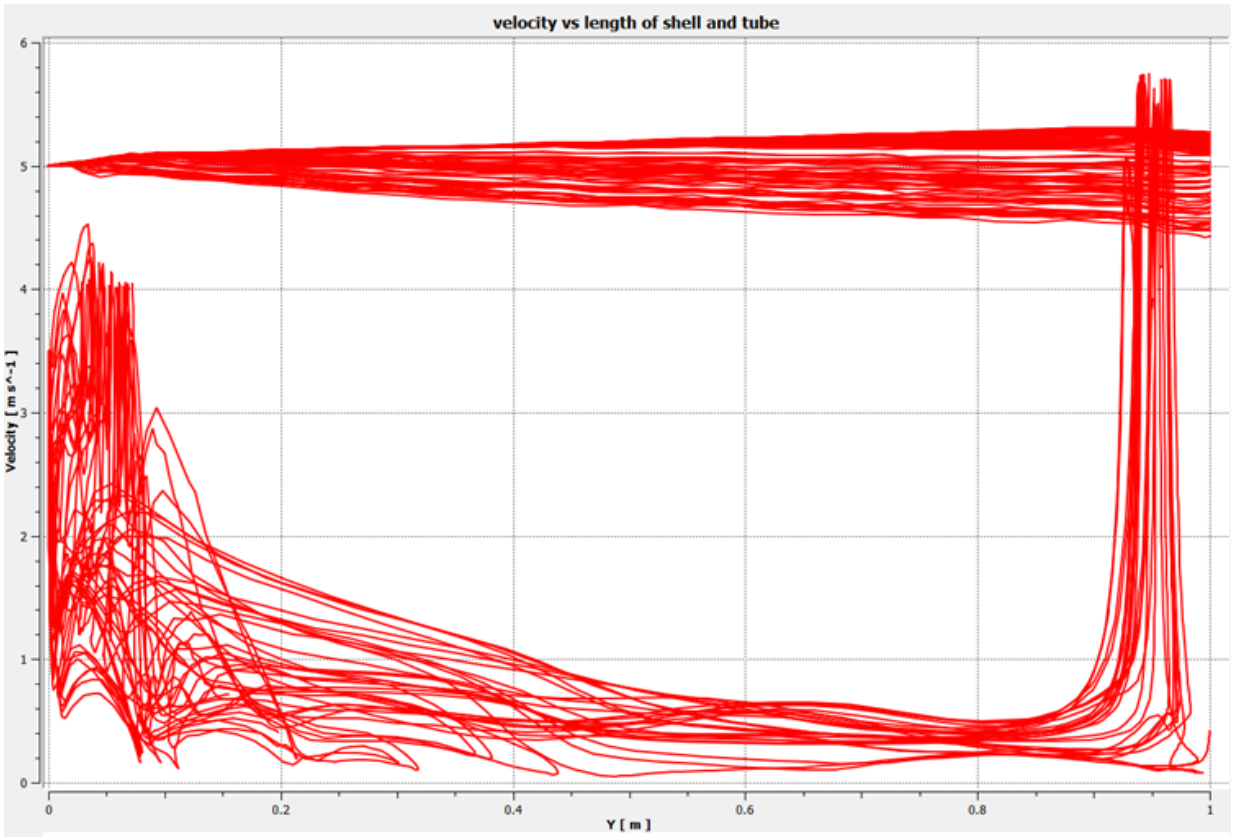

(a) Parallel fluid flow

Figure 15a. Velocity distribution graphs.

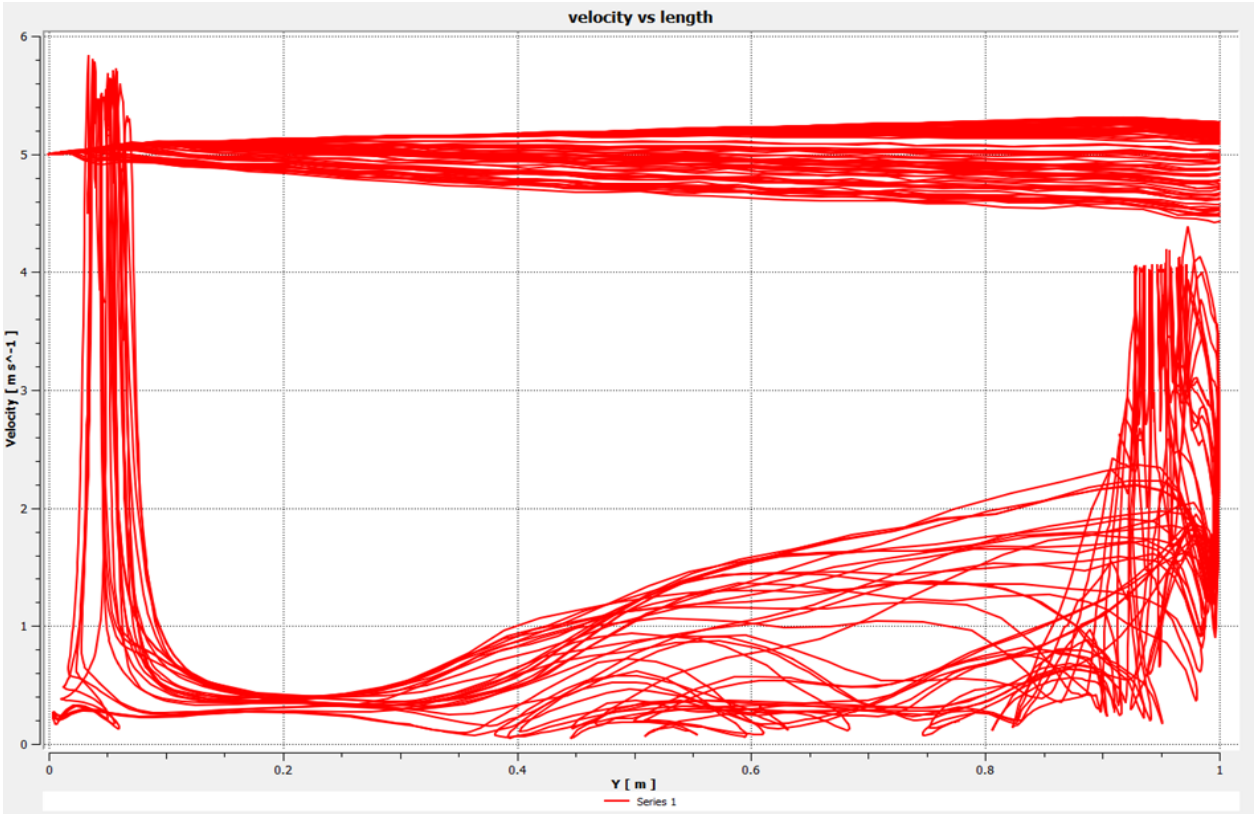

(b) Counter fluid flow

Figure 15b. Velocity distribution graphs.

The contour plots below represent the global temperature distribution for both (a) parallel fluid flow and (b) counter fluid flow, as seen in Fig. 16. The highest temperature is displayed by the red and the lowest is indicated by the blue. From the through head's intake to the out-through head on another, the heated fluid is continuously dripping out for either parallel fluid flow or counter fluid flow as show below temperature contour plots.

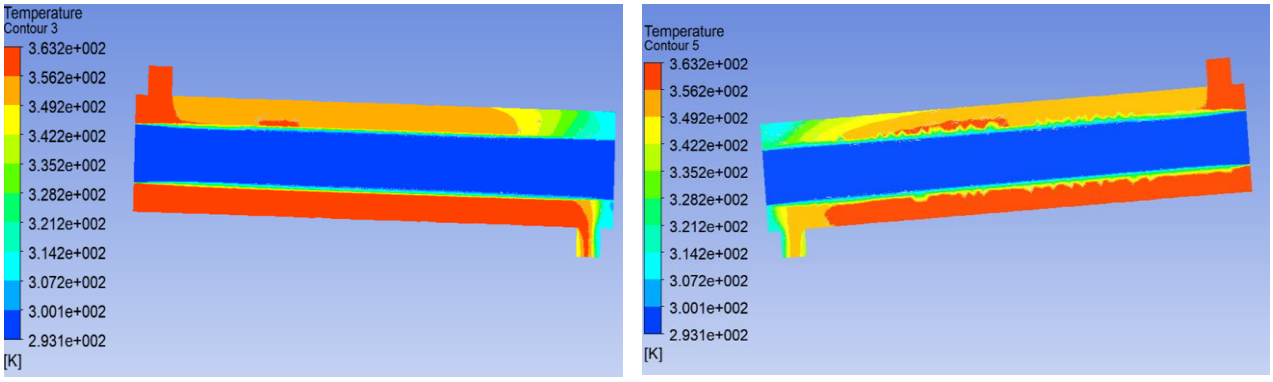

(a) Parallel fluid flow *(b)* Counter fluid flow

Figure 16. Global temperature distribution contour plots.

The temperature distribution charts for (a) parallel fluid flow and (b) counter fluid flow are displayed in Fig. 17 below. The chart of the temperature distribution (global) from 150 streamline collection dates. The temperature distribution is denoted by the y-axis, while the length is denoted by the x-axis. Temperature staring, dropping the hot fluid inlet through the head, and contact with cold fluid form a T-junction that is 50 mm away from the edge of cold fluid up to 950 mm away from the origin coordinate of cold fluid to hot fluid out, as shown in this temperature distribution chart in case of (a) parallel fluid flow in Fig. 17. From the

head's 950 mm T-junction, where the hot fluid begins to continually decrease in temperature, the cold fluid continues to do so until it reaches the head's hot flow outlet, which is located 50 mm from the cold fluid's source for the case of (b) counter fluid flow in Fig. 17.

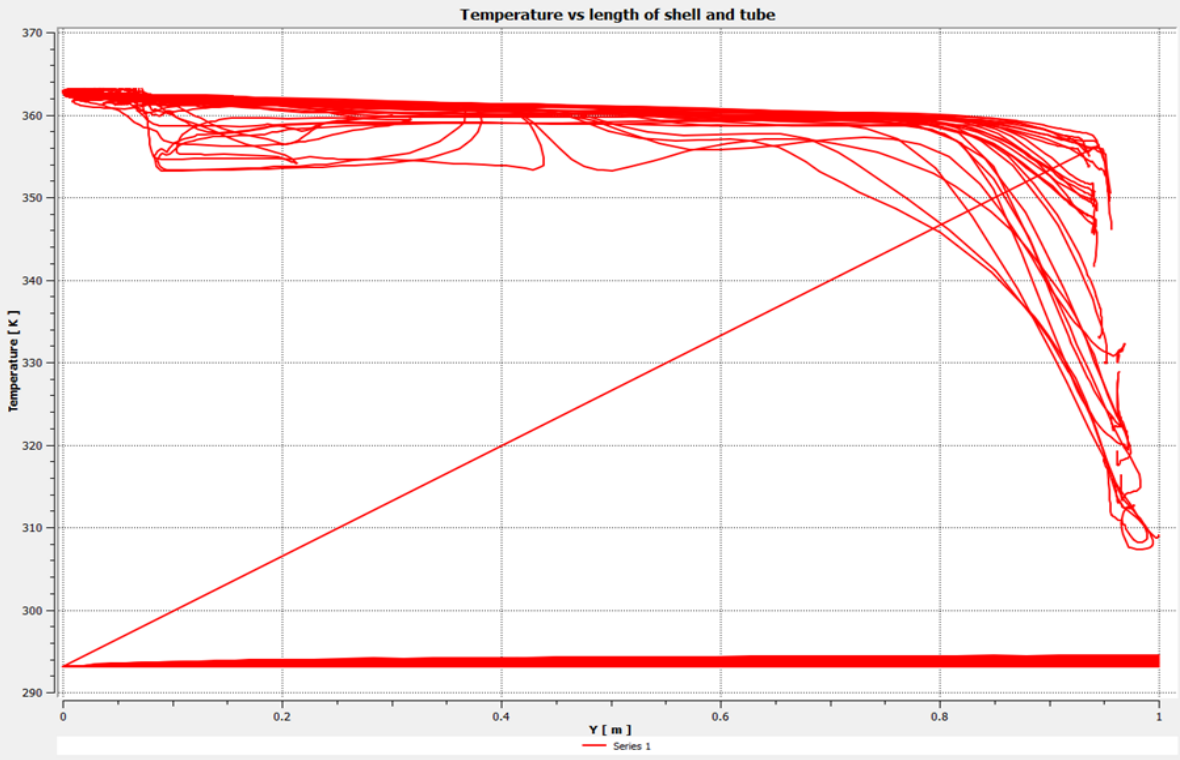

(a) Parallel fluid flow

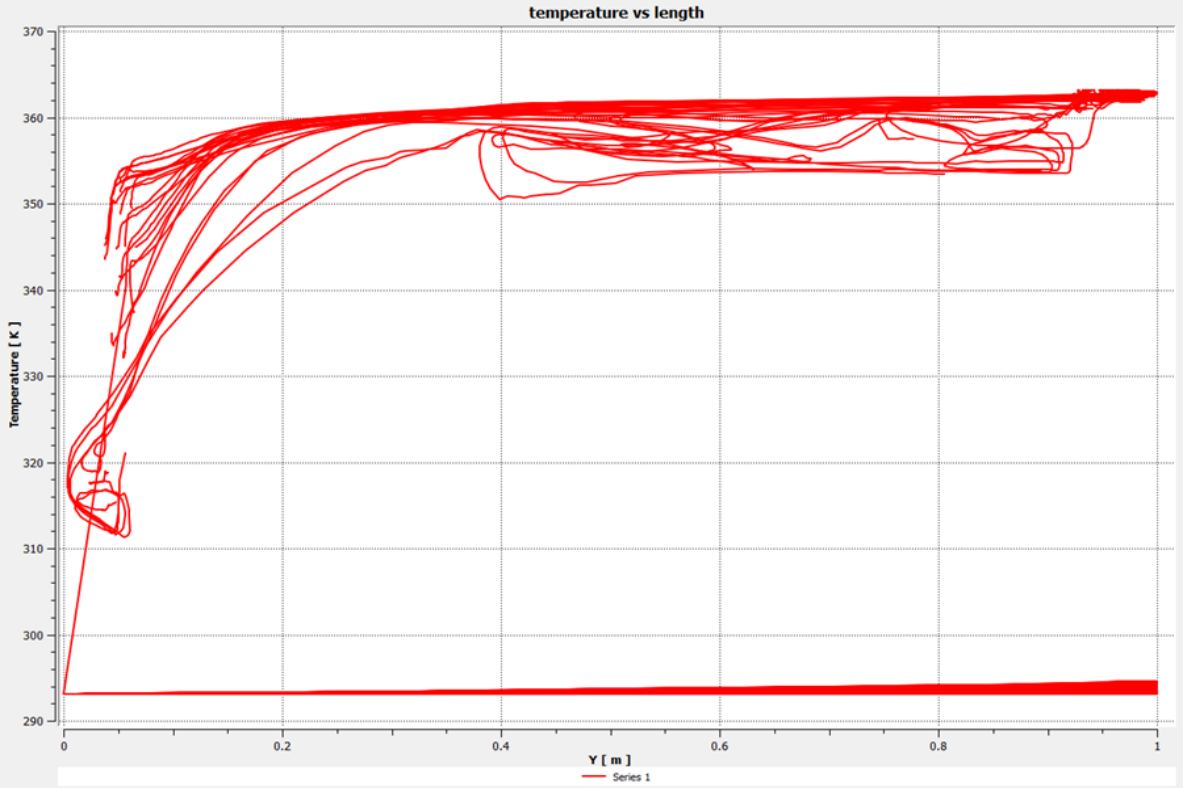

(b) Counter fluid flow

Figure 17. Temperature distribution plots.

4. Discussion

The overall results show that the parameters of pressure, temperature, and velocity do not significantly alter between parallel and counter fluid flow. The researchers demonstrated fluid flow animation using a velocity stream [11], [19], [31], [32], [37], [40], and [41]. The fluid flow character and pressure distribution approaching the T junction are complicated due to the sudden widening of the flow boundary, which results in flow separation and variable distribution [9], and [31]. The pressure is maximum at the end of the header and minimum at the entrance due to the jet caused at the inlet [27], [42], and [43]. In light of this, our findings were consistent with the study. Along the header inlet, the velocity is high, a clear vortex is circulated along the sides of the expanded jet flow, and a minor eddy flow is seen close to the header inlet because the vortex flow's circulation would slow down the first velocity [3], [27], [29], [37], [38], [39], and [42]. When the flow is flowing downstream, the turbulent kinetic energy and dissipation rate are greatest close to the T junction; they gradually decrease as the flow proceeds downstream, and they completely vanish near the closed end of the manifold [9]. As a result, our findings are consistent with those of other researchers. Researches demonstrated using velocity vectors [3], [9], [12], [16], [24], [25], [35], [37], [40] and [41]. Temperature measurements revealed a decrease in flow direction [6], [12], [20], [21], [22], [23] and [32]. A similar result occurs when hot fluid constantly transfers heat to cold fluid and hot fluid gradually decreases throughout the length, as shown in Fig. 17 global temperature distribution contour.

5. Conclusions

Fluid flows in the heat exchanger were analyzed using ANSYS Workbench CFX computational fluid dynamics, both parallel and counter types of heat exchangers. A detailed discussion was held regarding the temperature, pressure, and temperature throughout the entire heat exchanger. Here is a summary of the findings: The overall flow rate increases when the pressure differential decreases. High pressure and low velocity coexist at a T-junction, which is created when hot inlet fluid passes through the head and outer surface of cold fluid. Compared to parallel flow, counter flow has lower pressure and velocity distributions. Both parallel and counter types of heat exchangers can be successfully analyzed in all velocity distribution, pressure distribution, and temperature distribution using the ANSYS workbench (CFX) and computational fluid dynamics approach.

References

[1] **Zambaux, J. A., Harion, J. L., Russeil, S., & Bouvier, P.**, (2015). The effect of successive alternating wall deformation on the performance of an annular heat exchanger. Applied Thermal Engineering, 90, 286-295.

[2] **Sajadi, A. R., Sorkhabi, S. Y. D., Ashtiani, D., & Kowsari, F.**, (2014). Experimental and numerical study on heat transfer and flow resistance of oil flow in alternating elliptical axis tubes. International Journal of Heat and Mass Transfer, 77, 124-130.

[3] **Han, H. Z., Li, B. X., Wu, H., & Shao, W.**, (2015). Multi-objective shape optimization of double pipe heat exchanger with inner corrugated tube using RSM method. International Journal of Thermal Sciences, 90, 173-186.

[4] **Omidi, M., Farhadi, M., & Jafari, M.**, (2017). A comprehensive review on double pipe heat exchangers. Applied Thermal Engineering, 110, 1075-1090.

[5] **Yang, M., Low, E., Law, C. L., Chen, J. C., Show, P. L., & Huang, S. M.**, (2022). Heat and mass transfer in a counter flow parallel plate membrane-based absorption heat pump (PMAHP). International Journal of Thermal Sciences, 171, 107227.

[6] **Sheikholeslami, M., Hatami, M., Jafaryar, M., Farkhadnia, F., Ganji, D. D., & Gorji-Bandpy, M.**, (2015). Thermal management of double-pipe air to water heat exchanger. Energy and Buildings, 88, 361-366.

[7] **Yehia, M. G., Attia, A. A., Abdelatif, O. E., & Khalil, E. E.**, (2016). Heat transfer and friction characteristics of shell and tube heat exchanger with multi inserted swirl vanes. Applied Thermal Engineering, 102, 1481-1491.

[8] **Tavousi, E., Perera, N., Flynn, D., & Hasan, R.**, (2023). Heat transfer and fluid flow characteristics of the passive method in double tube heat exchangers: a critical review. International Journal of Thermofluids, 17, 100282.

[9] **Minocha, N., & Joshi, J. B.**, (2020). 3D CFD simulation of turbulent flow distribution and pressure drop in a dividing manifold system using openfoam. International Journal of Heat and Mass Transfer, 151, 119420.

[10] **Andhare, R. S., Shooshtari, A., Dessiatoun, S. V., & Ohadi, M. M.**, (2016). Heat transfer and pressure drop characteristics of a flat plate manifold microchannel heat exchanger in counter flow configuration. Applied Thermal Engineering, 96, 178-189.

[11] **Ozden, E., & Tari, I.**, (2010). Shell side CFD analysis of a small shell-and-tube heat exchanger. Energy conversion and Management, 51(5), 1004-1014.

[12] **Liu, J. J., Liu, Z. C., & Liu, W.**, (2015). 3D numerical study on shell side heat transfer and flow characteristics of rod-baffle heat exchangers with spirally corrugated tubes. International journal of thermal sciences, 89, 34-42.

[13] **Zhou, J., Sun, Z., Ding, M., Bian, H., Zhang, N., & Meng, Z.**, (2017). CFD simulation for flow distribution in manifolds of central-type compact parallel flow heat exchangers. Applied Thermal Engineering, 126, 670-677.

[14] **Yaïci, W., Ghorab, M., & Entchev, E.**, (2013). Numerical analysis of heat and energy recovery ventilators performance based on CFD for detailed design. Applied Thermal Engineering, 51(1-2), 770-780.

[15] **Huang, S. M., Yang, M., Huang, W. H., Tao, S., Hu, B., & Qin, F. G.**, (2018). An analytical solution of heat and mass transfer in a counter/parallel flow plate membrane module used in an absorption heat pump. International Journal of Thermal Sciences, 124, 110-121.

[16] **Gorman, J. M., Krautbauer, K. R., & Sparrow, E. M.**, (2016). Thermal and fluid flow first-principles numerical design of an enhanced double pipe heat exchanger. Applied Thermal Engineering, 107, 194-206.

[17] **Łopata, S., & Ocłoń, P.**, (2015). Numerical study of the effect of fouling on local heat transfer conditions in a high-temperature fin-and-tube heat exchanger. Energy, 92, 100-116.

[18] **Taler, D., & Ocłoń, P.**, (2014). Thermal contact resistance in plate fin-and-tube heat exchangers, determined by experimental data and CFD simulations. International Journal of Thermal Sciences, 84, 309-322.

[19] **Hari, B., Brouwer, J. P., Dhir, A., & Steinberger-Wilckens, R.**, (2019). A computational fluid dynamics and finite element analysis design of a microtubular solid oxide fuel cell stack for fixed wing mini unmanned aerial vehicles. International Journal of Hydrogen Energy, 44(16), 8519-8532.

[20] **Modi, N., Wang, X., Negnevitsky, M., & Cao, F.**, (2021). Melting characteristics of a longitudinally finned-tube horizontal latent heat thermal energy storage system. Solar Energy, 230, 333-344.

[21] **Hatami, M., Jafaryar, M., Ganji, D. D., & Gorji-Bandpy, M.**, (2014). Optimization of finned-tube heat exchangers for diesel exhaust waste heat recovery using CFD and CCD techniques. International Communications in Heat and Mass Transfer, 57, 254-263.

[22] **Kumar, P. M., & Chandrasekar, M.**, (2019). CFD analysis on heat and flow characteristics of double helically coiled tube heat exchanger handling MWCNT/water nanofluids. Heliyon, 5(7).

[23] **Zhou, F., Ling, W., Zhou, W., Qiu, Q., & Chu, X.**, (2019). Heat transfer characteristics of Cu-based microchannel heat exchanger fabricated by multi-blade milling process. International Journal of Thermal Sciences, 138, 559-575.

[24] **Gandhi, M. S., Ganguli, A. A., Joshi, J. B., & Vijayan, P. K.**, (2012). CFD simulation for steam distribution in header and tube assemblies. Chemical Engineering Research and Design, 90(4), 487-506.

[25] **Tamburini, A., Renda, M., Cipollina, A., Micale, G., & Ciofalo, M.**, (2016). Investigation of heat transfer in spacer-filled channels by experiments and direct numerical simulations. International Journal of Heat and Mass Transfer, 93, 1190-1205.

[26] **Su, L., Duan, Z., He, B., Ma, H., & Ding, G.**, (2019). Laminar flow and heat transfer in the entrance region of elliptical minichannels. International Journal of Heat and Mass Transfer, 145, 118717.

[27] **Cupiał, P., & Snamina, J.**, (2022). Analytical and numerical approach to convective heat transfer through a granular target with gas cooling. International Journal of Thermal Sciences, 171, 107196.

[28] **Yang, H., Wang, Y., Ren, M., & Yang, X.**, (2017). Effect of the rectangular exit-port geometry of a distribution manifold on the flow performance. Applied Thermal Engineering, 117, 481-486.
[29] **Jayakumar, J. S., Mahajani, S. M., Mandal, J. C., Vijayan, P. K., & Bhoi, R.**, (2008). Experimental and CFD estimation of heat transfer in helically coiled heat exchangers. Chemical engineering research and design, 86(3), 221-232.
[30] **Hashemian, M., Jafarmadar, S., & Dizaji, H. S.**, (2016). A comprehensive numerical study on multi-criteria design analyses in a novel form (conical) of double pipe heat exchanger. Applied thermal engineering, 102, 1228-1237.
[31] **Zhang, W., Li, A., Gao, R., & Li, C.**, (2018). Effects of geometric structures on flow uniformity and pressure drop in dividing manifold systems with parallel pipe arrays. International Journal of Heat and Mass Transfer, 127, 870-881.
[32] **Bezaatpour, M., & Goharkhah, M.**, (2020). Convective heat transfer enhancement in a double pipe mini heat exchanger by magnetic field induced swirling flow. Applied Thermal Engineering, 167, 114801.
[33] **Hashemian, M., Jafarmadar, S., Nasiri, J., & Dizaji, H. S.**, (2017). Enhancement of heat transfer rate with structural modification of double pipe heat exchanger by changing cylindrical form of tubes into conical form. Applied Thermal Engineering, 118, 408-417.
[34] **Li, B., Hou, J., Xu, K., Gao, Q., Zeng, M., & Wang, Q.**, (2023). Optimal designs for flow uniformity at inlet of microchannel flat tube heat exchanger. Applied Thermal Engineering, 226, 120300.
[35] **Sen, N., Tat, D., Singh, K. K., Goswami, A. K., Mukhopadhyay, S., & Shenoy, K. T.**, (2022). Single-phase flow distribution and mixing in a novel microfluidic header: Experimental and CFD studies. Chemical Engineering Research and Design, 188, 433-446.
[36] **Kirincic, M., Trp, A., & Lenic, K.**, (2021). Numerical evaluation of the latent heat thermal energy storage performance enhancement by installing longitudinal fins. Journal of energy storage, 42, 103085.
[37] **Raul, A., Bhasme, B. N., & Maurya, R. S.**, (2016). A numerical investigation of fluid flow maldistribution in inlet header configuration of plate fin heat exchanger. Energy Procedia, 90, 267-275.
[38] **Shojaeefard, M. H., Nourbakhsh, S. D., & Zare, J.**, (2017). An investigation of the effects of geometry design on refrigerant flow mal-distribution in parallel flow condenser using a hybrid method of finite element approach and CFD simulation. Applied Thermal Engineering, 112, 431-449.
[39] **Said, S. A. M., Ben-Mansour, R., Habib, M. A., & Siddiqui, M. U.**, (2015). Reducing the flow mal-distribution in a heat exchanger. Computers & Fluids, 107, 1-10.
[40] **Vali, A., Ge, G., Besant, R. W., & Simonson, C. J.**, (2015). Numerical modeling of fluid flow and coupled heat and mass transfer in a counter-cross-flow parallel-plate liquid-to-air membrane energy exchanger. International Journal of Heat and Mass Transfer, 89, 1258-1276.
[41] **Liu, H. L., Li, H., He, Y. L., & Chen, Z. T.**, (2018). Heat transfer and flow characteristics in a circular tube fitted with rectangular winglet vortex generators. International Journal of Heat and Mass Transfer, 126, 989-1006.
[42] **Wang, C. C., Yang, K. S., Tsai, J. S., & Chen, Y.**, (2011). Characteristics of flow distribution in compact parallel flow heat exchangers, part I: Typical inlet header. Applied Thermal Engineering, 31(16), 3226-3234.
[43] **Barrios, A. N. S., Silva, J. B. C., Rodrigues, A. R., Coelho, R. T., Junior, A. B., & Matsumoto, H.**, (2014). Modeling heat transfer in die milling. Applied thermal engineering, 64(1-2), 108-116.

HUNGARIAN AGRICULTURAL ENGINEERING
No 43/2024 18-25
Published online: http://hae-journals.org/
HU ISSN 0864-7410 (Print)
HU ISSN 2415-9751(Online)
DOI: 10.17676/HAE.2024.43.18
Received: 29.04.2024 - Accepted: 26.05.2024

PERIODICAL
OF THE COMMITTEE OF AGRICULTURAL AND BIOSYSTEM ENGINEERING OF THE HUNGARIAN ACADEMY OF SCIENCES
and
HUNGARIAN UNIVERSITY OF AGRICULTURE AND LIFE SCIENCES
INSTITUTE OF TECHNOLOGY

INFLUENCE OF AMBIENT STORAGE ON WEIGHT, COLOR, AND TSS IN GOLDEN DELICIOUS APPLES: A CORRELATIONAL STUDY

Author(s):
S. Kassebi [1], P. Korzenszky [2]

Affiliation:
[1] Doctoral School of Mechanical Engineering – Hungarian University of Agriculture and Life Sciences, 2100 Gödöllő, Páter Károly u. 1., Hungary;
[2] Institute of Technology – Hungarian University of Agriculture and Life Sciences, 2100 Gödöllő, Páter Károly u. 1., Hungary;

Email address:
kassebi.salma@phd.uni-mate.hu; korzenszky.peter.emod@uni-mate.hu

Abstract: This research explores the interplay between weight loss, color transformation, and total soluble solids (TSS) in Golden Delicious apples during storage at room temperature. Across six weeks, a freshly harvested batch of Golden Delicious apples underwent scrutiny in a controlled environment, maintaining around 24ºC and 60% humidity. The study aimed to unravel the post-harvest physiological shifts in apples, explicitly focusing on factors affecting consumer appeal and shelf life. Methodologically, weight loss was precisely tracked using a high-precision scale, while color alterations were quantified via a portable colorimeter, yielding CIELAB L*, a*, and b* values. A refractometer was used to assess TSS, which indicated sweetness and ripeness. Correlation analysis revealed a strong link between weight loss and color shift, with a less pronounced yet significant connection between TSS and the other variables. These findings enrich our comprehension of the post-harvest dynamics of Golden Delicious apples, carrying implications for adequate storage and marketing tactics. This research supports the principles of the circular economy by enhancing the efficiency of post-harvest processes and minimizing waste through better storage practices. By understanding these factors, producers can reduce spoilage and extend the shelf life of apples, contributing to more sustainable food systems.

Keywords: Apple, post-harvest changes, storage impact, correlation, mass loss

1. Introduction

Due to limited storage capacity compared to production levels, the costs associated with cold storage can increase. As a result, many consumers choose to purchase fruits that have been stored at room temperature in local markets. Therefore, assessing the quality of apples at room temperature is crucial, and non-destructive color measurement is a valuable indicator at purchase [1], [2]. A fruit's vibrant and fresh appearance is a consumer's initial interaction with it, significantly influencing their sensory experience. Traditionally, fruit quality assessment relied on visual inspection and destructive testing [3]. However, advancements in spectroscopic and imaging techniques offer effective and non-destructive alternatives that address the limitations of traditional methods [4].

The levels of total soluble solids (TSS) in apples are crucial in determining their texture and flavor, which in turn impact their overall quality and appeal to consumers [5], [6], [7].

Additionally, weight loss in fruits, mainly due to dehydration, affects their quality and economic value. The natural wax coating on apples plays a significant role in retaining moisture, and the structure and composition of the skin's wax are essential factors in mitigating weight loss [8]. Weight loss affects the fruit's visual appeal and textural quality, leading to softening and reduced turgor pressure. Therefore, measuring fruit weight is essential for fruit quality assessment [9], [10].

While there is existing research on fruit storage, further investigation is needed into color changes in fruits and the classification of ripening stages during shelf life [11] demonstrated that color changes during storage

could serve as a classification criterion for ripening stages. Apple quality deteriorates significantly during storage, which affects consumer acceptance [12], [13], [14]. This study highlights the relationship between weight loss, TSS and colorimetry data.

2. Materials and Methods

Fresh Golden Delicious apples were harvested from a farm near Kecskemét, Hungary. Three measurements were made for each sample to determine the weight and geometry. The average weight of the entire fruit sample was 150 ±12 g. The apples were kept for six weeks at room temperature (24 ± 1 C) with 60% relative humidity.

2.1. Measurement of Weight Loss

The samples of apple fruits were weighed using a precision scale type KERN (KERN & SHON GmbH, Balingen, Germany, KERN PCB 3500-2, max.: 3500 g ± 0.01 g).

Weight loss (%) was calculated using the following equation:

$$\textbf{Weight loss} = \frac{\mathbf{m_0 - m}}{\boldsymbol{m_0}} \cdot \mathbf{100}, [\%] \quad (1)$$

where:

m – the mass of apples during storage (g),

m_0 – the initial mass of apples (g).

2.2. Measurement of Color

The color characteristics of samples were measured with a wireless Nix Pro color sensor (Nix Sensor Ltd., Hamilton, Ontario, Canada, NixPro Mini).

Color parameters, precisely color difference (ΔE), and chroma (C) were calculated from the L*a*b* data. Chroma describes the saturation of a fruit's color, while Delta E is used to measure and compare color differences.

$$\mathbf{\Delta E} = \sqrt{(\mathbf{L_0^* - L^*})^2 + (\mathbf{a_0^* - a^*})^2 + (\mathbf{b_0^* - b^*})^2}, \quad (2)$$

$$\mathbf{C^*} = \sqrt{\mathbf{a^{*2} + b^{*2}}}, \quad (3)$$

where L_0^*, a_0^*, and b_0^* represent the initial color data based on the samples.

2.3. Measurement of Total Soluble Solids (TSS)

The TSS of extracted juice was determined with a digital hand refractometer (Ebro Electronic GmbH, Ingolstadt, Germany, Model: DR-10). The TSS values of the juice were measured in triplicate and the results were expressed in ºBrix (±0.2).

3. Results and Discussion

3.1. Correlation between weight loss and color parameters

Correlation analysis can assist in comprehending the connection between two variables. A significant linear trend can be identified by analyzing Golden Delicious apples' weight loss and L* value (lightness) stored at room temperature over six weeks. This trend indicates a link between increased weight loss and decreased lightness. The negative correlation between weight loss and the L* value suggests that as the apples lose water weight and undergo transformations during storage, they become less reflective or appear darker. The correlation also points to a change in color in the apples as they lose weight, which is linked to increased ethylene production and respiration [15]. Therefore, it is critical to understand how storage time influences

the apples' quality and marketability in terms of their visual appeal, which directly impacts how consumers perceive their freshness and quality. The solid linear correlation, with an R^2 value of 0.9075, indicates a robust connection, where the linear model explains most of the variance in the L* values. It implies that, by understanding the percentage of weight loss of the apples, their L* value can be predicted with a high degree of accuracy using this model. By understanding the correlation between weight loss and L* value in Golden Delicious apples, the quality and marketability of the fruit can be predicted based on its visual appeal. (Fig. 1.)

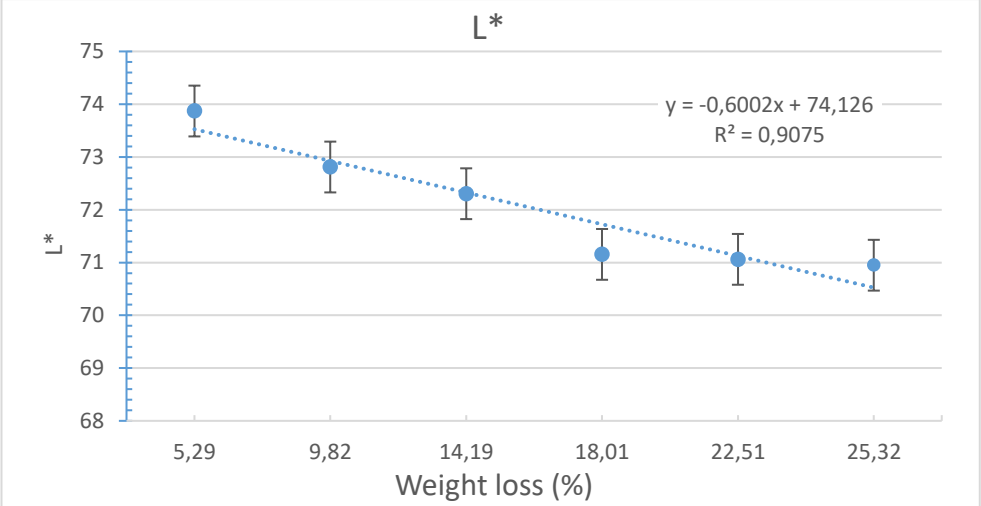

Figure 1. Correlation between Weight Loss and L* Values in Stored Golden Delicious Apples.

Fig. 2 shows the relationship between weight loss and the a* value (representing chromaticity on a green-to-red axis) of apples stored at room temperature over six weeks. The graph exhibits a positive correlation between weight loss and the a* value. As the weight loss percentage increases, the a* value increases, suggesting that the apples become redder as they lose weight and start rotting. The R^2 value of 0.9423 demonstrates a robust correlation between these two variables. As apples lose weight, mainly through water loss, there may be a concentration of pigments such as anthocyanins and carotenoids, which can cause the color to shift towards red [16]. Apples can undergo enzymatic reactions that may lead to a change in skin color. In the case of Golden Delicious apples, this might mean a shift from a greener to a redder hue as the weight loss progresses and red spots appear as a sign of rotten. The strong correlation between weight loss and color change affects apples' perceived freshness and quality. As the color shifts towards red, it may affect consumer preference significantly. In the case of Golden Delicious apples, a redder color is associated with ripeness and rottenness. This correlation is statistically robust, as indicated by the high R^2 value, and could be valuable for the agricultural industry to predict and assess color changes in apples due to weight loss during storage.

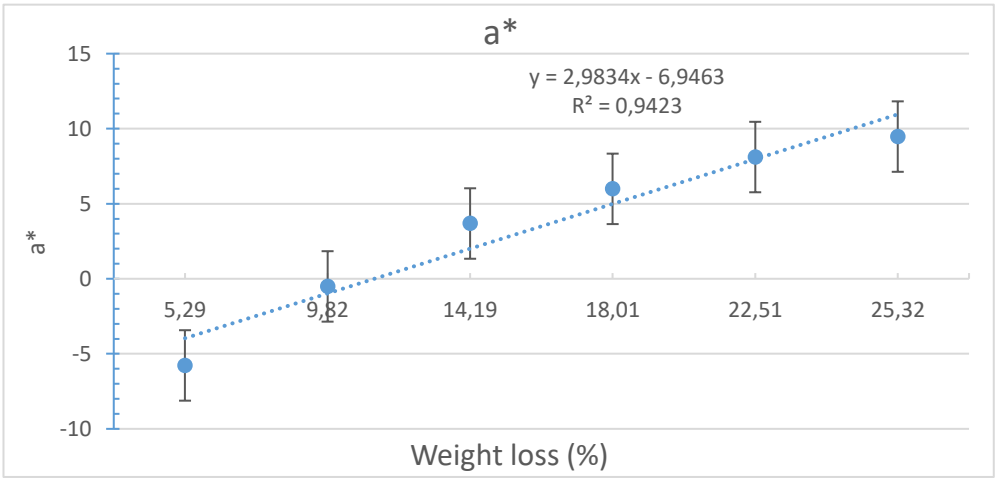

Figure 2. Correlation Between Weight Loss and Chromaticity (a*) of Golden Delicious Apples During Six Weeks of Room Temperature Storage.

Fig. 3 shows a positive correlation between weight loss and the b* value. As weight loss increases, the b* value increases, suggesting that the apples become more yellow as they lose weight. The R^2 value is 0.8523, which indicates a robust correlation between weight loss and b* value.

The increase in b* value with weight loss might be due to the natural ripening process, where chlorophyll breakdown and the synthesis of carotenoids can make the fruit appear more yellow over time [17].

Water loss may lead to a concentration of pigments within the apple, making the yellow color more pronounced. This is especially true if the water loss is more from the surface, where the color change is most noticeable. As they age and lose water, apples may undergo non-enzymatic browning reactions that can contribute to a change in color, potentially leading to an increase in the yellow component [18]. The strong correlation captured by the linear model and the high R^2 value suggests that this color change is consistent and can be reliably predicted by the extent of weight loss.

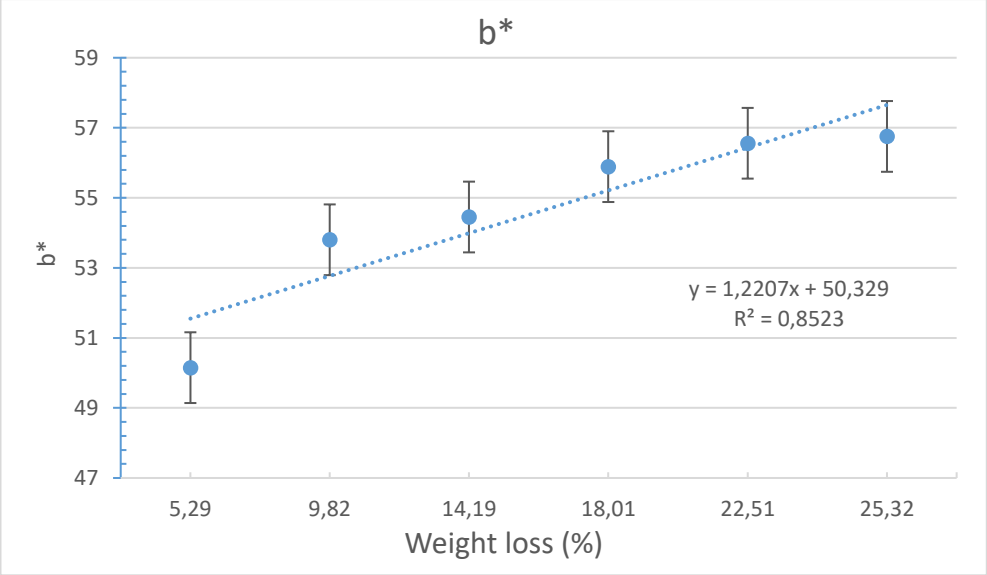

Figure 3. Correlation Between Weight Loss and Chromaticity (b*) of Golden Delicious Apples During Six Weeks of Room Temperature Storage

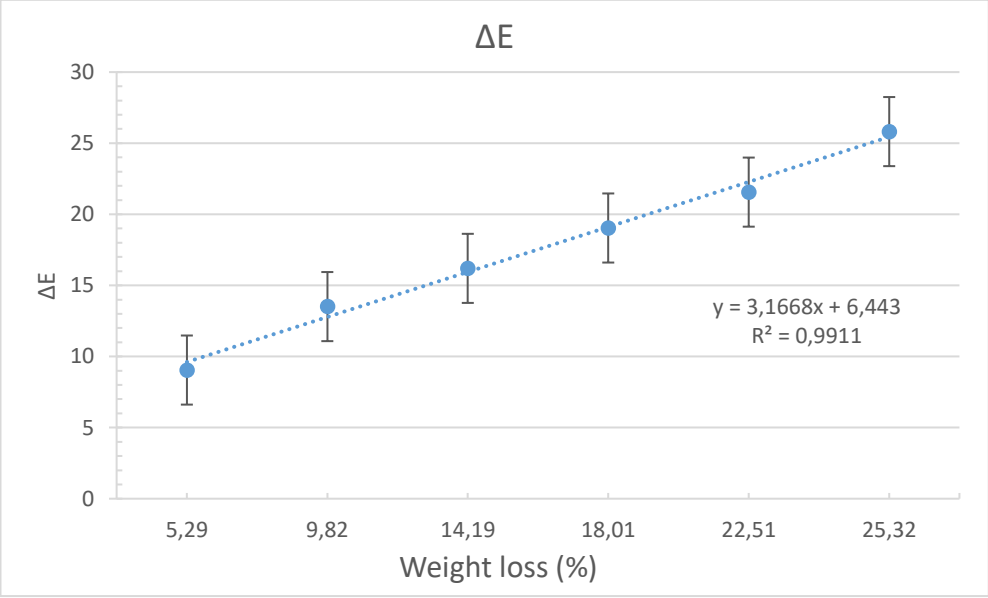

Figure 4. Relationship Between Weight Loss and Total Color Change (ΔE) in Golden Delicious Apples Over Six Weeks of Storage.

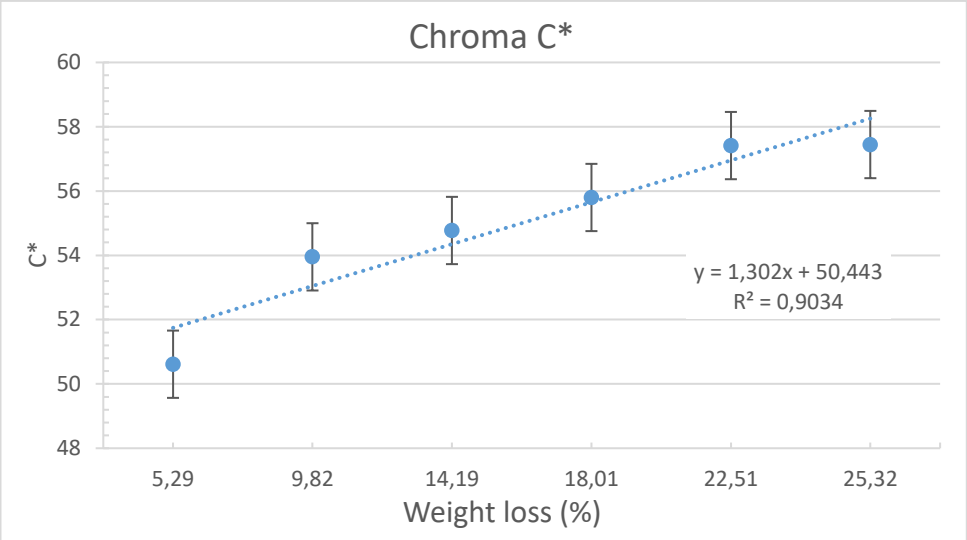

Figure 5. Impact of Weight Loss on Chroma Intensity (C*) in Golden Delicious Apples During Six Weeks at Ambient Temperature

The graphical analysis (Fig. 4) indicates a robust positive correlation between the weight loss of and ΔE, with an R^2 value of 0.9911. This strong correlation suggests that color changes are significant and directly related to the degree of weight loss.

In conjunction with ΔE, Chroma (C*) also exhibits a positive correlation with weight loss, as reflected by an R^2 value of 0.9034 (Fig. 5). This correlation demonstrates that as the apples lose weight, there is a concurrent increase in color intensity, leading to a more vivid and saturated appearance [11]. The initial weight loss stages are the most significant Chroma alterations, a trend consistent with the changes observed in ΔE.

The observed increase in both ΔE and Chroma during the early phase of weight loss can be attributed to the concentration of pigments due to moisture reduction and the potential degradation of chlorophyll. As a result, the apples exhibit a more pronounced color change, becoming noticeably different and more intense.

When apples ripen, the chlorophyll in their flesh and skin turns green. Chlorophyll is constantly renewed prior to maturation; however, once development starts, the rate of chlorophyll production slows down, initially leading to a loss of green tint. When more chlorophyll is lost, other pigmentation – typically yellow – takes centre stage. [19], [20].

3.2. Correlation between weight loss and Total Soluble Solids

Fig. 6 presents a correlation between the weight loss percentage of Golden Delicious apples and their Total Soluble Solids (TSS) measured during storage at room temperature. The graph illustrates a linear increase in TSS as the weight loss percentage rises. The pattern of change suggests that as apples lose moisture over time, the concentration of soluble solids like sugars increases [21]. The R^2 value of 0.9624 is very high, which means that the linear model can explain approximately 96.24% of the variance in TSS based on weight loss. This indicates a solid predictive relationship.

During storage, apples lose weight primarily due to water loss. As water content decreases, the components that make up the TSS, such as sugars, become more concentrated. TSS is a measure often associated with the sweetness and flavor intensity of the fruit. The increase in TSS as weight loss occurs may indicate that the apples could taste sweeter and have a more pronounced flavor as they dehydrate.

Given their perishable nature and high metabolic and respiratory rates, apples typically have a limited storage duration. Post-harvest losses, which can account for up to 25–28% of total yield [22], underscore the importance of enhancing post-harvest fruit management to bolster the food supply [23]. While apples are nutritionally rich, this value diminishes after harvest due to various factors.

Internal and external factors influence these losses during storage, with temperature and relative humidity playing a pivotal role [24]. The correlation between the weight loss of Golden Delicious apples and other parameters during post-harvest handling is particularly noteworthy. This weight loss is closely linked to changes in firmness, color, and total soluble solids content, reflecting the fruit's overall quality and shelf life.

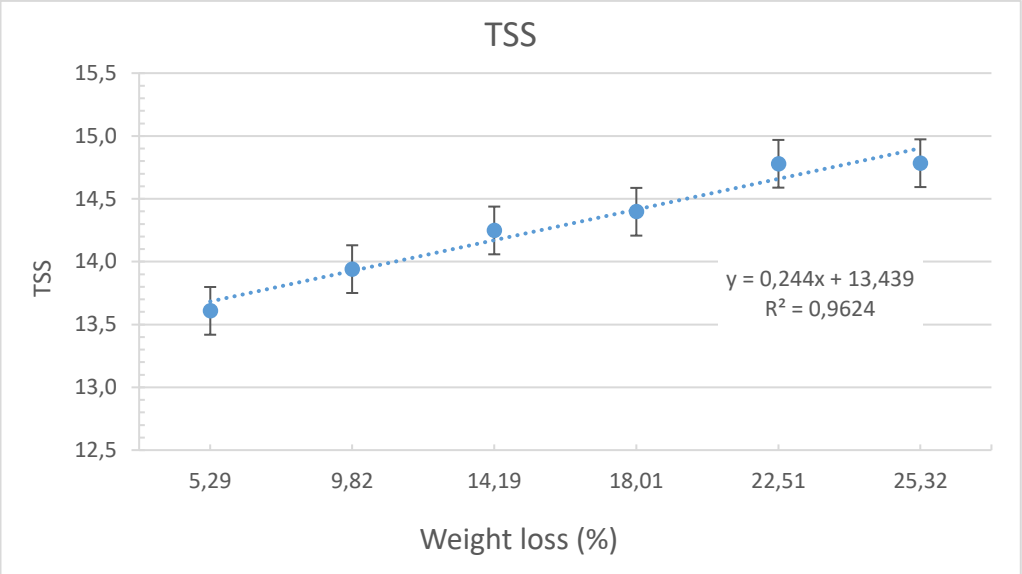

Figure 6. Correlation Between Weight Loss and TSS of Golden Delicious Apples During Six Weeks of Room Temperature Storage

The correlation between weight loss and total soluble solids (TSS) of Golden Delicious apples stored at room temperature has been a subject of interest in several studies. Juhnevica et al. assessed the impact of different storage conditions on apple quality [25]. This study provided insights into the various factors that influence the quality of apples during storage, including changes in TSS levels. Another study focused on the effect of post-harvest storage on the weight of Golden Delicious apples [26], highlighting the impact of storage conditions on weight loss, which can, in turn, influence TSS levels. Additionally, non-destructive methods for measuring chlorophyll content in the skin of Golden Delicious apples and evaluating quality were explored in a separate study by Rutkowski et al. shedding light on the potential indicators of apple quality beyond weight loss and TSS [27]. These findings collectively emphasize the multifaceted nature of apple quality during storage and the importance of considering various factors, including weight loss and TSS, in assessing and managing post-harvest apple quality.

4. Conclusions

This study established a definitive linear correlation between weight loss in Golden Delicious apples and critical quality attributes such as lightness, chromaticity, total color change, chroma intensity, and total soluble solids over a six-week storage period at room temperature. Analytical models explain most of the variability in these quality indicators, highlighting weight loss as a powerful predictive tool for assessing post-harvest quality deterioration. The implications for post-harvest apple management are substantial, presenting a metric for anticipatory quality control and increasing marketability through more informed storage strategies. This study highlights the importance of weight loss monitoring as a non-invasive but informative indicator of shelf life and sensory quality of Golden Delicious apples, offering real benefits to producers and consumers in the context of room-temperature storage. Some researchers have even modelled the indoor temperature of the containers, while others have analyzed the air quality in fruit storage facilities. [28], [29]. In this article, the temperature was kept constant, and the air quality was not analyzed. These insights are crucial for advancing the circular economy by reducing food waste and enhancing resource efficiency in the supply chain. Furthermore, these insights can encourage more sustainable farming methods, contributing to a more resilient food supply. Future studies could also investigate the impact of different storage strategies, such as modified atmosphere packaging, on the quality of Golden Delicious apples during storage.

Acknowledgement

The research was supported by the project ‘The feasibility of the circular economy during national defense activities’ of 2021 Thematic Excellence Programme of the National Research, Development and Innovation

Office under grant no.: TKP2021-NVA-22, led by the Centre for Circular Economy Analysis.
The study was supported by the Stipendium Hungaricum Program and the Doctoral School of Mechanical Engineering, The Hungarian University of Agriculture and Life Sciences, Gödöllő, Hungary.

References

[1] **Mardziah O., Mat Jafri M. Z., Abdul Aziz A., and Omar A.** (2015) Non-destructive quality evaluation of fruit by color based on RGB LEDs system, 2014 2nd International Conference on Electronic Design, ICED 2014, pp. 230–233, doi: 10.1109/ICED.2014.7015804.
[2] **Abasi S., Minaei S., Jamshidi B., Fathi D., and Khoshtaghaza M. H.** (2019) Rapid measurement of apple quality parameters using wavelet de-noising transform with Vis/NIR analysis, Scientia Horticulturae, vol. 252, pp. 7–13, doi: 10.1016/j.scienta.2019.02.085.
[3] **Pathmanaban P., Gnanavel B. K., and Anandan S. S.** (2019) Recent application of imaging techniques for fruit quality assessment, Trends in Food Science & Technology, vol. 94, pp. 32–42, doi: 10.1016/j.tifs.2019.10.004.
[4] **Caballero D. et al.** (2017) Prediction of pork quality parameters by applying fractals and data mining on MRI, Food Research International, vol. 99, pp. 739–747, doi: 10.1016/j.foodres.2017.06.048.
[5] **Yang S., Meng Z., Li Y., Chen R., Yang Y., and Zhao Z.** (2021) Evaluation of physiological characteristics, soluble sugars, organic acids and volatile compounds in 'Orin' apples (Malus domestica) at different ripening stages, Molecules, vol. 26, no. 4, p. 807, doi: 10.3390/molecules26040807.
[6] **Wani N. R. et al.** (2023) Predicting the optimum harvesting dates for different exotic apple varieties grown under North Western Himalayan regions through acoustic and machine vision techniques, Food Chemistry: X, vol. 19, p. 100754, doi: 10.1016/j.fochx.2023.100754.
[7] **Harker F. R., Marsh K. B., Young H., Murray S. H., Gunson F. A., and Walker S. B.** (2002) Sensory interpretation of instrumental measurements 2: sweet and acid taste of apple fruit, Post-harvest Biology and Technology, vol. 24, no. 3, pp. 241–250, doi: 10.1016/S0925-5214(01)00157-0.
[8] **Yang Y. et al.** (2017) Relationships between cuticular waxes and skin greasiness of apples during storage, Post-harvest Biology and Technology, vol. 131, pp. 55–67, doi: 10.1016/j.postharvbio.2017.05.006.
[9] [9] **Khodaei D., Hamidi-Esfahani Z., and Rahmati E.** (2021) Effect of edible coatings on the shelf-life of fresh strawberries: A comparative study using TOPSIS-Shannon entropy method, NFS Journal, vol. 23, pp. 17–23, doi: 10.1016/j.nfs.2021.02.003.
[10] **Sinha S. R. et al.** (2019) Post-harvest assessment of fruit quality and shelf life of two elite tomato varieties cultivated in Bangladesh, Bulletin of the National Research Centre, vol. 43, no. 1, p. 185, doi: 10.1186/s42269-019-0232-5.
[11] **Cárdenas-Pérez S. et al.** (2017) Evaluation of the ripening stages of apple (Golden Delicious) by means of computer vision system, Biosystems Engineering, vol. 159, pp. 46–58, doi: 10.1016/j.biosystemseng.2017.04.009.
[12] **Jha S. N., Rai D. R., and Shrama R.** (2012) Physico-chemical quality parameters and overall quality index of apple during storage, J Food Sci Technol, vol. 49, no. 5, pp. 594–600, doi: 10.1007/s13197-011-0415-z.
[13] **Bavisetty S. C. B., and Venkatachalam K.** (2021) Physicochemical qualities and antioxidant properties of juice extracted from ripe and overripe wax apple as affected by pasteurization and sonication, Journal of Food Processing and Preservation, vol. 45, no. 6, p. e15524, doi: 10.1111/jfpp.15524.
[14] **Bucher T., Malcolm J., Mukhopadhyay S. P., Vuong Q., and Beckett E.** (2023) Consumer acceptance of edible coatings on apples: The role of food technology neophobia and information about purpose, Food Quality and Preference, vol. 112, p. 105024, doi: 10.1016/j.foodqual.2023.105024.
[15] **Verde A., Míguez J. M., and Gallardo M.** (2023) Melatonin stimulates post-harvest ripening of apples by up-regulating gene expression of ethylene synthesis enzymes, Post-harvest Biology and Technology, vol. 195, p. 112133, doi: 10.1016/j.postharvbio.2022.112133.
[16] **Dar J. A., Wani A. A., Ahmed M., Nazir R., Zargar S. M., and Javaid K.** (2019) Peel colour in apple (Malus × domestica Borkh.): An economic quality parameter in fruit market, Scientia Horticulturae, vol. 244, pp. 50–60, doi: 10.1016/j.scienta.2018.09.029.

[17] **Sadat Razavi M. et al.** (2022) Impact of Bacterial Cellulose Nanocrystals-Gelatin/Cinnamon Essential Oil Emulsion Coatings on the Quality Attributes of 'Red Delicious' Apples, Coatings, vol. 12, no. 6, Art. no. 6, doi: 10.3390/coatings12060741.

[18] **Kassebi S., Farkas C., Székely L., Géczy A., and Korzenszky P.** (2022) Late Shelf Life Saturation of Golden Delicious Apple Parameters: TSS, Weight, and Colorimetry, Applied Sciences, vol. 13, no. 1, p. 159, doi: 10.3390/app13010159.

[19] **Łysiak G., Kurlus R., Zydlik Z., and Walkowiak-Tomczak D.** (2014) Apple skin colour changes during harvest as an indicator of maturity, Acta scientiarum Polonorum. Hortorum cultus = Ogrodnictwo, vol. 13, pp. 71–83.

[20] **Kingston C. M.** (2010) Maturity Indices for Apple and Pear, pp. 407–432, doi: 10.1002/9780470650509.ch10.

[21] **Arendse E., Fawole O. A., and Opara U. L.** (2014) Influence of storage temperature and duration on post-harvest physico-chemical and mechanical properties of pomegranate fruit and arils, CyTA - Journal of Food, Accessed: Dec. 13, 2022. [Online]. Available: https://www.tandfonline.com/doi/abs/10.1080/19476337.2014.900114.

[22] **Saletnik B., Zaguła G., Saletnik A., Bajcar M., Słysz E., and Puchalski C.** (2022) Method for Prolonging the Shelf Life of Apples after Storage, Applied Sciences, vol. 12, no. 8, Art. no. 8, doi: 10.3390/app12083975.

[23] **Ghazanfar M., Khan M., Khan C., and Bhatti R.** (2007) Post Harvest Losses in Apple and Banana During Transport and Storage, Pakistan Journal of Agricultural Sciences, vol. 44, pp. 534–539.

[24] **Tano K., Oulé M. K., Doyon G., Lencki R. W., and Arul J.** (2007) Comparative evaluation of the effect of storage temperature fluctuation on modified atmosphere packages of selected fruit and vegetables, Post-harvest Biology and Technology, vol. 46, no. 3, pp. 212–221, doi: 10.1016/j.postharvbio.2007.05.008.

[25] **uhnevica K., Seglina D., Krasnova I., Skudra G., Klava D., and Skudra L.** (2009) Evaluation of apple quality during storage in a controlled medium, Nr, vol. 3.

[26] **Kassebi S., and Korzenszky P.** (2021) The effect of post-harvest storage on the weight of Golden Delicious apples, Science Technology and Innovation, vol. 13, no.

[27] **Rutkowski K., Michalczuk B., and Konopacki P.** (2008) Non-destructive determination of 'Golden Delicious' apple quality and harvest maturity, Journal of Fruit and Ornamental Plant Research, vol. 16, pp. 39–52,

[28] **Patonai Z., Kicsiny R., Géczi G.** (2022) Multiple linear regression based model for the indoor temperature of mobile containers, HELIYON 8: 12 Paper: e12098

[29] **Patonai Z., Barczi A.** (2023) Monitoring air quality in fruit and vegetable storage facilities, Hungarian Agricultural Research: Environmental Management Land use Biodiversity 33 : 3-4 pp. 8-14. Paper: ISSN 1216-4526, 7 p.

HUNGARIAN AGRICULTURAL ENGINEERING
No 43/2024 26-36
Published online: http://hae-journals.org/
HU ISSN 0864-7410 (Print)
HU ISSN 2415-9751(Online)
DOI: 10.17676/HAE.2024.43.26
Received: 10.05.2024 - Accepted: 05.07.2024

PERIODICAL
OF THE COMMITTEE OF AGRICULTURAL AND BIOSYSTEM ENGINEERING OF THE HUNGARIAN ACADEMY OF SCIENCES
and
HUNGARIAN UNIVERSITY OF AGRICULTURE AND LIFE SCIENCES
INSTITUTE OF TECHNOLOGY

OPTIMAL MATERIAL FLOW CHANNELS OF CROSS FLOW DRYERS

Author(s):
I. Keppler[1], A. Bablena[1]

Affiliation:
[1] Institute of Technology – Hungarian University of Agriculture and Life Sciences, 2100 Gödöllő, Páter Károly u. 1., Hungary;

Email address:
keppler.istvan@uni-mate.hu; bablena.adrienn@uni-mate.hu

Abstract: Reducing the moisture content of harvested grains is crucial for their subsequent processing or storage. Given the substantial energy requirements and potential environmental consequences associated with artificial drying, it is imperative to optimize the efficiency of this process. The quality of the final product is significantly impacted by inadequate or excessive drying, which is heavily influenced by the duration of grain exposure to the drying environment. Advances in dynamic modeling, facilitated by enhanced computational capabilities, have empowered researchers to intricately examine particle movement phenomena within drying equipment. In our study, we investigate variations in particle residence times under diverse geometric and tribological boundary conditions.

Keywords: granular materials, discrete element method, cross flow dryers, particle flow unevenness

1. Introduction

Reducing the moisture content of harvested grains is an essential part of preparing them for further processing or storage. Ideally, this task can be accomplished through natural drying, utilizing direct solar energy. However, the quantity of grains required to meet the food and raw material demands of developed industrial countries cannot be dried naturally; artificial drying is necessary. Due to the high energy demands and potential environmental impact of artificial drying, we must strive to perform the drying process with the highest possible efficiency.

2. The drying efficiency problem

In agriculture, drying can account for 60-80% of direct energy consumption [1], [2]. Therefore, it is evident that increasing drying efficiency is a fundamental interest for all enterprises involved in drying. There are two main directions for enhancing efficiency: optimizing thermodynamic processes (for example, by reducing the specific amount of fossil fuels used) and exploiting the potential opportunities in influencing particle movement processes.

In our article, we examine the second possibility. The development of explicit dynamic modeling methods, particularly the significant increase in computational capacity, has enabled researchers to study the particle movement processes occurring in drying equipment in detail [3], [4].

The quality of the final product is significantly affected by under-drying or over-drying, which is greatly influenced by the time the grain spends in the dryer [5]. The duration spent in the dryer depends on the velocity conditions of particle movement, which can be excellently analyzed using the discrete element method (DEM) [6].

To improve the efficiency of the drying process, we intend to investigate the following questions:

1. What dimensionless characteristic can be used to describe the uniformity of material flow within the dryer?

2. How do the tribological characteristics of interactions between particles and the wall affect the uniformity of material flow within the dryer?

3. How do the tribological characteristics of interactions between particles affect the uniformity of material flow within the dryer?
4. Is there a lamella geometry (different from straight) that can further improve the uniformity of material flow and thus enhance drying efficiency?

Theoretical considerations, experimental investigations and numerical simulations were conducted to achieve these objectives.

3. The Brachistochrone problem

The movement of grain in a dryer can be related to the solution of an ancient mathematical problem. The question of the downward motion of a particle sheds light on a classic problem in mechanics: the brachistochrone (shortest time) problem. This was first formulated by Johann Bernoulli [7], with the first solutions independently published by Newton and Leibniz [8], [9].

Bernoulli's question was as follows: What is the shape of the frictionless path along which a point mass will travel between two points, A and B, that are vertically aligned but not on the same vertical line, in the shortest possible time? (Figure 1.) This problem is one of the classic problems in the calculus of variations. The mathematical formulation of the problem is as follows [10]

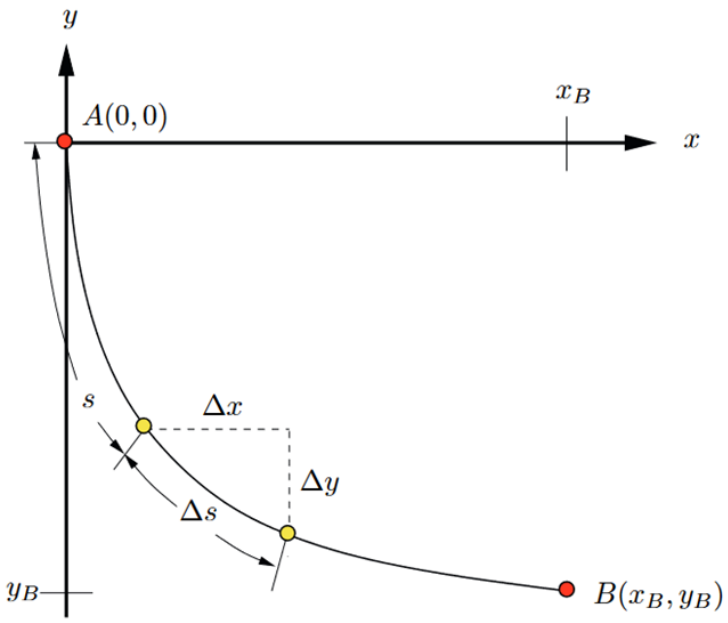

Figure 1. The Brachistochrone problem [11]

Time needed to move from *A* to *B*:

$$\int_A^B \frac{ds}{v} = \int_A^B \frac{ds}{\sqrt{2gy}}$$

Distance between points *A* and *B* is: $ds = \sqrt{x'(y)^2 + 1}dy$, so

$$t_{AB} = \frac{1}{\sqrt{2g}} \int_0^{y_B} \frac{\sqrt{x'(y)^2 + 1}}{\sqrt{y}} dy.$$

In this case, we seek the equation for the function $x(y)$ that minimizes the integral. To determine this, we write the Euler-Lagrange equation for the problem:

$$\frac{\partial f}{\partial x} = \frac{d}{dy}\frac{\partial f}{\partial x'}$$

where $f(x, x', y) = \frac{\sqrt{x'^2+1}}{\sqrt{y}}$. The solution of this differential equation is a cycloid:

$$x = a(\theta - \sin\theta)$$

$$y = a(1 - \cos\theta),$$

where parameter *a* is chosen according to the geometrical boundary conditions.

When considering friction, an analytical solution still exists, although it is significantly more complex. Numerous researchers have addressed this topic [12], [13], [14], [15], and the resulting curves differ only negligibly from the cycloid-shaped curve obtained in the frictionless case in practical applications [16]:

$$x(\theta) = \frac{C}{2}\left(\theta - \sin\theta + \mu\,(1 - \cos\theta)\right)$$

$$y(\theta) = \frac{C}{2}\left(1 - \cos\theta + \mu\,(\theta + \sin\theta)\right) + y_0,$$

where C and y_0 are chosen according to the geometrical boundary conditions.

Naturally, the motion of an entire granular assembly within a drying apparatus is a far more complex problem, as it requires considering interactions between the grains as well as between the grains and the walls. Therefore, we cannot expect an analytical solution to the proposed problem; instead, a numerical solution is necessary. The occasional interruption of material flow continuity precludes the use of finite element-based numerical methods, leading us to opt for the discrete element method.

4. Experimental investigations

Cross-flow drying equipment typically operates in a batch mode. During drying, the grain moves downward in a vertical direction, with deflector vanes ensuring that an adequate amount of air enters the equipment and that the grains remain in the dryer for the appropriate amount of time. We conducted particle movement experiments on both a large-scale industrial dryer and a model dryer. The obtained velocity values are shown on Figure 2.

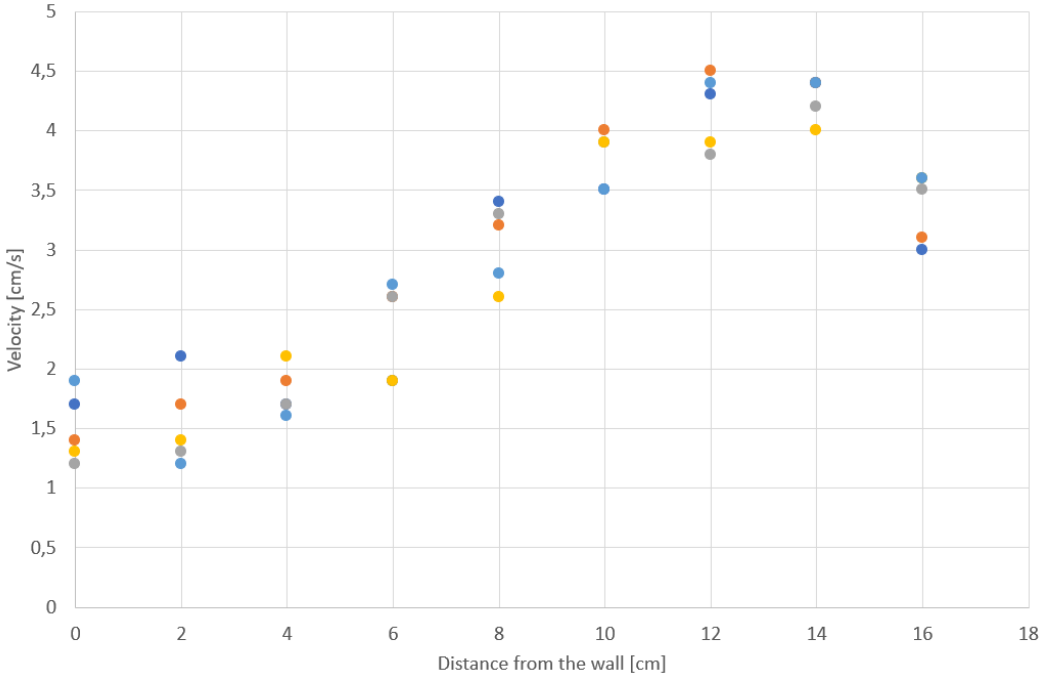

Figure 2. Velocity values measured around the lamella in the drying equipment

Figure 2. clearly shows that the presence of the lamellae significantly affects the flow velocity of the particles. A characteristic number that can describe the unevenness of the flow could be the

$$\vartheta = \frac{v_{\max} - v_{\min}}{v_{\max}}$$

quantity (velocity coefficient), which has a value of 0 for perfectly uniform flow, and approaches 1 as the unevenness increases. Based on the current measurement results, the average velocities corresponding to each distance value yield 0.65.

Particle movement studies were conducted both on the standalone drying module and inside the operational industrial drying equipment. Comparing the particle movement characteristics (velocity coefficients) between the standalone drying module and the operational industrial drying equipment, no significant differences in velocity coefficient values were observed.

Since measurements on the large dryer indicated that the vanes significantly influence the unevenness of particle flow, it was necessary to examine the effect of the vanes' inclination angle on velocity conditions. To facilitate this task, a model drying apparatus was constructed, consisting of two columns from the original drying module. The structure of the model dryer is depicted in Figure 3.

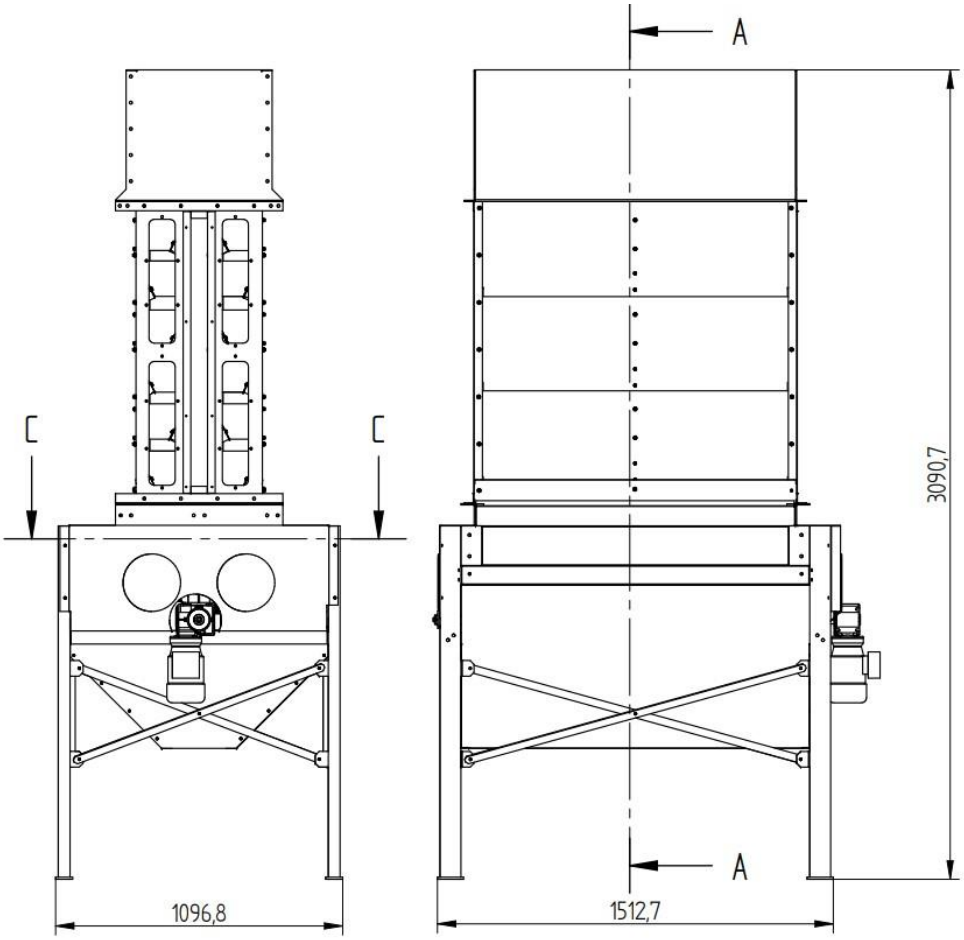

Figure 3. The model dryer apparatus

The flow velocity is primarily determined by the opening time of the discharge system. The rotational speed of the discharge unit in the model dryer was adjusted to generate velocity values that closely match those of the industrial dryer. We used painted layers to evaluate the particle displacements (Figure 4.).

Figure 4. Painted layers to analyze the particle displacement

As shown in Figure 5., good agreement in velocity ratios between the model dryer and the industrial drying equipment can be achieved by appropriately adjusting the opening time of the discharge unit.

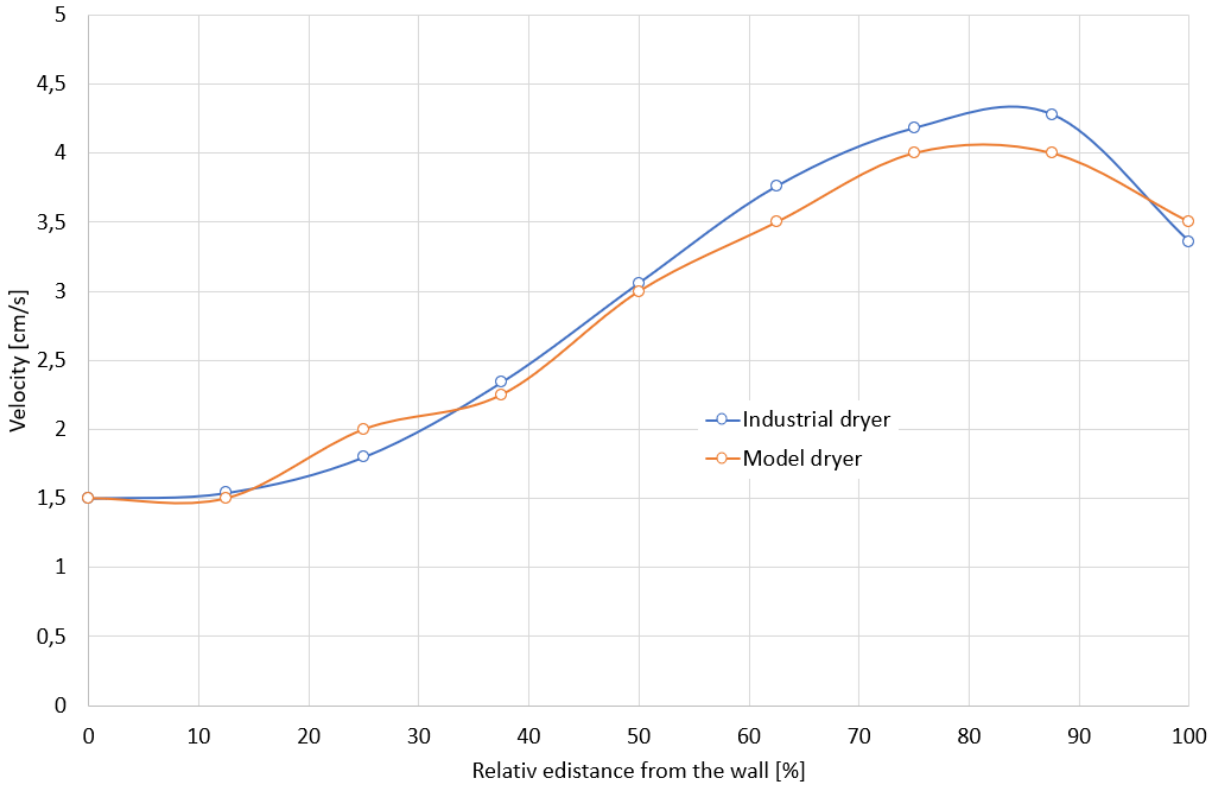

Figure 5. Comparison of the material flow conditions between the industrial and model dryers

5. The discrete element model

The discrete element method was developed by Cundall and Strack in the 1970s. When applying this method, the system solves the equations of motion for each individual particle in the assembly, taking into account the interactions between particles as well as between the particles and the bounding walls. To ensure adequate accuracy, calculations must be performed with very small time steps, making the method extremely computationally intensive for assemblies containing large quantities of particles [17].

To investigate the particle movements within the drying apparatus, we used the academic version of the EDEM 2.7 discrete element software. During the simulations, we consistently employed the "Hertz-Mindlin with no slip" contact model for calculating the contact forces between particles. The specified material characteristics and contact properties significantly influence the magnitudes of the normal and tangential force components. When using the mentioned contact model, the normal and tangential components of the forces can be calculated as follows:

$$F_n = \frac{4}{3}E_0\delta^{\frac{3}{2}}\sqrt{R_0} - 2\sqrt{\frac{5}{6}}\frac{\ln C_r}{\sqrt{\ln^2 C_r + \pi^2}}\sqrt{2E_0}\sqrt[4]{R_0\delta}\sqrt{m_0}v_{\mathrm{nrel}},$$

$$F_t = -8G_0\sqrt{R_0\delta}\delta_t - 2\sqrt{\frac{5}{6}}\frac{\ln C_r}{\sqrt{\ln^2 C_r + \pi^2}}\sqrt{2G_0}\sqrt[4]{R_0\delta}\sqrt{m_0}v_{\mathrm{trel}},$$

where $\frac{1}{E_0} = \frac{1-\nu_1^2}{E_1} + \frac{1-\nu_2^2}{E_2}$ gives us the reduced elastic modulus E_0. The normal overlap δ plays a significant role in the calculation of contact forces and can be determined as follows: consider two particles labeled *i* and *j*, with centers at positions x_i and x_j, and radii $R_i$and R_j. Then, $\delta = R_i + R_j - (x_j - x_i)$. The reduced radius in can be calculated as $R_0 = \frac{R_1R_2}{R_1+R_2}$, and the reduced mass is similarly calculated as $\mathrm{m}_0 = \frac{\mathrm{m}_1\mathrm{m}_2}{\mathrm{m}_1+\mathrm{m}_2}$. Finally, v_{nrel} represents the normal component of the relative velocity between the particles. $\frac{1}{G_0} = \frac{2-\nu_1}{G_1} + \frac{2-\nu_2}{G_2}$ and δ_t is the tangential deformation.

The normal F_n and tangential F_t force components between particles are related by Coulomb's law, such that $F_t = \mu_s F_n$, where μ_s is the coefficient of static friction. This relationship ensures that the tangential component cannot exceed the normal component.

In addition to the forces acting on the particles, the torque arising from these components can also be defined. The rolling torque M_r is given by $M_r = -\mu_r F_N R_i \omega_i$, where R_i denotes the distance between the centroid of particle *i* and the contact point, ω_i is the unit vector in the direction of the angular velocity vector, indicating the rotation direction of particle *i*, and μ_r is the coefficient of rolling friction. Similarly, the torque M_t due to the tangential force component F_t can be determined as $M_t = F_t R_i$.

During the simulations, the motion of each particle can be determined using the principles of linear and angular momentum. This defines a system of differential equations that can be solved numerically using many small time steps. The choice of the time step has a significant impact on the results and their accuracy. In my simulations, I used 25% of the Rayleigh time step (T_R) for the time increment (δt), that is:

$$\delta t = 0{,}25T_R = 0{,}25 \cdot (0.1631\nu + 0{,}8766)^{-1}\pi R\left(\frac{\rho_p}{G_p}\right)^{\frac{1}{2}}.$$

We have created the geometric model of the discharge opening and bottom lamellae (both straight and cycloidal case) of the drying apparatus (Figure 6.) for performing discrete element numerical simulations. The details of the model, boundary conditions, determination of micromechanical properties, and their values can be found in reference [18].

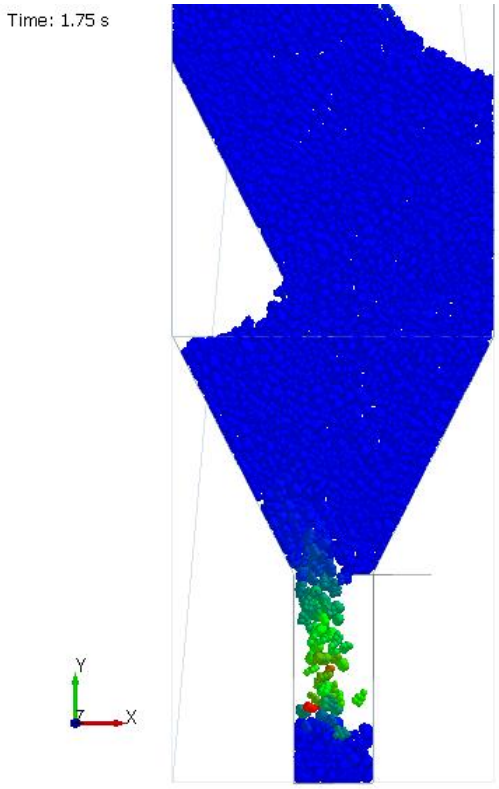

Figure 6. Discrete element model of the drying apparatus

Instead of studying velocity unevenness, in DEM investigations, we shifted our focus to examining the unevenness of the displacement field (Figure 7.):

$$\xi = \frac{y_{max} - y_{min}}{y_{max}}.$$

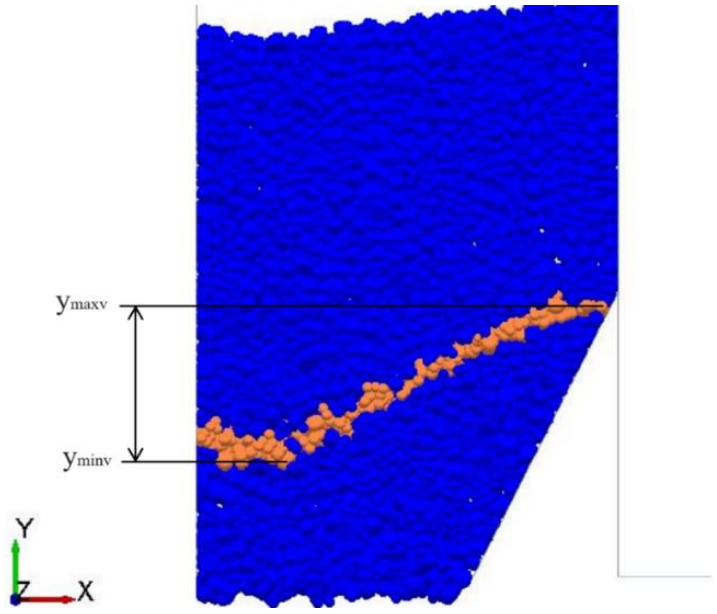

Figure 7. Determining flow unevenness from the displacement of particles

Based on analytical considerations in our earlier work, we demonstrated that cycloid-shaped vanes cause less flow unevenness.

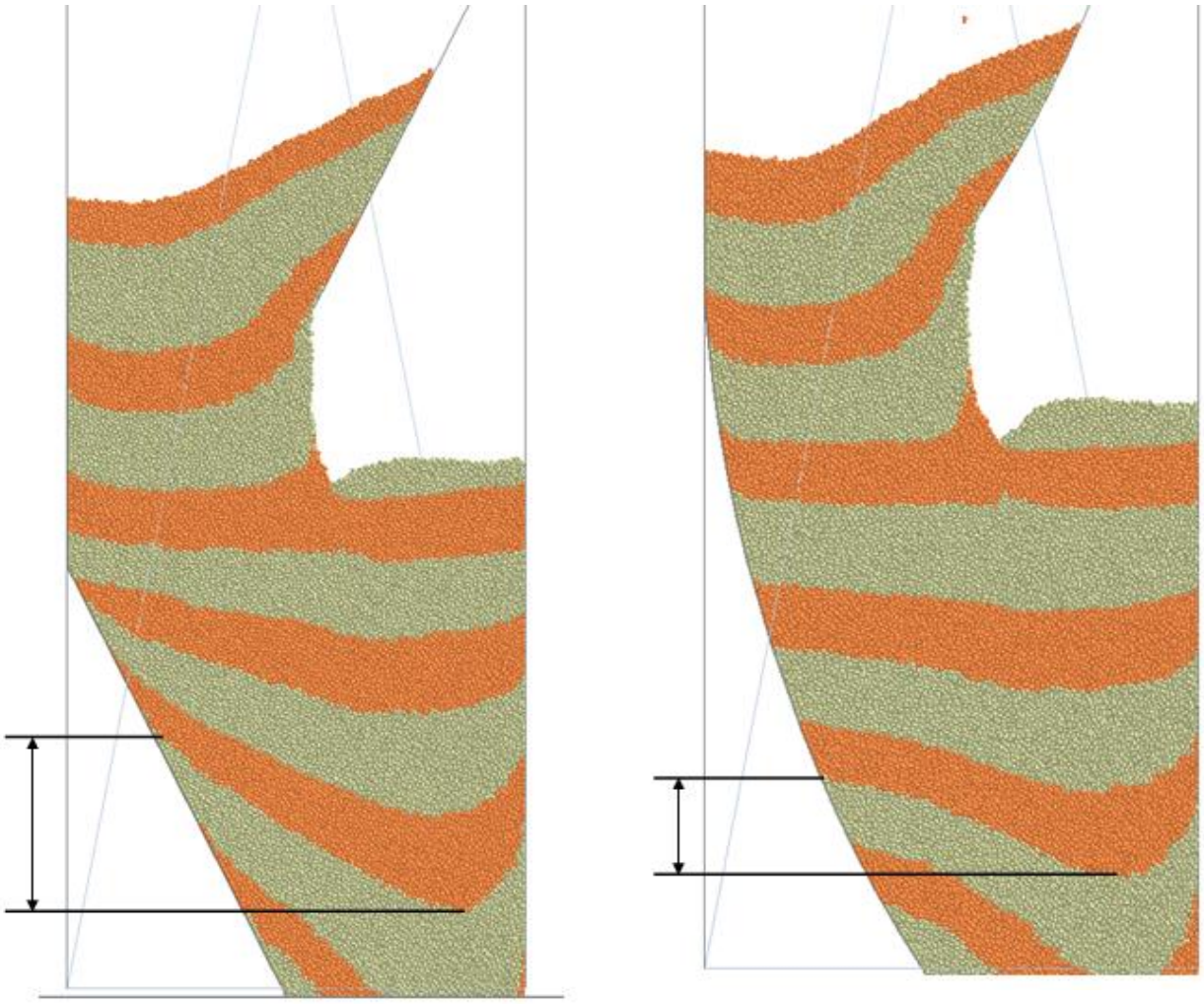

a., straight lamella *b.*, cycloidal lamella

Figure 8. Flow unevenness of different lamella geometries

Figure 8. shows a comparison of the uniformity of material flow. We can see the distortion of the originally horizontal striping after the same amount of time for both straight and cycloidal lamella cases. It can be observed that in the case of cycloidal lamella, this unevenness is much smaller. We also examined the value of flow unevenness for different particle-particle friction and wall friction values.

6. Results

To analyze the difference between the two types of lamella geometry, we introduced the flow unevenness difference as

$$\Delta = \frac{\xi_{straight} - \xi_{cycloidal}}{\xi_{straight}}.$$

As we can see on the following figures (Figure 9. and Figure 10.), the cycloidal lamella gives better results for all practically possible particle - wall and particle – particle friction values.

This result remarkably demonstrates that results developed through classical mechanical methods for the motion of a single particle remain applicable to some extent even when dealing with interactions among a large number of particles.

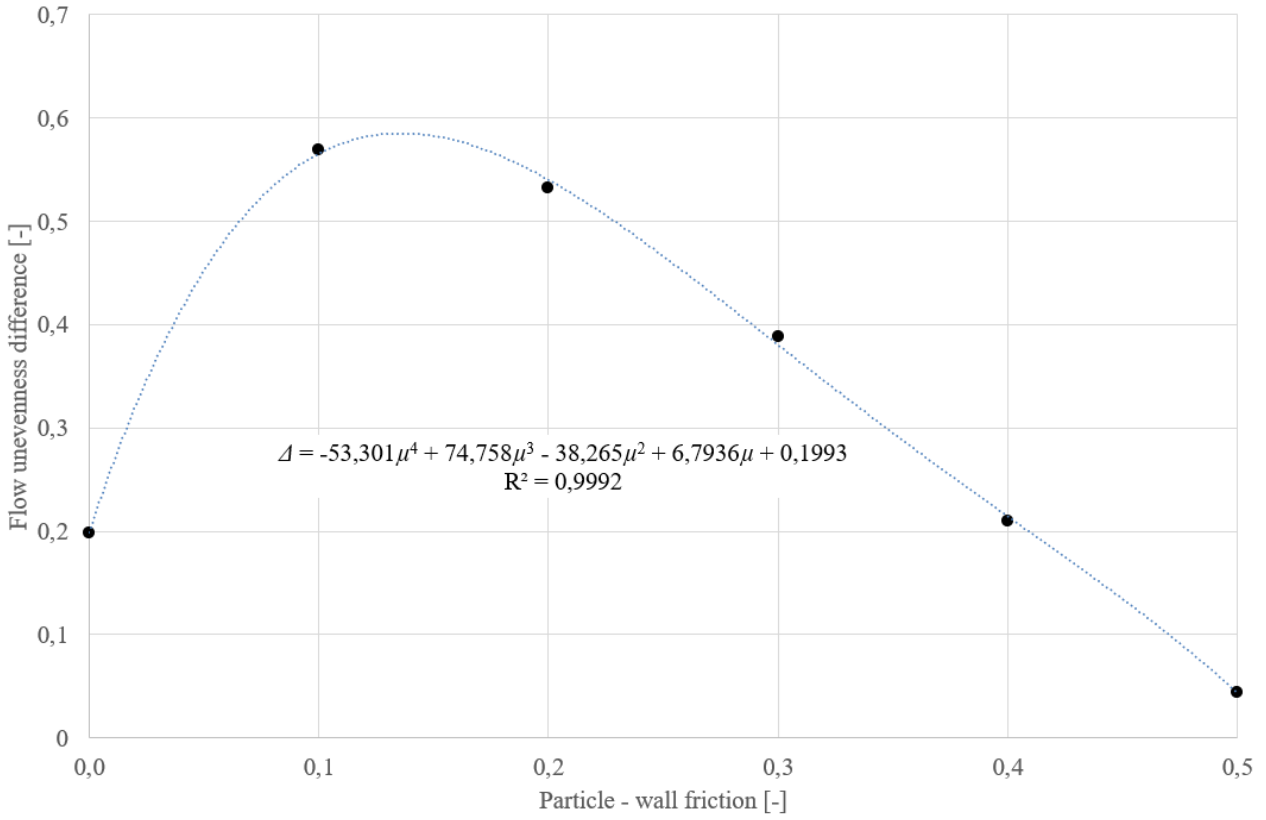

Figure 9. Flow unevenness difference as a function of particle – wall friction

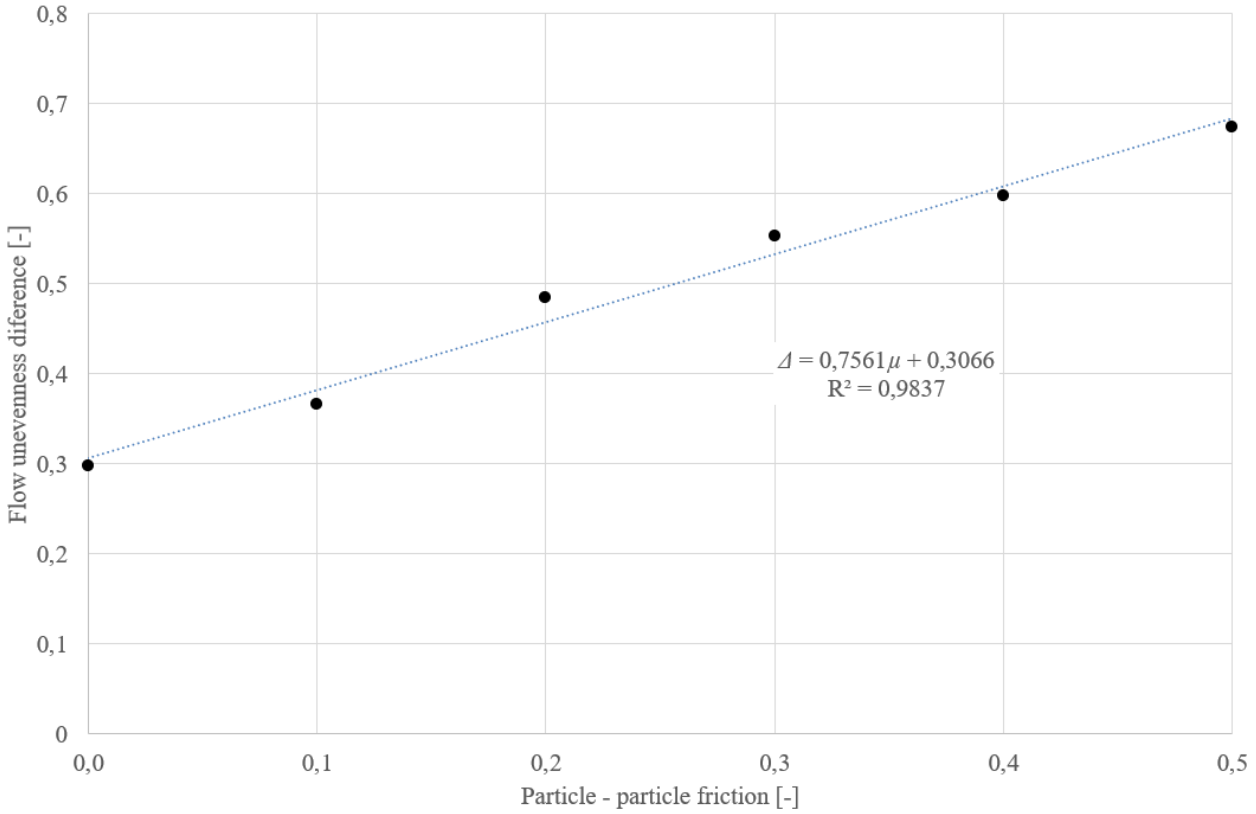

Figure 10. Flow unevenness difference as a function of particle – particle friction

From the above diagrams, we can see that the cycloidal-shaped lamella design ensures less flow velocity unevenness in all cases. Its effect on improving the flow pattern is particularly pronounced in cases of high internal friction (contamination).

7. Conclusions

To characterize the unevenness of material flow (by examining the movement of a designated strip in the material mass), we introduced the unevenness factor ξ. Using experimental investigations and numerical simulations, we demonstrated that the value of wall friction has a significant impact on the unevenness of material flow. Using experimental investigations and numerical simulations, we also demonstrated that the value of friction between particles has a significant impact on the unevenness of material flow. Using experimental investigations and numerical simulations, we showed that it is advisable to use cycloidal-shaped lamella in drying equipment. The cycloidal lamella resulted in a better unevenness factor for all particle-wall and particle-particle friction coefficient values we examined. To analyze the difference between the two types of lamella geometry, we introduced the flow unevenness difference. Its use enabled the quantitative determination of the results.

We found, that the flow unevenness difference as a function of particle-wall friction can be approximated with the polynomial equation

$$\Delta = -53.301\mu^4 + 74.758\mu^3 - 38.265\mu^2 + 6.7396\mu + 0{,}1993$$

within the interwall of particle – wall friction from 0 to 0.5. As the function of particle – particle friction we got a much simpler linear correlation:

$$\Delta = 0.7561\mu + 0{,}3066$$

within the interwall of particle – particle friction from 0 to 0.5.

Even though these two results provide an empirical formulation of the relationship between friction coefficients and the unevenness of material flow, they are surprisingly accurate in predicting the phenomenon. They can provide valuable insights into improving the understanding of the operational processes of drying equipment.

Acknowledgement

The authors appreciate the support of projects GINOP-2.1.2-8-1-4-16-2017-00285, GINOP-2.1.2-8.1.4-16-2017-00187 and GINOP-2.1.2-8-1-4-16-2017-00188.

References

[1] **Beke J.** (1997): Terményszárítás, Agroinform, Budapest, 419 p.
[2] **Baker, C.G.J.** (1997): Industrial Drying of Foods, Springer US, 978-0-7514-0384-8
[3] **Mellman, J., Teodorov, T.** (2011): Solids transport in mixed-flow dryers. Powder Technology, 205, 117-125. p.
[4] **Keppler, I., Kocsis, L., Oldal, I., Farkas, I., Csatár, A.** (2012): Grain velocity distribution in a mixed flow dryer. Advanced Powder Technology, 23, 824-832. p.
[5] **Mellman, J., Iroba, K.L., Meztger, T., Tsotas, E., Mészáros, Cs., Farkas, I.** (2011): Moisture content and residence time distributions in mixed-flow grain dryers. Biosystems Engineering, 109, 297-307. p.
[6] **Cundall, P.A. and Strack, O.D.L.** (1979) A discrete numerical model for granular assemblies. Geotechnique, 29(1), 47-65.
[7] **Bernoulli, J.** (1696): Problema novum ad cujus solutionem Mathematici invitatur. Acta Eruditorum, 18, 269 p.
[8] **Newton**, **I.** (1697): Philosophical Transactions of the Royal Society of London, 19, 424-425 p.
[9] **Leibnitz, G.W.** (1697): Acta Eruditorum, 19, 201-205 p.
[10] **Taylor, J.R.** (2005): Classical Mechanics. University Science Books, Colorado, 786 p.
[11] **Pesch H. J.** (2012): The Princess and Infinite-Dimensional Optimization Documenta Mathematica Extra Volume ISMP 345–356 p.

[12] **Wensrich, C.M.:** Evolutionary solutions to the brachistochrone problem with Coulomb friction. Mechanics Research Communications, 31, 151-159 p.
[13] **Hayen, J.C.** (2005): Brachistochrone with Coulomb friction. International Journal of Non-Linear Mechanics, 40, 1057-1075 p.
[14] **Čović, V., Vesković, M.** (2008): Brachistochrone on a surface with Coulomb friction. International Journal of Non-Linear Mechanics, 40, 437-450 P.
[15] **Sumbatov, A.S.** (2017): Brachistochrone with Coulomb friction as the solution of an isoperimetrical variational problem. International Journal of Non-Linear Mechanics, 88, 135-141 p.
[16] **Barsuk, A.A., Paladi, F.** (2023): On parametric representation of brachistochrone problem with Coulomb friction. International Journal of Non-Linear Mechanics, 148, 104265
[17] **Bagi, K.** (2007): A diszkrét elemek módszere, BME Tartószerkezetek Mechanikája Tanszék, Budapest, 73 p.
[18] **Keppler, I., Bablena, A**. (2024): Optimal lamella geometry for mixed flow dryers. Arch Appl Mech 94, 961–972.

HUNGARIAN AGRICULTURAL ENGINEERING
No 43/2024 37-52
Published online: http://hae-journals.org/
HU ISSN 0864-7410 (Print)
HU ISSN 2415-9751(Online)
DOI: 10.17676/HAE.2024.43.37
Received: 20.05.2024 - Accepted: 05.08.2024

PERIODICAL
OF THE COMMITTEE OF AGRICULTURAL AND BIOSYSTEM ENGINEERING OF THE HUNGARIAN ACADEMY OF SCIENCES
and
HUNGARIAN UNIVERSITY OF AGRICULTURE AND LIFE SCIENCES INSTITUTE OF TECHNOLOGY

HUNGARIAN UNIVERSITY OF AGRICULTURE AND LIFE SCIENCES
Institute of Technology

OVERVIEW OF THE UTILIZATION AND DISPOSAL OF WASTE FROM MARITIME SHIPPING AND EXAMINATION OF POSSIBLE SOLUTIONS

Author(s):
A. Kári-Horváth[1], Zs. Lantos[2], Á. Sztancsek[2]

Affiliation:
[1] Institute of Technology - Hungarian University of Agriculture and Life Sciences, 2100 Gödöllő, Páter Károly u. 1., Hungary;
[2] Gyémánt-Pirazol Kft. 4031 Debrecen, Nívó utca 11. Hungary;

Email address:
kari-horvath.attila@uni-mate.hu; zsolt.lantos@gyemantpirazol.hu; akos.sztancsek@gyemantpirazol.hu

Abstract: Towards the middle of the XXI. century, environmental protection is becoming more and more of a focus in the world. According to not only environmentalists but also many politicians, economists, and even historians, the biggest threat to the world is environmental pollution and climate change caused by global warming. Accordingly, the development of environmentally friendly technologies, which does not only apply to the automotive industry, is also in full swing in the transport industry. Much attention is paid to reducing the environmental burden of shipping as well. This is all the more justified since nowadays, the most common ship fuel, the so-called heavy oil, contains 3500 times more sulfur than conventional diesel fuel. Accordingly, there are now floating hotels operating around the world that use LNG as a green fuel. In this article, we try to collect the literature strongly related to the topic in order to develop detailed technology in our further work.

Keywords: shipboard waste, waste utilization, MARPOL convention, Rankine-Clausius cycle, heat treatment technologies

1. Introduction

1.1. Concepts of waste and its utilization

Defining waste involves many difficulties. On the one hand, waste is a set of substances that are created during many human activities, so their physical and chemical properties can be different. And on the other hand, waste management is one of the youngest areas of environmental protection, so its legal background is constantly changing [1]. The nature of waste is not directly an environmental concept but rather an economic and legal formulation [2]. As a result, in practice, there are definitions that need to be explained or supplemented. Certain terms are not clear, so their redefinition is inevitable in future legislation. In addition, several definitions are known in international practice that accurately interpret each type of waste, so their introduction in Hungary is becoming more and more urgent. This subsection provides a brief overview of the world and interpretation of the basic concepts of waste management.

We use several definitions to define waste. In a more general sense, "waste is a substance, product, residue, object, isolated pollutant, contaminated area, which cannot be used or sold directly by their owner, and which must be treated separately" [1].

According to this formulation, waste is a completely unnecessary set of materials for the owner which cannot be utilized. Since most waste contains recoverable components, it is justified to modify this definition. The official concept of waste is much simpler than this. CLXXXV of 2012 on waste. (Section 2, paragraph (1), point 23) waste is defined as "any substance or object that the owner throws away, intends to throw away or must throw away". This wording is very simplistic, but it also includes materials and objects that are not considered waste under any circumstances. In international practice, components suitable for energy production are called RDF (Refuse-Derived Fuel) or SRF (Solid Recovered Fuels), i.e. waste-derived fuel or

alternative fuel [3], [4], [5].

1.2. Integrated waste management pyramid

The waste pyramid establishes a hierarchical ranking in terms of waste management (Figure 1.).

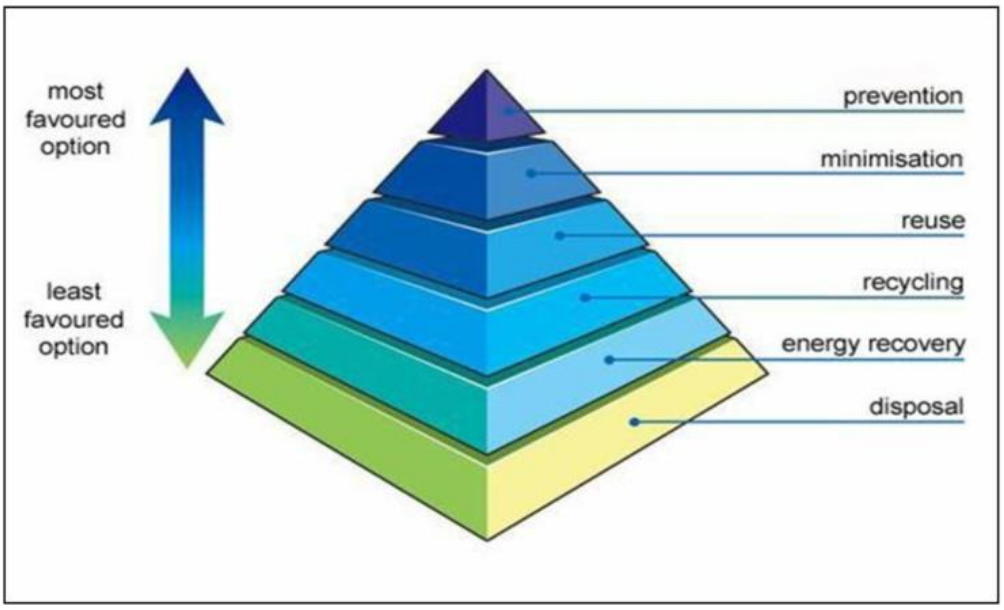

Figure 1. Integrated waste management pyramid

From an environmental protection point of view, prevention is the most important thing because if no waste is generated, then we don't have to think about further treatment. Nowadays, it is difficult to imagine a production or consumption process that produces or uses products without generating waste. Consequently, the principle of minimization should be applied, which aims to formulate the maximum possible recycling of waste and by-products generated during the production process [3]. During production, auxiliary streams are used to maximize the incorporation of raw materials into the final product, thereby ensuring that waste generation is minimized.

2. Materials and methods

2.1. The MARPOL convention

The purpose of the MARPOL 1973/1978 Convention (International Convention for the Prevention of Pollution from Ships) is to protect the marine environment and prevent pollution caused by ships at sea. The convention, which is mandatory for all seagoing vessels over 500 GT participating in international trade, covers the management of the following potential hazards and sources of pollution:

Annex I: Regulations for the prevention of oil spills
Annex II: Provisions for the prevention of contamination caused by bulk liquid toxic substances
Annex III: Regulations for the prevention of pollution caused by packaged hazardous materials transported by sea
Annex IV: Regulations for the prevention of pollution caused by wastewater generated on ships
Annex V: Regulations for the prevention of pollution caused by household and other waste on ships
Annex VI: Air pollution caused by ships

Especially highlighting Annex IV., as it is the most important in relation to our work.
Wastewater:

a) drainage and other waste from any type of toilet, urinal and toilet sink;
b) drainage from the medical rooms (pharmacy, patient bay, etc.) on the wash basins in such rooms,
c) removal from places containing live animals;
d) other wastewater if it is mixed with the above drains.

2.2. Energetic utilization of waste

Utilization for energetic purposes in the narrower sense means the production of electricity and heat; in addition, it is advisable to list the production of mechanical energy as a viable energy type because biofuels are increasingly important in addition to power plant energy consumption. Thermal waste management technologies are used to utilize waste for energy purposes. In international practice, the term energy from waste (WtE) is widespread and includes all processes that enable the recovery of the amount of energy in waste in the form of useful heat and/or electricity [6], [7].

Depending on their composition, we use different types and temperatures of waste treatment (Figure 2.). Processes that also take place at normal atmospheric temperatures are classified as traditional technologies. The most well-known traditional technology is fermentation, which results in the biological degradation of devices. The final product in the form of gas is biogas, which can be used to replace natural gas. Many technologies can be used to separate carbon dioxide from biogas and other energy-neutral gases; after removing these gases, we get so-called biomethane of the same quality as natural gas. Biomethane can be introduced into the natural gas network if it complies with MSZ 1648:2000.

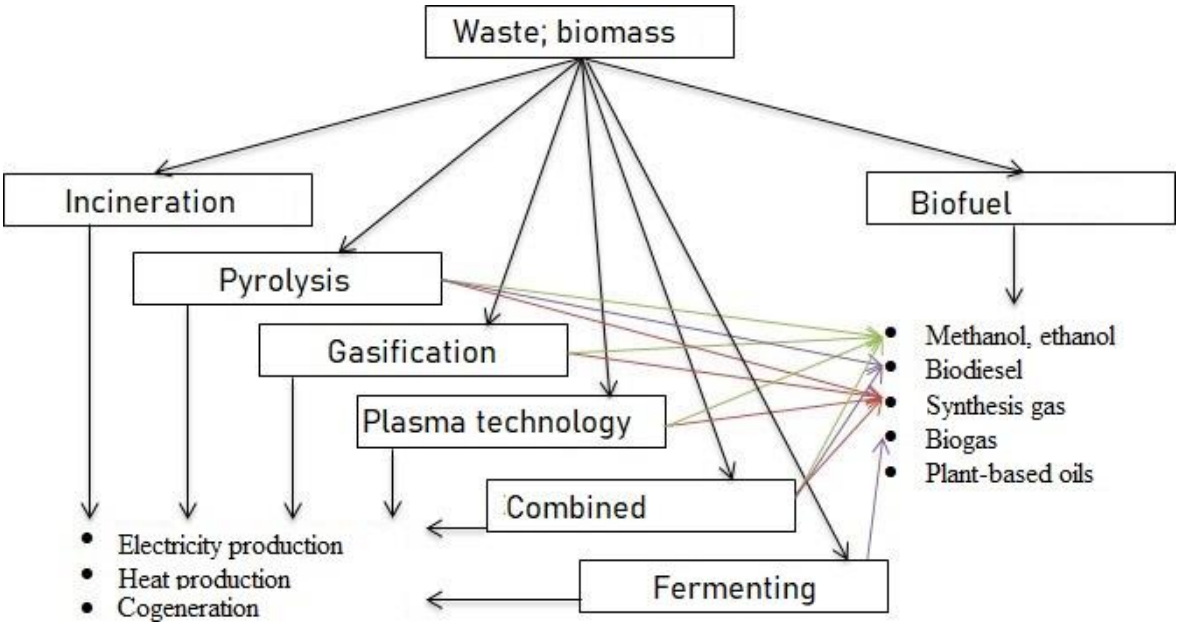

Figure 2. Possibilities of using waste for energy purposes

Thermal technologies can be divided into two main groups. The first group is represented by basic technologies. The most well-known technology is traditional incineration, where the calorific value of the waste is extracted simply by incineration and used in the form of heat and/or electricity. During combustion, non-combustible flue gas and ash are formed in the solid phase, and their release into the environment leads to the deterioration of air quality.

New technologies such as pyrolysis, gasification and plasma technology, as well as their combinations, make it possible to produce a gaseous energy carrier (wood gas) from solid biomass. In addition to the gas phase, pyrolysis still produces combustible carbon dioxide-rich pyrocoke and pyrrole oil, which can be used for power generation or further gasification in coal and oil power plants. During gasification, the solid final product is the slag and ash produced during combustion. Among the new thermal technologies, plasma technology should be prioritized because the solid phase here is vitreous slag (glass slag), a product that is completely indifferent to the environment, particularly suitable for construction use. Keeping all of this in mind, plasma technology achieves the complete disposal of waste while recovering energy, but it requires electricity for its operation, which reduces the energy efficiency of the technology [8], [9].

In addition to traditional incineration, alternative technologies produce useful products that can be used with favourable efficiency in the energy, chemical and construction industries, among others. Nevertheless, more than 95% of thermal waste treatment plants today use traditional incineration technology [8]. The

biggest electrical disadvantage of this technology is the low electrical efficiency. During the implementation of the Rankine-Clausius cycle (Figure 3.), the available net electrical efficiency is usually between 19 - 27% [10].

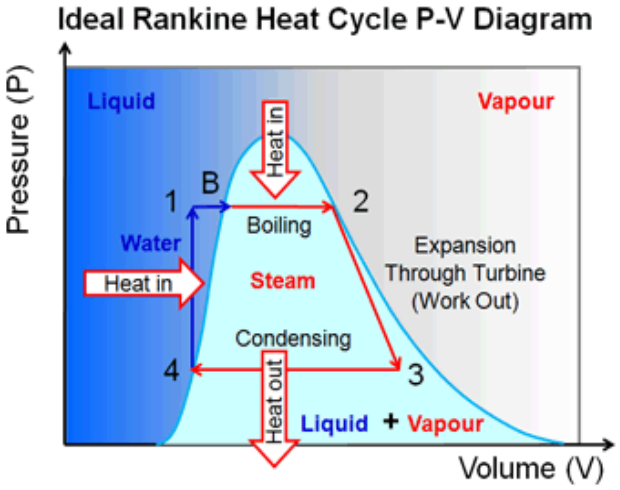

Figure 3. Rankine-Clausius cycle

On the other hand, new thermal technologies represent the first step in converting waste into high-energy synthesis gas, which can operate in a diesel cycle, gas engine or gas turbine with a net electrical efficiency of up to 35% [11], [12]. With this solution, the specific electricity production can even be doubled,

2.3. Composition of shipboard waste

EMSA assists the European Commission in the work of the possible revision of Directive 2000/59/EC [13] on port reception facilities for ship-generated waste and cargo residues, also known as the PRF Directive. One issue raised is the amount and management of ship-generated waste (SGW) on board ships. The relevant literature is out of date and does not reflect new developments in waste treatment and management. Better information on the volume of waste generated during voyages, waste management practices on board ships, and waste discharged at ports would help regulators, ports and waste managers plan for waste reception and transport.

2.3.1. Oily bilge water

A bilge is a mixture of liquids that collect in the bilge of a ship. It comprises a mixture of fresh water, seawater, oil, mud, chemicals and various other fluids that lead to the water house. Seawater and freshwater can enter the deck water well from the engine room or engine room due to deck drains, piping leaks, and pump and valve gland leaks.

Bilge water is produced by condensation, seepage and cleaning. As a general rule, bilge water contains oil from the engine room; hence the term "oily bilge". Fluid entering the bilge system, including bilge wells, bilge lines, tank top or bilge holding tanks, is classified as oily bilge water [14], [15], [16], [17], [18]. All boats have oily bilges, although recreational boats have a minimal amount.

Although there are many technologies for separating water and oil, such as absorption/adsorption, biological treatment, coagulation/flocculation, flotation and membranes, the most commonly used technology for ship inspections is oil-water density differences is based on. This type of treatment can reduce the amount of bilge water by 65-85%.

MARPOL mandated that all ships over 400 gross tons (GT) must be fitted with equipment to limit the release of oil into the oceans to 15 ppm when a ship is underway. They must also have an oil content monitor (OCM) and a bottom alarm to determine if the treated bottom water meets the emission requirements.

2.3.2. Oily residue (sludge)

Oil residue (sludge) is waste from the cleaning of fuel or lubricating oil, or oil collected in oil water

separators, oil filter equipment or drip trays, and waste from hydraulic and lubricating oils [19].
Sludge is usually collected in a sludge tank, waste fuel tank, waste oil tank, or lube oil or fuel oil drain tank. It can then be transferred directly from the tank to a port receiving facility.

The amount of sludge from lubricating oil depends on the type of lubricating oil and the consumption of lubricating oil. It is usually several orders of magnitude less than the oil residues in the fuel. Thanks to the automatic lubrication system, usage can be reduced by 70% [20], [21].

Oil sludge is the residual waste from fuel consumption. Treatment of oily sludge can be achieved by evaporation and/or incineration. Most of the sludge is stored and disposed on PRF without treatment.

The generation of oily sludge water depends on many factors, including the type and amount of fuel. Ships produce 0.01 - 0.03 m^3 of sludge. Evaporation can reduce the amount of sludge by up to 75% while burning the remaining sludge by 99% or more.

2.3.3. Oil tank washing

Cargo tanks in oil tankers must be cleaned before new cargo incompatible with the previous cargo is loaded or before dry docking. Tank cleaning can be done by spraying with crude oil (crude oil wash or COW), seawater or fresh water and cleaning agents. The former does not produce waste because the remains are converted into useful cargo.

Regulation 34 of MARPOL Annex 1 allows controlled unloading if the ship is en route, not in a special area and more than 50 nautical miles from the coast. The water fraction has a maximum volume of 30 litres per nautical mile. If the vessel has an Oil Discharge Monitoring and Control System (ODMCS) and a slop tank, no additional requirements are required for discharges at sea. [22], [23], [24], [25]. Unlike the discharge of bottom water to the sea, no ppm limits are required for the disposal of sedimented slopes, and therefore, oil water separators are not usually used. The total amount of oil discharged into the sea shall not exceed 1/30,000 of the total amount of the cargo, the remainder of which is intended for tankers built/delivered after 31 January 1979.

2.3.4. Sewage

Sewage is any form of drainage and other waste from toilets and urinals; water drainage from medical rooms (office, patient room, etc.) through the sinks, bathtubs and drains located in such rooms; drainage from spaces containing live animals; or other wastewaters, if mixed with the channels defined above [26], [27]. This is commonly referred to as "black water". It does not include greywater, which is the drain from dishwashers, showers, laundry, bathtubs and sinks [28].

MARPOL IV prohibits the discharge of sewage into the sea unless the ship has an approved sewage treatment plant or the ship discharges the shredded and disinfected sewage more than three nautical miles offshore using an approved system nearest land. Unshredded or disinfected sewage may be discharged more than 12 nautical miles from the nearest land.

The size of the tank should take into account the capacity to hold all the sewage, the operation of the vessel, the number of persons on board and other relevant factors. The storage tank must have means of visually indicating its contents.

The storage tank can also be used to collect grey water and/or galley water. However, grey water is not always piped to the tank and is sometimes stored in separate storage tanks. Grey water can sometimes be discharged directly into the sea or must be mixed with the wastewater to be treated. It can also be recycled into the toilet flushing system.

About a quarter of cruise ships have installed an advanced wastewater treatment system (AWTS), which mixes and cleans grey and black water and produces a bioresidue or sewage sludge that must be preserved for discharge ashore [29]. It is common on cruise ships to have a separate tank for galley water, which is emptied in accordance with food waste regulations. It is common for cruise ships to chop, mix and disinfect the water before it is released into the sea.

The main factors of the amount of wastewater are:

- number of crew and passengers;
- type of toilets: flush toilets produce a larger amount of wastewater than vacuum toilets;
- the length of the trip;
- the type of treatment: the presence of a sewage treatment plant or a shredding and disinfection system ensures different amounts of waste.

The amount of wastewater produced in the sewage depends on the size of the ship and the technology used [30].

2.3.5. Plastic

Plastic waste can be generated in all types of containers and often originates from domestic provisions and supplies used for shipboard operations.

Plastic waste typically includes sheets, packaging, bottles, cans, synthetic ropes, synthetic fishing nets, plastic trash bags, and empty chemical cans.

Plastics on board can be handled in two ways: they are stored separately (compacted or otherwise) and transported to the PRF, or they can be incinerated, and the ash treated as incinerator ash. Incineration is restricted by MARPOL VI. Regulation 16 prohibits the burning of polyvinyl chloride (PVC) on board ships, except in shipboard incinerators for which an IMO-type approval certificate has been issued in accordance with MEPC.244 [31], [32]. Burning plastics with PCBs is always prohibited.

According to the literature, each person produces 1 kg of solid waste per day, and other sources give an estimate of 3 kg/day for staff members [33]. Maintenance-related solid waste is 11 kg/ship-day for all ships [34].

These estimates are not specific to plastic waste but are on the order of 0.06 - 0.2 m^3 per person per day and 0.7 per day [35].

2.3.6. Food waste

Food waste is generated on all kinds of dishes in the kitchen and/or restaurant. The IMO defines this as any spoiled or intact food material and, including fruit, vegetables, dairy products, poultry, meat products, and food scraps generated on board. However, onboard large ships (cargo and cruise ships), sometimes a distinction is made between soft organic food waste (shells, leftovers, etc.) and hard organic (bone) and packaging (even though the packaging is not food waste according to Annex V of MARPOL). This separation is not based on regulation but comes from practical management on board ships.

Organic food waste can be discharged directly into the sea 12 km from the nearest land or shredded and then discharged into the sea 3 km from the nearest land (12 km in special areas).

Ships that generate a lot of food waste (e.g. cruise ships or work ships) should sometimes be dried to reduce odours and reduce the risk of rotting [36].

Solid organic waste, waste from plates and packages, is collected in bags and bins and disposed of in port reception facilities [37], [38]. In some cases, this is delivered to the household waste category instead of food waste. Regarding the treatment of food waste, we found no difference between cruise ships and normal cargo ships. The exception is that cruise ships usually have galley waste tanks that are emptied under the same regulations as food waste and/or greywater.

2.3.7. Household waste

Household waste is any waste that originates from the domestic spaces on board the vessel and is not food waste, cooking oil or plastic. The IMO defines this as “all other waste generated in the accommodation spaces on board a ship, not covered by another Annex. Household waste does not include greywater. "Household waste is therefore typically paper, cardboard, fluorescent tubes, synthetic material, foil, metal cans, lids, glass, chamber packaging waste and so on. Domestic waste is generated on board by crew and passenger accommodation and is generated on all types of ships. Waste minimization measures are mostly found on cruise ships to reduce the amount generated inland. [39], [40]

2.3.8. Cooking oil

Cooking oil waste is produced on board during food preparation and is produced in most types of ships. In most cases, cooking oil is collected and delivered to the PRF. In some cases, they are burned. On some ships, it was customary to mix cooking oil with sludge and treat it as sludge. However, MEPC 68 decided that this was inconsistent with MARPOL Annex V [32].

Large cruises have a separate tank for storing large-capacity (up to 1000 m3) cooking oil. The used oil is sold in the port, and e.g. biofuel production.

2.3.9. Operational waste

Many different types of waste are classified as 'operational waste'.

Most ships include engine room waste such as oily rags and batteries in this category, but it can also include other waste from ship operations such as old ropes, glassware, wood, washing machines, debris, refrigerators, aerosols, ladders, fireworks and flares, chemical residues, asbestos and paint. Therefore, some of these wastes must be classified as hazardous materials. Some ships also report cargo handling waste in this category, such as wooden pallets, storage materials and rubber gloves.

On other ships, the category is used for other household waste, such as fluorescent lamps, torn work clothes, etc. [19], [41].

2.3.10. Cargo residue

MARPOL Annex V defines cargo residues as “remains of all cargo not covered by other Annexes of the Convention which remain on board or in a hold after loading or unloading, including loading or unloading excess or spillage, whether wet or dry or in washing water, but does not include cargo dust left on deck after sweeping or dust on the outer surface of the ship" [41].

Cargo residues can remain in the corner of the hold or in other places that are not accessible during unloading and are highly dependent on the efficiency and methods of unloading the cargo.

2.3.11. Ozone-depleting substances

MARPOL VI. Its annex defines ozone-depleting substances as controlled substances listed in Annex A, B, C or E of the then-current Montreal Protocol on Substances that Deplete the Ozone Layer, as defined in Article 1(4) of the 1987 Montreal Protocol on Substances that Deplete the Ozone Layer. The application or interpretation of Annex.

Examples include Halon 1211, Halon 1301, Halon 2402, CFC-11, CFC-12, CFC-113, CFC-114 and CFC-115 [19], [41].

Substances that deplete the ozone layer are used on board ships in air conditioning or refrigeration equipment. They can also be placed in mobile devices (refrigerators, mobile air conditioners).

Equipment containing ozone-depleting substances produces ozone-depleting substances during renovation, but this is likely to be removed by repair companies.

2.3.12. Other uncommon waste streams

Dirty ballast water

Ballast water is carried in ships' ballast tanks to improve stability, balance and equipment. If oil tanks are used to transport ballast water, the water is contaminated with oil and is classified as waste in MARPOL Annex I [26].

It is very rare to produce oily ballast water on board. A likely waste from onboard ballast water operations is when sediment in the ballast water tank needs to be removed during a port state control tank integrity assessment or when the ship needs to treat its ballast water and is unable to do so. Both of these circumstances are very rare, and in such circumstances, the ports are likely to put the ship in touch with specialist waste management contractors.

Animal carcasses

Animal carcasses are the remains of deceased livestock. The discharge of animal carcasses is allowed only outside special areas, as far as possible from the nearest land and on the road. So, the possibility of disposal of animal carcasses is to release them into the sea or transport them to the PRF. If the vessel has adequate storage space on board, a limited amount of carcasses can be stored for a short time before unloading. In case of health and safety threats, it is recommended to release it into the sea, but more than 12 km from the nearest land. Before release into the sea, animal carcasses must be dismembered/shredded or treated to facilitate the sinking or dispersal of the carcasses [41].

Fishing equipment

Fishing equipment waste is generated when fishing equipment wears out and tears beyond repair. It only occurs on fishing boats.

2.4. Heat treatment technologies

Heat treatment technologies are operations that are suitable for transforming waste awaiting disposal into a product or energy with more favourable properties from certain points of view. The main end products of the applied processes are gaseous and solid materials [9].

Heat treatment technologies are usually compared based on their typical reaction conditions. One of the most important reaction conditions is the applied temperature, which provides preliminary information on the impact of the technology on the environment and the costs of the investment. The higher temperature requires the use of special materials, metal alloys and technical ceramics, which leads to a significant increase in costs. The most decisive factors in investment costs are operating temperature and pressure.

The second and most important reaction condition is the excess air factor. This characteristic partly shows the chemical composition and specific quantity of the emitted gas product. In the case of perfect combustion, we must expect a significant air surplus (a surplus of air greater than one), which directly increases the amount of flue gas emitted (containing more air) and indirectly - through the flue gas cleaning system - the investment and operating costs.

The third reaction condition is the operating pressure, which determines the relationship between the reactions. It plays an important role in the chemical composition of the resulting gas product and is a determining factor in investment costs.

The fourth reaction condition involves the type of auxiliary currents. The auxiliary flows can be divided into two groups; on the one hand, we distinguish material flows and on the other energy flows. The auxiliary gas used affects the composition, handling, and physical and chemical properties of the final products obtained.

2.4.1. Basic technologies

Table 1. Typical reaction conditions of thermal treatment technologies

Proceedings	Temperature [°C]	Excess air factor	Operating pressure [bar]	Auxiliary currents
Pyrolysis	300−600(1,600)	$\lambda = 0$ endothermic	$p \leq 1$ bar $p \geq 1$ bar	- nitrogen
Pyrolytic-gassing	800−1,000°C	$0 < \lambda < 0.5$	$p \geq 1$ bar	air, water vapour
Traditional firing	850−1,200°C	$\lambda \geq 1$ $1.1 \leq \lambda \leq 2.5$ exothermic	$p \geq 1$ bar	air, natural gas supplementary heating
Gasification	600−1,600	$\lambda < 1$ $0.5 \leq \lambda \leq 0.8$ is partial oxidation	$1 \leq p \leq 20$ bar	air, water vapour, CO_2 and O_2 mixture, a combination of these
Plasma technology	2,000−6,000	$\lambda = 0.5$ endothermic	$1 \leq p \leq 20$ bar	air, water vapour, CO_2 and O_2 mixture, a combination of these
Reference: Natural gas-powered gas engine torus power plant	600−1,200	$\lambda = 1.8$ exothermic	$p = 1$ bar	air

The basic technologies are all thermal treatment technologies, during which the waste undergoes chemical

changes that cause the decomposition of individual components and the evaporation of volatile compounds. The basic technologies differ in their characteristic reaction conditions. In a basic technology, the characteristic chemical reactions are decisive, but different processes can also take place, which influence the composition of the resulting gas product. If the chemical reactions characteristic of different technologies take place to a similar degree within a device, then we are talking about a single-step or process-integrated combined heat treatment technology.

Tables 1. and 2. show the typical reaction conditions of the basic technologies, as well as the final products produced and the type of power plants used. The names of the residues generated after energy production are also indicated in the tables [8], [9], [10], [42], [43], [44].

Table 2. Products of thermal treatment technologies and the used power machines

Proceedings	Emerging product before power machine	Power machine	Eastern end product after power plant
Pyrolysis	pyrogas, pyro oil, pyrocoke	gas engine, gas turbine, diesel engine, steam boiler-steam turbine	flue gas (<5 % combustible), slag, ashes, cinders
Pyrolytic gasification	pyrogas, less pyrocoke and oil		
Traditional firing	fuel, waste [1]	steam boiler steam turbine	
Gasification	synthesis gas, slag, ashes, cinders	gas turbine, gas engine	flue gas (<5 % combustible)
Plasma technology	synthesis gas, glass slag slag	gas turbine, gas engine	
Reference: Natural gas-powered gas engine power plant	natural gas [2]	gas turbine, gas engine	flue gas (<3% CH4 content)

Notes:
[1] is not the product of the technology, but the raw material entering the technology, which is the same for all technologies
[2]at the reference power plant, the fuel is natural gas instead of waste

Traditional combustion

Conventional incineration is a technology that allows simple burning of the amount of energy contained in waste and fuel [45]. During the combustion process, we can utilize the so-called reaction heat released as a result of the chemical reactions taking place, which corresponds to the calorific value of the waste. Combustible materials in the waste are sufficient under appropriate conditions [42]. Waste incineration is a heat-generating, i.e. exothermic, process where the amount of oxygen required for perfect combustion can be provided with a sufficiently high air surplus. During incineration, the organic components of the waste react with the oxygen in the air to form gases and water vapor and leave the flue gas as flue gas [46].

Incombustible inorganic materials, such as ash, slag, and fly ash, usually remain in a solid state [47]. Due to the diversity of waste, different types, chemical compositions and states of materials must be burned, which makes the burning process complex. A number of conditions must be met to achieve perfect oxidation. 29/2014 on the technical requirements, operating conditions and technological emission limit values of waste incineration. FM regulation provides. The decree stipulates strict conditions for the placement of waste incinerators. The regulation covers the temperature and residence time of the flue gas leaving the combustion equipment. In order to satisfy the conditions, the flue gas is led to an afterburner, where the remaining combustible material is burned, so the combustion is completed. The required temperature in the afterburner is usually 850 °C, or in the case of hazardous waste, the temperature 1100 °C can only be reached with the help of a supporting burner. The large amount of secondary air introduced into the chamber mixes with the flue gas in a turbulent flow, resulting in significant heat loss, which is why a heat supply is needed. In order to achieve mixing and burnout, the residence time is a minimum of 2 seconds. For the perfect, soot-free

combustion of hydrocarbons and plastics, the residence time of 2 seconds is usually short [42], [43.].

Pyrolysis

Pyrolysis is a process based on the thermal decomposition of organic matter, which takes place with the complete exclusion of oxygen. The treatment of organic waste includes transformation by chemical decomposition under the influence of heat, usually under pressure, usually under pressure [6], [7], [48], [49]. During the treatment, a gaseous energy carrier is released, which is called pyrolysis gas or pyrogas. Pyrogas is a gas mixture rich mainly in carbon monoxide, hydrogen and methane, the heating value of which can be close to that of natural gas. It may also contain energetically inert components, especially carbon dioxide and water vapour [10], [50], [51], [52]. Utilization of gas products in power plants are primarily advisable in a gas turbine or gas-fired systems, which makes it suitable for replacing natural gas-fired power plants [31], [51].

In the solid phase, pyrolysis coke, or coke for short, remains, in which the carbon content of the given waste is enriched [9], [53], [54]. The energy produced in this way can be used to replace coal in ironworks, cement production and coal-fired power plants. In the case of waste contaminated with heavy and light metals, the metals usually remain in the solid phase, so the pyrocoke must be further treated in order to recover it [55]. Pyrolysis, like traditional burning, is one of the heat treatment processes, but we are basically talking about two different processes. Combustion requires three basic things: combustible material, oxidizing material, and heat. In contrast, pyrolysis requires only combustible material and heat [56.]. Pyrolysis is an umbrella term that includes several technologies. The main purpose of a very low temperature (<300 °C) process such as torrefaction is to remove volatile compounds from the fuel and reduce moisture content, thereby increasing the energy density of the remaining solid product.

Gasification

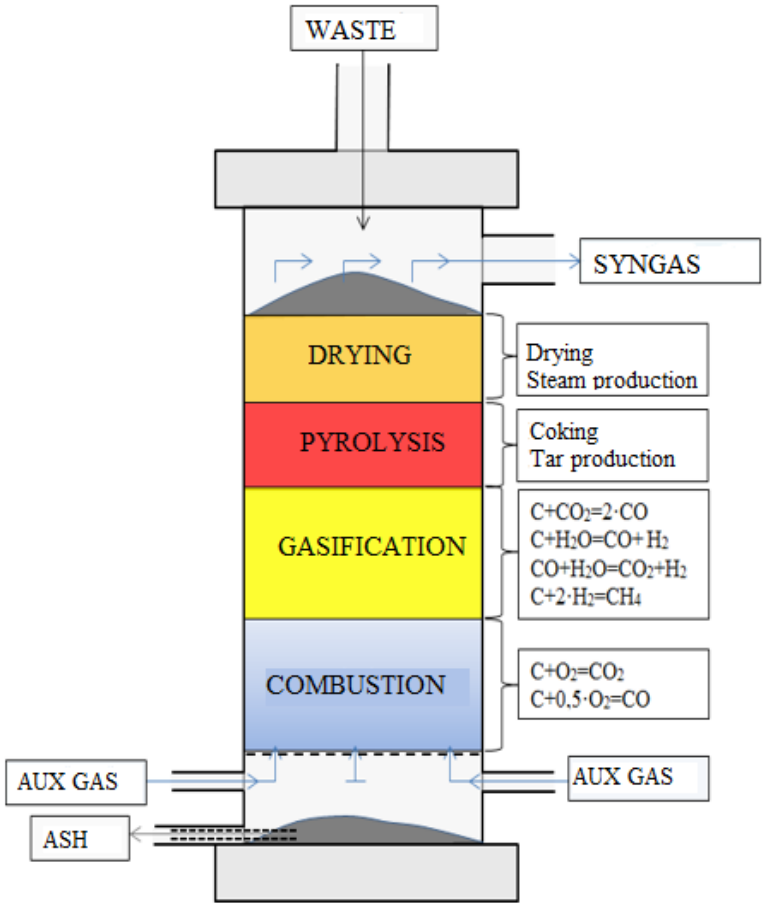

Figure 4. The principle structure of the zones formed in an upper outflow gasification reactor

Gasification is one of the oldest processes for converting solid fossil and renewable energy sources into combustible syngas and liquid fuels. Gasification was first used by Thomas Shirley to produce hydrogen in 1659. The first patent was filed by Robert Gardner in 1788, marking the beginning of the spread of gasification. Gasification is a process based on the rapid thermal decomposition of materials by partial oxidation, which thus requires less oxygen than the theoretical amount of oxygen required for perfect combustion [46]. During the partial oxidation of the organic compounds in the raw material, synthesis gas is released, which can be used either as a raw material, in chemical syntheses or as a fuel [55], [51.]. Due to the sensitivity of the process, it is important that the characteristics of the fed waste (size, moisture content, consistency) remain within certain predetermined limits [43]. The effect of sensitivity is typically manifested in energy and environmental efficiency.

In addition to waste management, the main goal of the process is the highest gas emission, which is accompanied by the achievement of optimal energy efficiency. The synthesis gas produced during gasification is a gas mixture rich in hydrogen and carbon monoxide, which, depending on the gasification medium, may also contain other energetically neutral components. Gasification is not an independent technology, as both pyrolysis and the combustion zone are formed in the reactor designed for this purpose. However, the name is correct because the reactions taking place in the case of thermodynamic equilibrium result in a self-sustaining process, except for radiation losses [6]. The relative location of the zones and the flow direction affect the chemical composition and temperature of the resulting synthesis gas [7], [57]. Figures 4. and 5. illustrate the basic structure of the reactor in two versions [7], [58], [59].

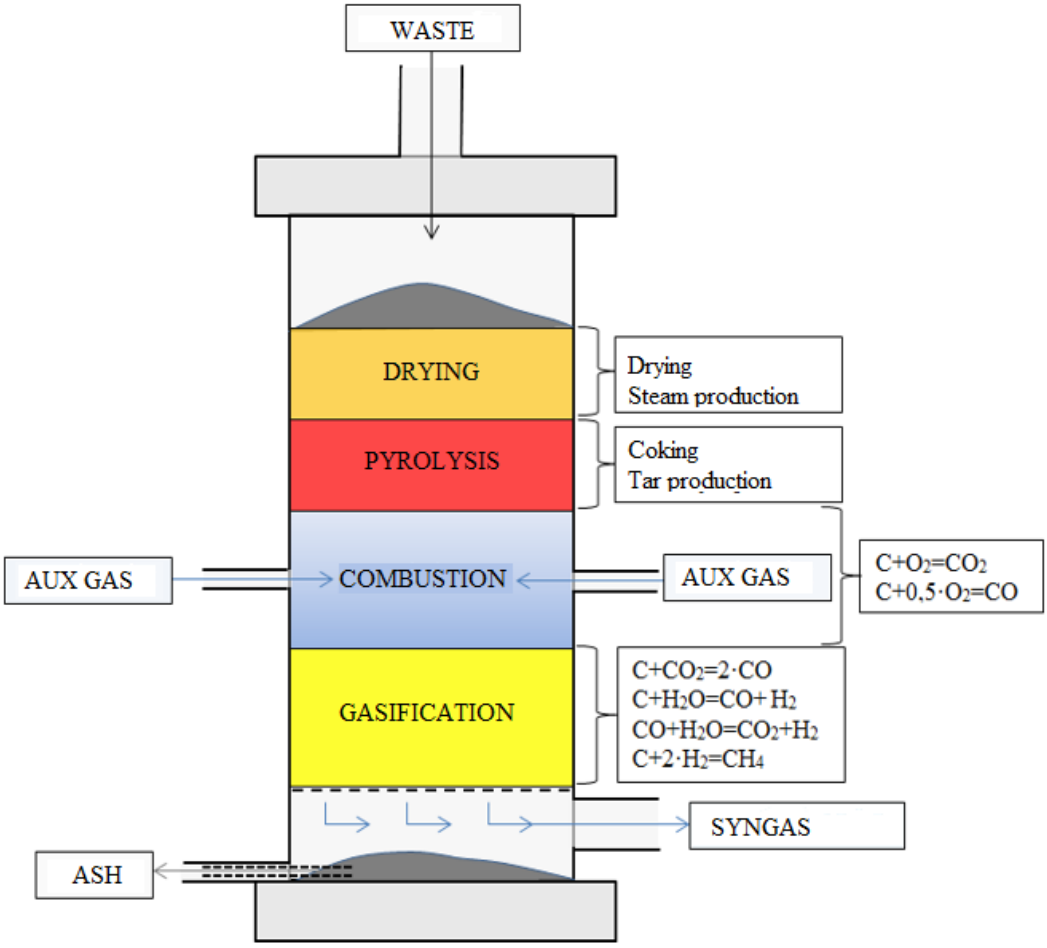

Figure 5. The principle structure of the zones formed in a bottom outflow gasification reactor

Plasma technology

To understand how plasma technology works, it is helpful to first define the concept of plasma. Plasma is an

ionized gas formed by a high-current electric arc between electrodes in an inert gas stream. During the process, the charged electrons leaving the cathode excite the atoms and particles in the arc. The excitation causes a light phenomenon called an electric arc. Due to the large flowing currents, the materials enter the plasma state, which can be considered the fourth state [60], due to the high temperature of the arc space. In the case of plasma technologies, the core temperature would normally be between 3000 and 5000°C, but up to 30,000°C could be achieved [60], [61].

The temperature of 5000°C is also a significant problem, as it requires expensive technical ceramics and metal alloys [45]. At this temperature, waste components, such as toxic substances, break down into their components. Above 5000°C, chemicals and toxic gases (dioxins and furans) completely decompose. Substances harmful to the environment are produced only in small quantities or not at all [62]. Although this is a common commercial technology, the process is extremely complex and expensive and requires the involvement of a skilled operator [42], [57]. Figure 6. illustrates the structure and operation of the plasma reactor through the material flows. The reactor provides overcurrent and countercurrent operation.

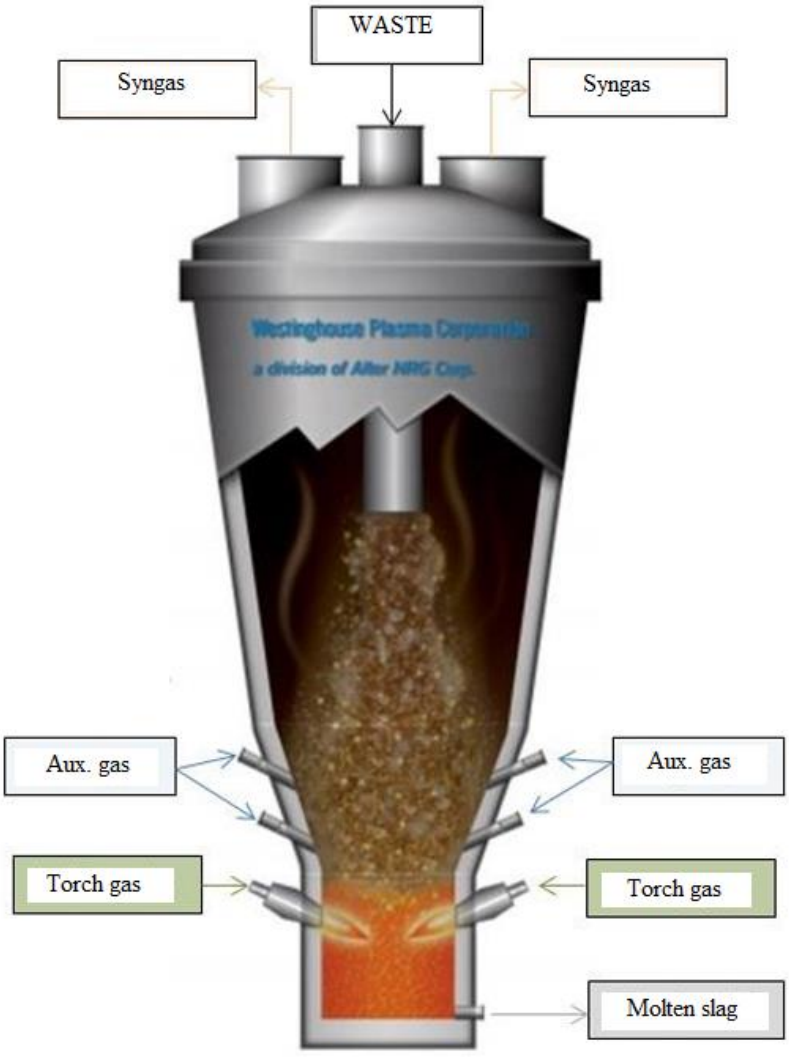

Figure 6. Construction and material flows of a plasma reactor

The operating pressure affects the nature of the reactions taking place and, through this, the composition and calorific value of the synthesis gas produced [31].

1. Disadvantages of plasma technology [9], [10], [62], [63], [64], [65]:
   - In plasma-based processes with lower temperatures (below 2000 ° C), gas purification is more complex and complicated.
   - The most heavily polluted washing water produced during the application of the technology must

also be treated in a complex manner.
- Compared to combustion, there is a greater possibility of the formation of imperfect combustion products that are difficult to decompose.

2. Environmental advantages of plasma technology [9], [10], [62], [63], [64], [65]:
   - It does not require pre-sorting of the waste, so regardless of its composition, it can be sent mixed.
   - Inorganic wastes partially decompose, partially melt and vitrify.
   - Organic materials are completely decomposed.
   - Halogens are chemically bound to the resulting glass and do not dissolve from it.
   - The strong ultraviolet radiation emitted by the plasma accelerates the decomposition of chlorine-containing organic compounds.
   - The ultraviolet radiation generated in the plasma space gets "stuck" in the plasma arc, thereby causing additional excitation, which increases with increasing temperature.
3. Technical and economic advantages of plasma technology [9], [10], [62], [63], [64], [65]:
   - Due to the high temperature, plasma technology can be effectively used to break down all types of waste (dangerous, toxic, deadly).
   - The process takes place in a completely closed space, so no harmful substances enter the environment.
   - The by-products of the process are harmless and can be used as raw materials in the metallurgical and construction industries.
   - The reduction in the amount of waste is 300:1 compared to conventional incineration, where this ratio is only 5:1 (for solid waste) due to the large amount of ash.
   - The maximum daily capacity of plasma technology is up to 500 tons/day.
   - Machines using plasma technology are computer-controlled, silent, and can be stationary or mobile.
   - During the application of plasma technology, impurities entering the slag, such as mercury, cadmium, sulfur, various dioxins and heavy metals, can be significantly reduced by using special washing water, dry washers and filters.

Combined technologies

Combined heat treatment technologies are alternative solutions created by combining basic technologies. The purpose of these technologies is to eliminate the disadvantages of the underlying technologies and combine their advantages. The most common reasons are to reduce investment and operating costs, increase energy efficiency and improve environmental performance.

3. Conclusion

In the study, we summarized the possibilities for the utilization and destruction of waste. In the first part, we studied the utilization and grouping of waste. We examined the legal background and regulations of waste management and disposal, as well as land and settlement regulations (Hungarian and international), as well as maritime and shipping regulations. Afterwards, we studied the disposal of waste and the composition of the waste generated on the ship.

The technology we have designed reduces the moisture content of very mixed waste below 15 m/m%, after which we obtain a material that is easy to handle and suitable for further utilization(s). The utilization, destruction and use of this material can be decided after various chemical analyses. Recyclability and environmental protection are the primary considerations, taking into account the quantities generated on ships. According to our plans, with the technology, we can reduce the amount of hazardous substances produced and increase the recyclability of waste. The project (2019-1.1.1-PIACI-KFI-2019-00320) aimed at the development of a product and technology that complies with current shipping regulations and offers a new and efficient solution for the treatment and disposal of wet waste generated on board ships.

Acknowledgement

The research was supported by the project 'The feasibility of the circular economy during national defense activities' of 2021 Thematic Excellence Program of the National Research, Development and Innovation Office under grant no.: TKP2021-NVA-22, led by the Center for Circular Economic Analysis.

References

[1] **Barótfi** I., (2000) Környezettechnika, Mezőgazda Kiadó, Budapest, 2000: p. 981.
[2] **Kun-Szabó T**. (1999) A Környezetvédelem minőségmenedzsmentje. (The Quality Management of Environmental Care) Műszaki Könyvkiadó, Magyar Minőség Társaság, Budapest p. 396. ISBN 9789631630480
[3] **Antonio C. Caputo, Pacifico M. Pelagagge** (2002) RDF production plants: I Design and costs. Applied Thermal Engineering 22. pp. 423−437. 2002, https://doi.org/10.1016/S1359-4311(01)00100-4
[4] **Fellner J., Rechberger H**. (2009) Abundance of 14C in biomass fractions of wastes and solid recovered fuels. Waste Management 29. pp. 1495−1503. 2009, https://doi.org/10.1016/j.wasman.2008.11.023
[5] **Basu P**. (2013) Biomass gasification, pyrolysis and torrefaction, Practical design and theory, Second edition, Elsevire, San Diego, 2013. p. 529.
[6] **Szuhi A**. (2009) Új termikus technológiák és hagyományos hulladékégetők. Környezetvédelmi és Vízügyi Minisztérium (New thermal technologies and traditional waste incinerators) 2009. p. 36.
[7] **Red T. B., Das A**. (1988) Handbook of biomass downdraft gasifier engine systems, Solar Energy Research Institute, Colorado, 1988. p. 140.
[8] **Szuhi A**. (2013) Az új termikus technológiák környezeti hatásai (pirolízis, elgázosítás és plazma technológia). Humusz Szövetség és Vidékfejlesztési Minisztérium 2013. p. 14.
[9] **Hornyák M., Bánhidy J., Kovacs E., Kovacs L., Varga P**. (2008) Útmutató az elérhető legjobb technika meghatározásához a hulladékégetők engedélyezése során, Környezetvédelmi és Vízügyi Minisztérium, Budapest 2008. p. 386.
[10] **Büki G**. (2007) Kapcsolt energiatermelés. Műegyetemi Kiadó, Budapest 2007. p. 420.
[11] **Gróf Gy., Könczöl S**. (2008) Gázmotoros kapcsolt hő- és villamosenergia-termelés. Háttértanulmány az üzemeltetési ajánlás kidolgozásához 2008. (Gas engine combined heat and electricity production. Background study for the development of the operating recommendation)
[12] **Committee on Shipborne Wastes**; Marine Board; Commission on Engineering and Technical Systems: National Research Council, 1995. Clean ships clean ports clean oceans: Controlling garbage and plastic wastes at sea. Washington DC: National Academy Press.
[13] **MEPC, 2006**. Resolution MEPC.157(55) Adopted on 13 October 2006: Recommendation on Standards for the Rate of Discharge of Untreated Sewage from Ships, London: The Marine Environment Protection Committee.
[14] **MEPC, 2007**. Prevention of Air Pollution from Ships: Washwater Discharge Criteria for Exhaust Gas-SOx Cleaning Systems, MEPC 56/INF5, London: IMO, Marine Environmental Protection Committee (MEPC)
[15] **MEPC, 2011a**. ANNEX 12: Resolution MEPC.200(62), Adopted on 15 July 2011: Amendments to the annex of the protocol of 1978 relating to the international convention for the prevention of pollution from ships, 1973.
[16] **MEPC 62/24**, London: The Marine Environment Protection Committee (MEPC). MEPC, 2011. ANNEX 12: Resolution MEPC.200(62), Adopted on 15 July 2011: Amendments to the annex of the protocol of 1978 relating to the international convention for the prevention of pollution from ships, 1973. MEPC 62/24, London: The Marine Environment Protection Committee (MEPC).
[17] **MEPC, 2011**. Resolution MEPC 201(62) adopted on 15 July 2011: Amendments to the Annex of the Protocol of 1978 relating to the International Convention for the prevention of pollution from ships, 1973 (Revised MARPOL Annex V), London: International Maritime Organization (IMO).
[18] **IMO, 2006d**. Marpol Consolidation 2006: Annex VI Regulations for the Prevention of Air Pollution from Ships.
http://www.marpoltraining.com/MMSKOREAN/MARPOL/Annex_VI/r12.htm.
[19] **NEA**; PM Group, 2009. Annex 2: Ship Generated Waste Analysis, Zoetermeer: NEA.
[20] **Netherlands Maritime Technology**, 2016. Sustainable Maritime Solutions: Waste. http://sustainable-maritime-solutions.nl/waste/
[21] **HELCOM, 2013**. HELCOM interim guidance on technical and operational aspects of delivery of sewage by passenger ships to port reception facilities: 2013 HELCOM Ministerial Declaration, Helsinki: HELCOM, Baltic Marine Environment Protection Commission.
[22] **HELCOM, 2015**. Baltic Sea Sewage Port Reception Facilities: *HELCOM Overview 2014, Revised*

Second Edition, Helsinki: HELCOM, Baltic Marine Environment Protection Commission.

[23] **HPTI, 2007**. Study on Ships producing reduced quantities of ships generated waste: present situation and future opportunities to encourage the development of cleaner ships, Lissabon: European Maritime Safety Agency (EMSA), Unit D – Implementation EU maritime legislation.

[24] **MEPC, 2016**. ANNEX 9 (Adopted on 22 April 2016): Amendments to the Annex of the International Convention for the Prevention of Pollution from Ships, 1973, as modified by the Protocol of 1978 relating thereto Amendments to MARPOL Annex IV, Resolution MEPC. 274(69), London: The Marine Environment Protection Committee (MEPC).

[25] **IMO, 1983**. Annex I- Regulations for the Prevention of Pollution by Oil: Chapter 4, Part B, Regulations 33: Crude oil washing requirements, London: IMO.

[26] **IMO, 2006a**. Marpol Consolidation 2006: Annex I- Regulations for the Prevention of Pollution by Oil. [Online]http://www.marpoltraining.com/MMSKOREAN/MARPOL/Annex_I/index.htm

[27] **MEPC, 2012**. Annex 24: Resolution MEPC.219(63) : Guidelines for the Implementation of MARPOL Annex V.
www.imo.org/en/OurWork/environment/pollutionprevention/garbage/documents/219(63).pdf.

[28] **Handson tv/e, 2004**. Fishing for Litter – Denmark. [Online] http://handson.tve.org/series-5/green-current/fishing-litter-denmark/.

[29] **MEPC, 2015**. Report of the Marine Environment Protection Committee on its sixty-eighth Session, MEPC 68/21, London: International Maritime Organization (IMO), Marine Environment Protection Committee (MEPC).

[30] **Mountouris A., Voutsas E., Tassios D**. (2006) Solid waste plasma gasification: equilibrium model development and exergy analysis. Energy Conversion and Management. Vol. 47. 2006. pp. 1723−1737.

[31] **MEPC, 2014**. Resolution MEPC.244(66) Adopted on 4 April 2014: The 2014 Standard specification for shipboard incinerators, London: The Marine Environment Protection Committee (MEPC).

[32] **ASCI, 2000**. Alaska Cruise Ship Initiative Part I Final Report: Activities and Workproducts up to June 1, 2000, sl: Alaska Cruise Ship Initiative (ASCI).

[33] **Mohammed J., Torres R., Obenshain E**. (1998) Waste Reduction at Sea: Pollution prevention Strategies on Miami-Based Cruise Lines, Ann Arbor: National Pollution Prevention Center for Higher Education, University of Michigan.

[34] **Brandstoftafel scheepvaart**, 2014. Visie Duurzame Brandstoffenmix: Dealrapport Brandstoftafel scheepvaart, sl: Brandstoftafel scheepvaart

[35] **TEN ECOPORT**, 2014. Common Action Plan for ship-generated waste Ports of Bari and Durres, sl: Transnational Enhancement of ECOPORT8 network (TEN ECOPORT)

[36] **MMPA, 2012**. Ship-generated waste management plan at the maritime port of Dudinka. Dudinka: Murmansk Maritime Port Administration (MMPA), Dudinskiy Branch.

[37] **Environmental Board**, 2015. Ship-generated waste and cargo residues reception and handling plan, Tallinn: Environmental Board of Port of Tallinn

[38] **IMO, 2006b**. Marpol Consolidation 2006: Annex IV- Regulations for the Prevention of Pollution by Sewage from Ships.
http://www.marpoltraining.com/MMSKOREAN/MARPOL/Annex_IV/index.htm.

[39] **IMO, 2006c**. Marpol Consolidation 2006: Annex V- Regulations for the Prevention of Pollution by Garbage from
Ships.http://www.marpoltraining.com/MMSKOREAN/MARPOL/Annex_V/index.htm

[40] **IMO, 2008**. 2008 Revised Guidelines for Systems for handling Oily Wastes in Machinery spaces of Ships incorporating Guidance Notes for an Integrated Bilge Water Treatment System (IBTS), MEPC.1/Circ.642, London: International Maritime Organization (IMO).

[41] **Csőke B**. (2011) Hulladékgazdálkodás (Waste management), Pannon Egyetem – Környezetmérnöki Intézet, 2. javított kiadás, 2nd revised edition, Veszprém, 2011. p. 699.

[42] **Örvös M**. (2011) Disposal with thermal processes. Educational aid BME, 2011. p. 31IMO, 2006d. Marpol Consolidation 2006: Annex VI Regulations for the Prevention of Air Pollution from Ships. http://www.marpoltraining.com/MMSKOREAN/MARPOL/Annex_VI/r12.htm

[43] **Mannheim V**. (2010) Thermal treatment of organic chemical industrial waste with plasma technology. Energy management. Budapest, 2010. 51st year. No. 3 p. 21−23.

[44] **Murphy JD, Mckeogh E**.: Technical, economic and environmental analysis of energy production from municipal solid waste. Renewable Energy 29. pp. 1043−1057. 2004.

[45] **Woodhead Publishing**, Philadelphia, USA, 2013. p. 234.

[46] **Young G. C**. (2010) Municipal solid waste to energy conversion processes: Economic, technical, and renewable comparisons. John Wiley & Sons, Inc., New Jersey. 2010 p. 398

[47] **V. Madár, A. Betovics, L. Tóth**: Production and Production-Increasing Factors of Biochar, Hungarian Agricultural Engineering No 42/2023 14-25.

[48] **Korzenszky P.; Lányi K.; Simándi P.**, (2015) Test Results of a Pyrolysis Pilot Plant in Hungary Hungarian Agricultural Engineering 2015: 28 pp. 48-52, 5 p.

[49] **Lányi K., Molnar E., Vanó I., Korzenszky P.** (2014) Looking Behind The Process of Pyrolysis in Waste Management: Questions on The Composition and Quality of End-Product and Their Answers by Meas of Analytical Chemistry, Hungarian Agricultural Engineering 26 pp. 25-28, 4 p.

[50] **Virág S, Montvajszki M, Korzenszky P.** (2015) Thermal waste treatment procedures, 295 p. Szarvas, 2015. Project TÁMOP-4.2.2.A-11/1/KONV-2012-0015: Basic research and development at the Pyrolysis Technology Center of Szent István University.

[51] **Korzenszky P., Simándi, P.** (2015) Results of a thermolysis pilot plant in Hungary, In: Futó, Zoltán (ed.) The latest development possibilities of waste management, Szarvas, Hungary: Szent István University Faculty of Economics, Agriculture and Health 126 p. pp. 22-30, 9 p.m.

[52] **Korzenszky P., Puskás J., Mozsgai, K., Lányi K., Mák Z.,** (2014) Innovation possibilities of a thermolysis plant to be established in Hungary, In: Marianne, Bell (ed.) 20th International Symposium on Analytical & Applied Pyrolysis: Birmingham Pyro2014, Paper: B143.

[53] **Bártfai Z., Korzenszky P., Szalkai I.** (2019) Preprocess Variations of Plastic Waste Recycling, In: Magó L., Kurják Z. (ed.) SYNERGY - Engineering, Agriculture and Green Industry Innovation: ABSTRACTS of the VI. International Conference of CIGR Hungarian National Committee and the Szent István University, Faculty of Mechanical Engineering and the XXXIX. R&D Conference of Hungarian Academy of Sciences, Committee of Agricultural and Biosystems Engineering, Gödöllő, Hungary, 4 – 6 November 2019. Gödöllő, Hungary: Szent István University Faculty of Mechanical Engineering 96 pp 36, 1 p.

[54] **Hill T., Dowen S**. (2010) Pyrolysis and gasification. Briefing (Draft 2), UK Without Incineration Network (UK WIN), 2010. pp. 1-9.

[55] **Helsen L., Bosmans A**. (2010) Waste-to-Energy through thermochemical processes: matching waste with process. Proceedings of the International Academic Symposium on Enhanced Landfill Mining, Houthalen-Helchtern, Belgium, pp. 133−180. 2010.

[56] **Huang H., Tang L**. (2007) Treatment of organic waste using thermal plasma pyrolysis technology. Energy Conversion and Management 48. pp. 1331−1337. 2007

[57] **Rajvanshi K. A**. (1986) Biomass gasification. Alternative Energy in Agriculture. Vol. 2. No. 4. 1986. pp. 83−102

[58] **Schuster G., Löffer G., Weigel K., Hobfauer H**. (2001) Biomass steam gasification – an extensive parametric modeling study. Bioresource Technology. Vol. 77. 2001. pp. 71−79,

[59] **Lee S., Speight J. G., Loyalka S. K**. (2015) Handbook of alternative fuel technologies. Taylor & Francis, 2015. p. 686.

[60] **Klinghoffer N. B., Castaldi M. J**. (2013) Waste to energy conversion technology, Woodhead Publishing, pp. 3-14., https://doi.org/10.1533/9780857096364.1.3.

[61] **Mountouris A., Voutsas E., Tassios D**. (2008) Plasma gasification of sewage sludge: Process development and energy optimization. Energy Conversion and Management 2008 49. pp. 2264−2271.

[62] **Szépvölgyi J**. (2000) Transformation of substances in high-temperature plasmas. Instrumentation and Measurement Technology Bulletins. 2000 (vol. 36) No. 65 p. 4

[63] **Morly C**. (2005) Method for calculating equilibrium compositions at specified temperature. Gaseq, the chemical equilibrium program for windows 2005 p. 6. www.gaseq.co.uk

[64] **Corti A., Lombardi L**. (2004) Biomass integrated gasification combined cycle with reduced CO2 emission: Performance analysis and life cycle assessment (LCA). Energy, Vol. 29. 2004. pp. 2109−2124.

HUNGARIAN AGRICULTURAL ENGINEERING
No 43/2024 53-64
Published online: http://hae-journals.org/
HU ISSN 0864-7410 (Print)
HU ISSN 2415-9751(Online)
DOI: 10.17676/HAE.2024.43.53
Received: 22.08.2024 - Accepted: 18.10.2024

PERIODICAL
OF THE COMMITTEE OF AGRICULTURAL AND BIOSYSTEM ENGINEERING OF THE HUNGARIAN ACADEMY OF SCIENCES
and
HUNGARIAN UNIVERSITY OF AGRICULTURE AND LIFE SCIENCES INSTITUTE OF TECHNOLOGY

HUNGARIAN UNIVERSITY OF AGRICULTURE AND LIFE SCIENCES
Institute of Technology

OPTIMIZING THERMAL MANAGEMENT IN PHOTOVOLTAIC PANELS: EXPERIMENTAL STUDY

Author(s):
H. Saadi [1], P. Hermanucz [2]

Affiliation:
[1] Doctoral School of Mechanical Engineering – Hungarian University of Agriculture and Life Sciences, 2100 Gödöllő, Páter Károly u. 1., Hungary;
[2] Institute of Technology - Hungarian University of Agriculture and Life Sciences, 2100 Gödöllő, Páter Károly u. 1., Hungary;

Email address:
saadi.hasna@phd.uni-mate.hu, Hermanucz.Peter@uni-mate.hu

Abstract: This study investigates the enhancement of thermal management in photovoltaic (PV) systems by implementing a modified setup with copper pipes and an aluminium-based adhesive to boost thermal conductivity. Conducted over a four-month period at the Hungarian University of Agriculture and Life Sciences, the research examined the impact of varying cooling flow rates, insulation levels, and inlet temperatures on the working temperature of a modified PV system. Findings demonstrate that full insulation significantly raises working temperatures up to 67%, while lower inlet temperatures and increased cooling flow rates effectively decrease them to 11,54% and 18,97% respectively. The results suggest that optimizing thermal management can enhance PV efficiency in high-temperature environments, promoting the system's resilience and efficiency in diverse climatic conditions.

Keywords: photovoltaic systems, radiation, insulation, inlet temperature, flow rate

1. Introduction

As the global demand for sustainable energy continues to rise, solar photovoltaic (PV) technology remains a vital component of the renewable energy landscape. However, the efficiency of PV systems is significantly influenced by various environmental factors, particularly temperature. Managing these factors effectively is crucial for optimizing the performance of solar cells and maximizing energy output. Typically, solar panels are produced under standard test settings (STC). These parameters specify that for every one degree increase in temperature, the efficiency of the PV panel decreases by 0.004-0.005 % [1]. Al-Ghezi et. al. investigates the impact of solar radiation and operational temperatures on photovoltaic (PV) panels, employing both PVsyst simulation software and outdoor experiments [2]. The results indicate that elevated operating temperatures have a detrimental effect on the performance of the panels. Specifically, a 1°C rise in temperature leads to a slight increase in current (approximately 0.068%), but results in a decrease in voltage (around 0.34%), output power (about 0.489%), and efficiency (approximately 0.586%). And the other hand Ale et. al. demonstrates that the temperature of PV modules, along with various other elements, significantly influences the performance of PV systems [3]. Additionally, it establishes a strong and positive linkage between module temperature and key performance indicators, including solar irradiance, short circuit current, output power, and conversion efficiency.

Tripathi et. al. investigates the impact of solar radiation and ambient temperature on the temperature of solar PV panels [4]. The experiments were carried out in Telangana, India, specifically during the sunny days of February 2020. The studies have confirmed that higher temperatures can reduce the efficiency of a panel and potentially harm its cells when exposed to lengthy periods of elevated temperatures. The high level of accuracy observed indicates the model's efficacy in forecasting panel temperatures. Specifically, the panel temperature reached 78.50°C when exposed to solar radiation of 1140 W/ m^2 and an ambient temperature of 36°C. Continued exposure to such high temperatures can have a negative impact on the performance and

structural integrity of the panel. Many previous researches have investigated the possibility of using solar energy in domestic hot water production [5], [6], [7]. The results of these researches have often had difficulties in storing and utilizing heat produced at low temperature levels at higher temperature levels. Han et. al. also examines the electrical and thermal performance of two solar energy systems, a combined Photovoltaic-Thermal (PVT) system with a Solar Thermal (ST) system (PVT-ST), and a separate Photovoltaic (PV) system with a Solar Thermal (ST) system (PV-ST) [8]. The research examines the effectiveness of these systems under varied environmental variables, such as varying levels of solar radiation, ambient temperatures, and inlet water temperatures, by developing a detailed heat transfer model. The results indicate that the PV-ST system demonstrates exceptional performance in situations with lower ambient temperatures and solar radiation. This is attributed to its effective cooling mechanism, which improves its electrical efficiency. In contrast, the PVT-ST system demonstrates superior performance in situations with elevated ambient temperatures and intense solar radiation. This is due to its efficient combination of photovoltaic and thermal elements, resulting in increased electro-thermal efficiency and primary energy conservation. Boumaaraf et al. evaluates the performance of a locally manufactured photovoltaic/thermal (PV/T) collector versus a traditional PV module under the climatic conditions of Ghardaia city, Algeria, aiming to address individual housing energy needs in semi-arid regions [9]. A detailed mathematical model incorporating heat transfer balance equations, along with electrical and thermo-physical properties, was developed and converted into a numerical program within the MATLAB environment for theoretical simulations and experimental validations. The findings reveal that the PV/T collector demonstrates a slightly higher electrical efficiency of 7% compared to 6.78% for the PV module, alongside a remarkable thermal efficiency of 61% and an overall efficiency of 79.43%. Boumaaraf et al. embark on an investigative journey to transform a conventional photovoltaic (PV) panel into a photovoltaic-thermal (PVT) collector, with the aim of enhancing both electrical and thermal energy production [10]. Outdoor experiments were conducted, and a data collecting system based on a personal computer (PC) was used to assess the effectiveness of the system. The findings revealed a marginal increase in electrical energy production by 0.32% and a notable gain in thermal energy with an average efficiency of 20.33%. However, it was observed that the PVT collector's moderate thermal insulation considerably impeded its ability to generate thermal energy. Several studies have also investigated the use of solar energy in the food industry [11], [12], [13], but these studies have not addressed the optimal solution to the simultaneous demand for heat and electricity.

The determination of the temperature of photovoltaic cells is a distinct and captivating issue, as the effectiveness of converting solar radiation into electrical energy is contingent upon it. Various research has examined different methods of cooling photovoltaic (PV) modules, highlighting the importance of maintaining ideal operating temperatures to improve efficiency and avoid harm. The hybrid PVT (HPVT) system combines a PV module and a traditional thermal collector into a single piece of equipment, allowing for the simultaneous availability of both thermal and electrical energy. Despite extensive research on thermal management in PV systems, the concept of "heat capacity" has remained largely unexplored in this context. Recognizing this gap, my research aims to systematically compare the heat capacity of conventional and modified PV systems. The study involves continuous modifications to a PV system, with the goal of minimizing its working temperature, consequently, maximize its ability to maintain stable temperatures and high electrical output under hot weather conditions.

2. Material and methods

In this experiment, we worked with both a conventional PV panel and a modified version that has copper pipes attached with a specialized aluminium adhesive to boost thermal conductivity. By tweaking factors like the cooling flow rate, insulation, and inlet temperature, we aimed to find the best setup to maximize the system's heat capacity. Using sensors, we closely monitored temperature changes, sunlight intensity, and electrical output, all with the goal of developing a PV system that can maintain or even improve its efficiency as temperatures climb ultimately enhancing solar energy performance.

2.1. Material

The experimental setup used to evaluate the impact of heat capacity improvements on photovoltaic (PV) systems, The experimental setup includes a standard PV panel and a modified version (Figure 1.). The modified panel features copper pipes adhered to its backside (Figure 2.) using a Synthetic Resin adhesive

containing 75% aluminium (Figure 3.) with different thicknesses (3 to 5 mm). The system also includes adjustments to the flow rate of the cooling medium to optimize heat removal. As well as XPS Insulation (20 mm) to minimize heat loss and maintain effective temperature control. Central to our experimental setup is the Arduino-based control unit (Figure 4.), which plays a critical role in orchestrating data acquisition and real-time monitoring of the PV systems. This robust platform interfaces seamlessly with a network of strategically placed sensors throughout the systems. The system includes a 10-liter thermal storage tank (Figure 4.), which plays a crucial role in the cooling process of the modified PV-T panel. This tank is designed to hold and manage the cooling fluid, ensuring a stable and consistent supply for the cooling system. Our system is equipped with a Perion 95 Ah battery which serves as the primary electrical storage solution. This high-capacity battery is essential for storing the electrical energy generated by the PV systems, ensuring that power is available for use even when sunlight conditions are less favourable. With its substantial 95 Ah capacity, the Perion battery offers robust performance and reliability, supporting extended periods of energy storage and usage.

Figure 1. Experimental Setup, Conventional PV and modified PV panels

In our experimental setup, a network of carefully chosen sensors is employed to monitor and optimize the performance of both the conventional and modified PV systems. These sensors play a vital role in capturing real-time data, which is crucial for evaluating system behaviour and effectiveness. The LM335 temperature sensor was used to provide precise temperature readings at various points in the system, offering reliable accuracy within 1°C over a broad range. To measure solar irradiance, we used the TF 6003.0000 BG irradiance sensor, which captures global radiation with a silicon diode and PMMA dome perfect for photovoltaic applications and useful in fields like climate research and agriculture. For current measurement, the ACS712 sensor handled both AC and DC currents by translating them into a proportional voltage. Lastly, a 10:1 voltage divider was employed to scale down voltages for safe monitoring by the Arduino, providing essential data on the system's electrical output and efficiency.

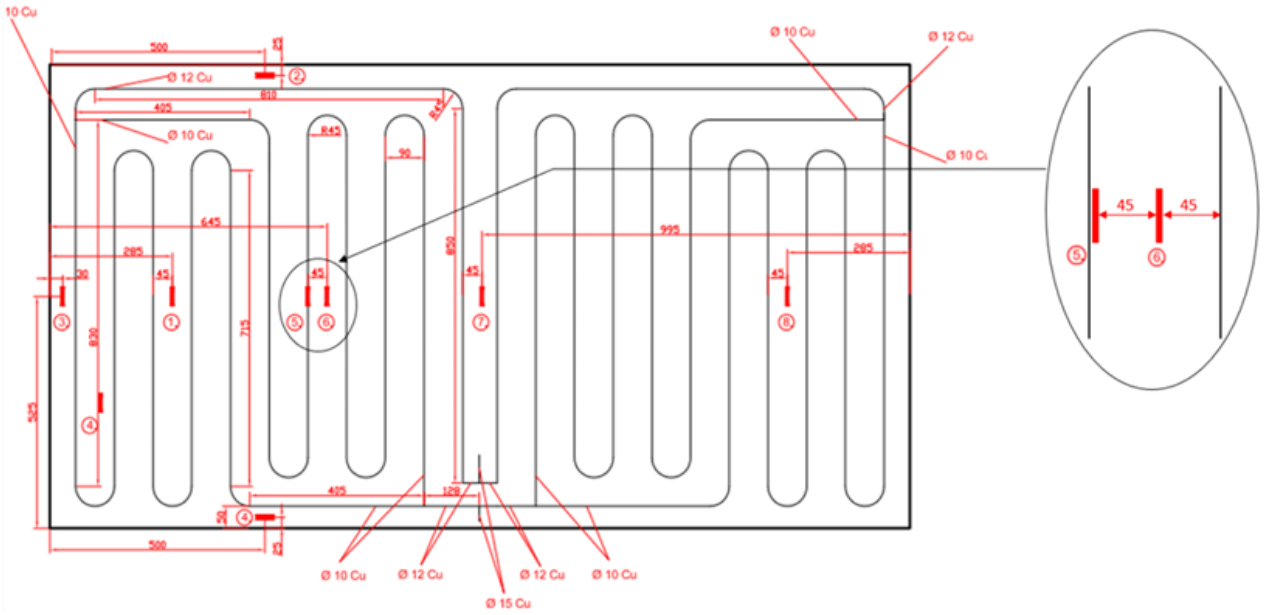

Figure 2. Cooling system and Temperature sensors distribution

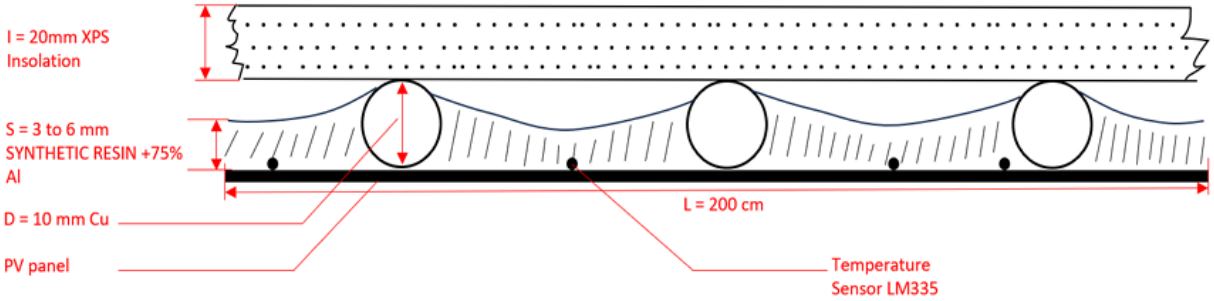

Figure 3. PVT module design cross section

Figure 4. Arduino-based control unit and the storage tank

2.2. Methods

The experiment was conducted over a four-month period (June, July, August and September 2024) in the energetic building's laboratory at the Hungarian University of Agriculture and Life Sciences from 10:00 AM to 04:00 PM. The experimental setup includes a modified PV system equipped with copper pipes adhered to the backside of the panel using a specialized adhesive material containing 75% aluminium. This setup is designed to enhance thermal conductivity and improve cooling efficiency. By incrementally adjusting variables such as cooling flow rate, insulation, inlet temperature, the study seeks to identify the optimal configuration for achieving the highest possible heat capacity in a PVT system. Throughout this process, an array of sensors is used to monitor temperature variations across different components of both the modified and unmodified PV systems, as well as other critical parameters like irradiance, ambient temperature, and electrical output. The ultimate goal is to develop a PV system capable of maintaining or even improving electrical production in the face of rising temperatures, thereby pushing the boundaries of solar energy efficiency.

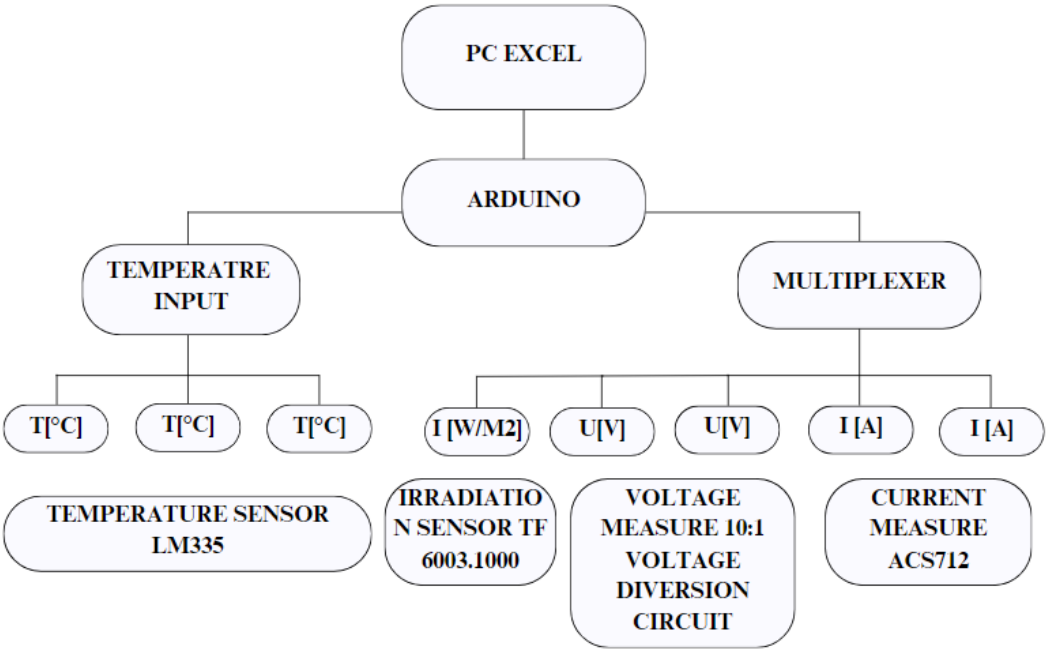

Figure 5. Data acquisition Architecture

3. Results

For the purpose of this analysis, data from 10 selected days were chosen to examine the primary objectives. The results focus on the impact of system insulation, as well as the effects of inlet temperature and cooling flow rate. By analyzing these critical variables, we aim to understand how modifications impact the working temperature of the modified photovoltaic panel.

3.1. Insulation effect

To analyze the impact of insulation on the modified PV panel's temperature Table 1. shows a comparison of the working temperature of the modified PV panel with that of the unmodified panel, under similar conditions, including irradiation, ambient temperature, flow rate, and inlet temperature. With full insulation, the modified PV panel consistently exhibits significantly higher working temperatures than the conventional PV panel. In mostly sunny conditions (Figure 6.), the modified PV panel's temperature is about 67% higher than that of the conventional PV (Figure 7.), while under mostly cloudy weather, it is approximately 63% higher. This indicates that the full insulation retains more heat within the modified system, amplifying its working temperature.

Table 1. Impact of PV system insulation during sunny and cloudy weather conditions.

Date	Periods	Ts [°C]	Q [l/min]	Insulation	T amb [°C]	PV-T [°C]	PVT-T [°C]	G [W/m2]	Weather
19 June	Morning	15	4	Full	26.28	27.34	43.68	778.10	**Mostly sunny**
	Noon				27.85	30.52	52.25	966.77	
	Afternoon				30.13	31.32	53.55	924.13	
14-Aug	Morning	15	7	No	33.52	39.51	31.77	823.26	**Mostly sunny**
	Noon				36.22	42.64	34.28	914.45	
	Afternoon				40.70	41.56	33.44	751.13	

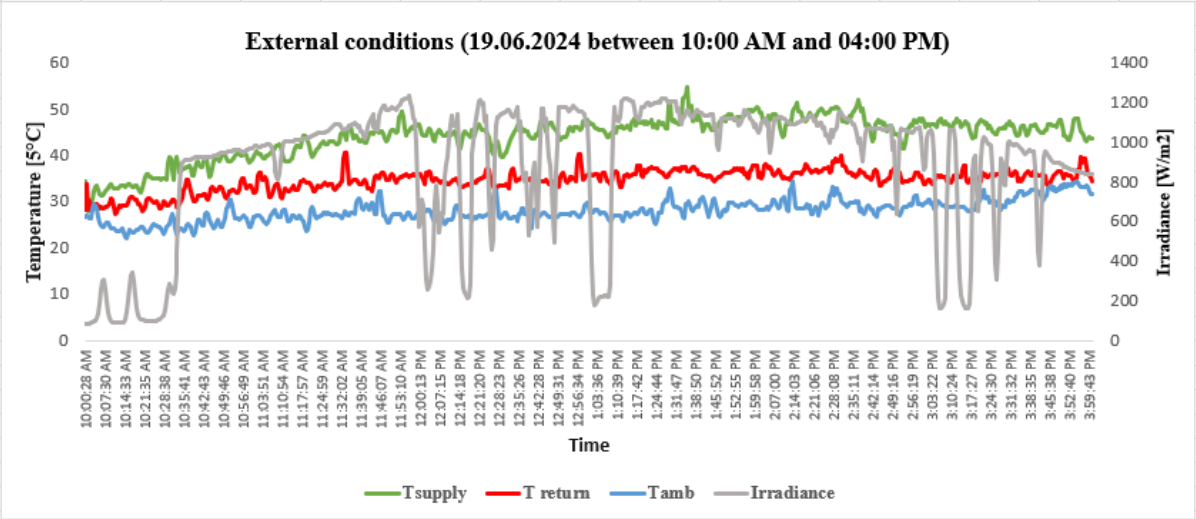

Figure 6. External Condition and the ON state of the system insulation

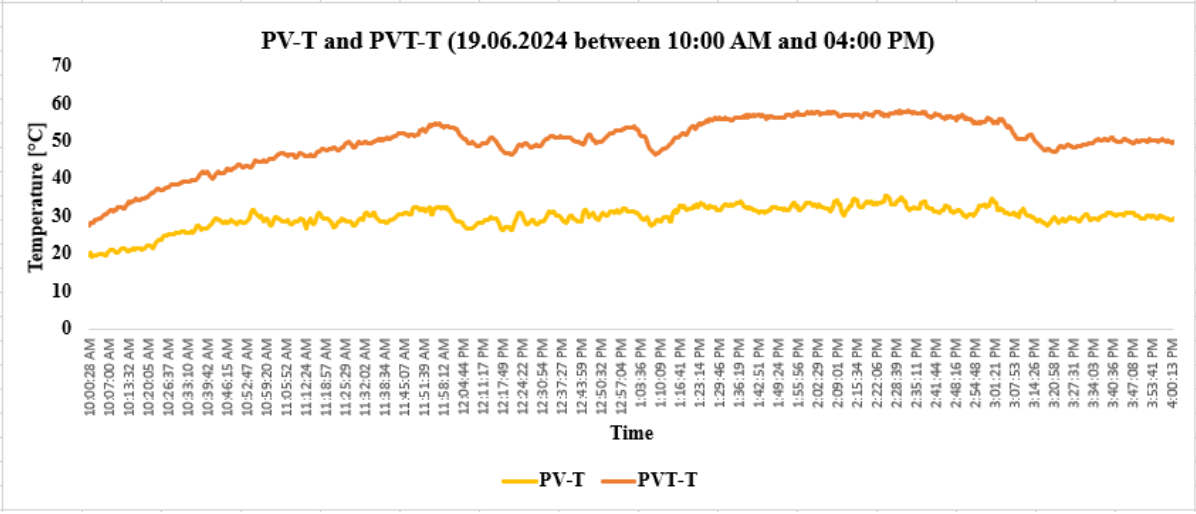

Figure 7. PV-T and PVT-T while the ON state of the system insulation

However, when the insulation is removed, the modified PV panel experiences a substantial temperature reduction. Specifically, the temperature decreases by around 19.58% during severe weather conditions (Figure 8.) and by approximately 21.82% in mostly cloudy weather (Figure 9.). This indicates that the absence of insulation allows for better heat dissipation, significantly lowering the working temperature of the

modified PV panel. Overall, insulation has a substantial impact on increasing the working temperature of the modified PV panel, particularly under more extreme weather conditions.

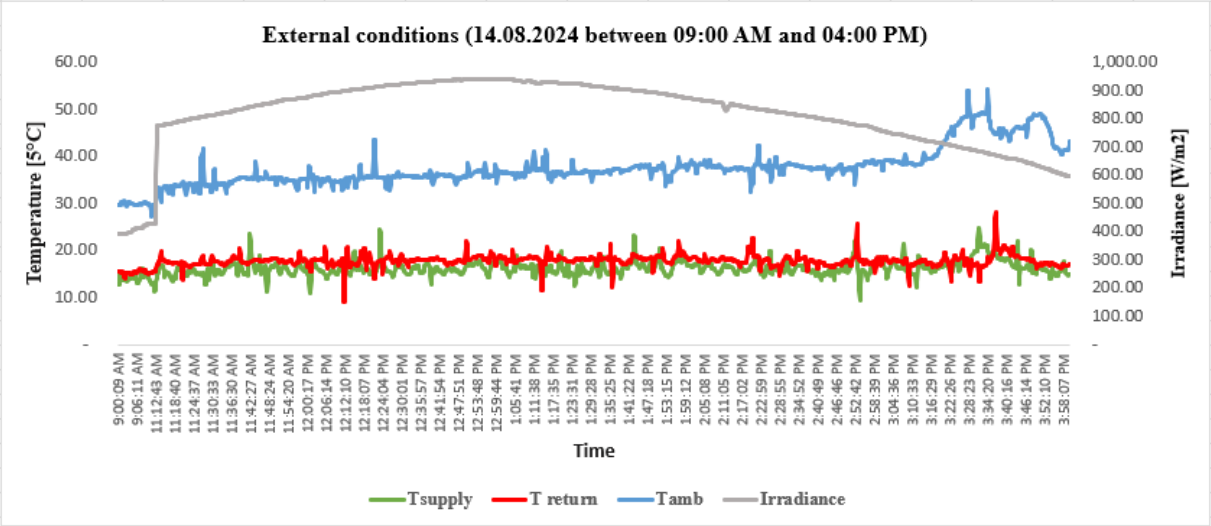

Figure 8. External Condition and the OFF state of the system insulation

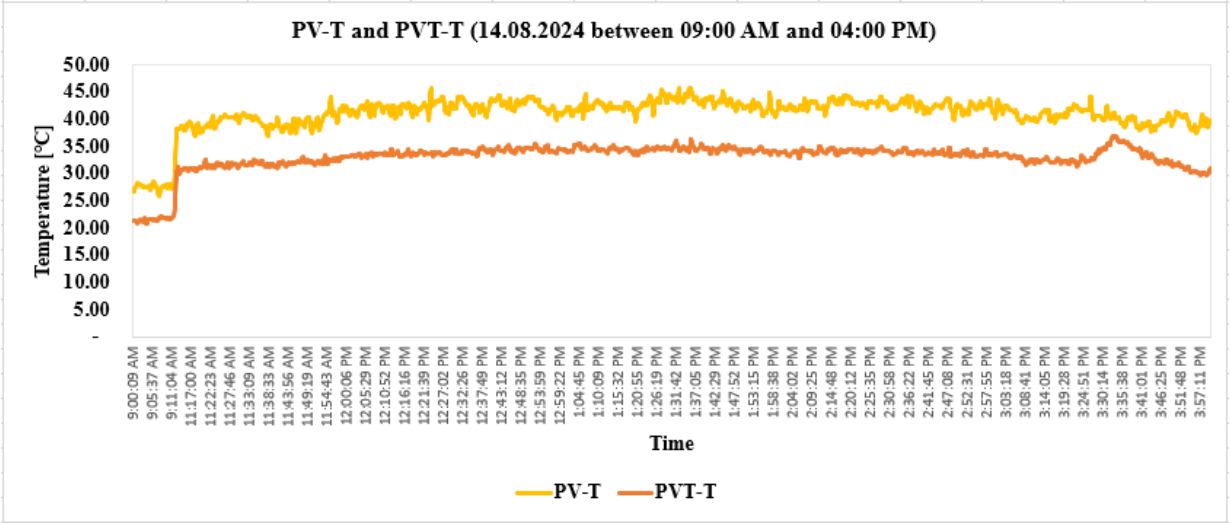

Figure 9. PV-T and PVT-T while the OFF state of the system insolation

3.2. The impact of the inlet Temperature

Table 2. illustrates the impact of inlet temperature on the working temperature of the modified PV panel by comparing the temperature difference between the PV-T and PVT-T systems. This comparison was made under consistent flow rate conditions (4 l/min) and similar external conditions over three sunny days (20 June, 7 July, and 3 July). For a clearer assessment of the inlet temperature's effect, all selected days reflect conditions where the modified PV panel was fully insulated.

Starting with the non-cooling state on 20 June (Figure 10.), where the inlet temperature was not set, the working temperature of the modified PV panel (PVT-T) was 64.4% higher than that of the conventional PV panel. When the cooling system was activated and the inlet temperature was set to 10°C on 7 July (Figure 11.), this temperature difference decreased to 34.32%, indicating a significant cooling effect. Furthermore, with an even lower inlet temperature of 8°C on 3 July (Figure 12.), the difference was reduced to a more desirable level of 11.54%. These results highlight the substantial impact of lower inlet temperatures on reducing the working temperature of the modified PV panel when fully insulated.

Table 2. PV-T and PVT-T under different inlet temperatures.

Date	Periods	Cooling state	T_s [°C]	Q [l/min]	Insulation	T_{amb} [°C]	PV-T [°C]	PVT-T [°C]	Weather
20-June	Morning	NO	NO	NO	Full	28.01	25.89	40.10	**Mostly sunny**
	Noon					30.10	29.77	50.95	
	Afternoon					31.61	29.81	49.82	
7-Jul	Morning	C	10	4	Full	28.68	22.39	30.14	**Mostly sunny**
	Noon					33.71	26.53	35.51	
	Afternoon					31.57	24.22	32.58	
3-Jul	Morning	C	8	4	Full	27.61	17.36	19.60	**Mostly sunny**
	Noon					30.38	18.86	21.42	
	Afternoon					31.13	27.67	29.92	

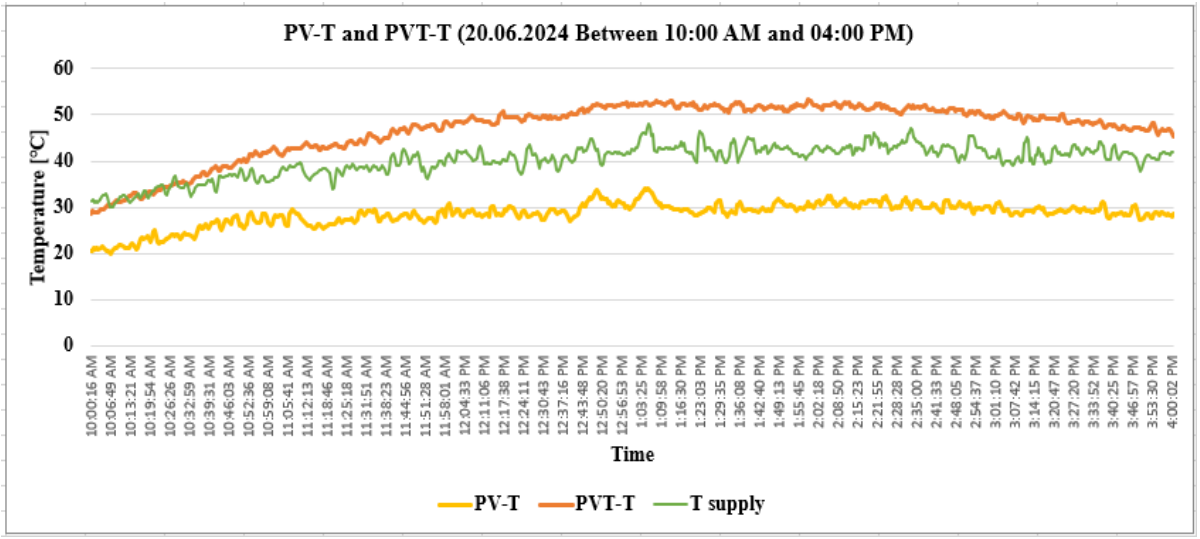

Figure 10. PV-T and PVT-T while the cooling system is OFF

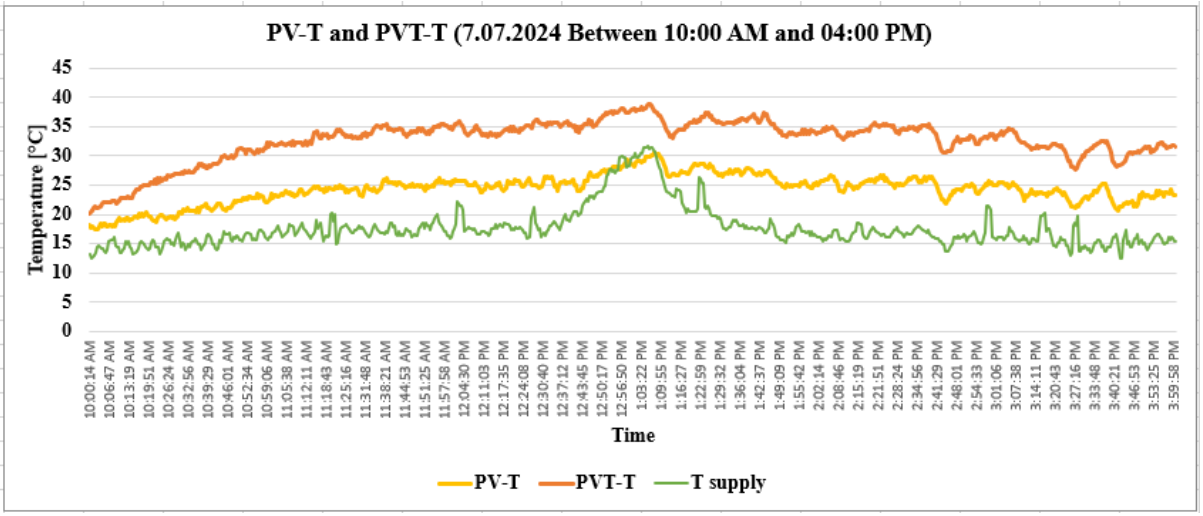

Figure 11. PV-T and PVT-T with an inlet Temperature of 10°C

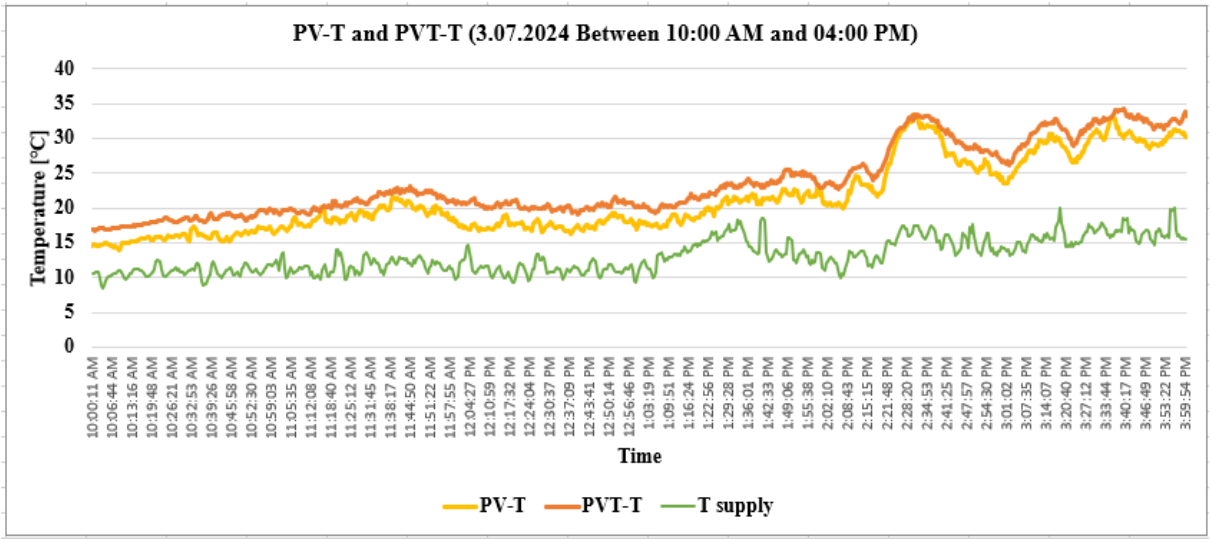

Figure 12. PV-T and PVT-T with an inlet Temperature of 8°C

3.3. The volum flow rate effect

Table shows the impact of flow rate on the working temperature of the modified PV panel compared to the conventional PV panel, under similar weather conditions and ambient temperatures. For this analysis, we selected four sunny days with no insulation applied to the modified PV panel (31 August, 1 September, 19 September, and 20 September). Two different flow rates were tested: 4 l/min and 7 l/min. To assess the real impact of flow rate, we used a lower inlet temperature with the lower flow rate and a higher inlet temperature with the higher flow rate, based on previous findings that lower inlet temperatures generally lead to a lower working temperature for the modified PV panel. For the lower flow rate (4 l/min) with an inlet temperature of 10°C on 19 and 20 September (Figure 13.), the PVT-T system operated only 7.65% and 6.43% lower than the PV-T, respectively, despite the favorable inlet temperature and lack of insulation.

Table 3. PV-T and PVT-T under different flow rate conditions.

Date	Periods	T_s [°C]	Q [l/min]	Insulation	T_{amb} [°C]	PV-T [°C]	PVT-T [°C]	G [W/m^2]	Weather
19-Sep	Morning	10	4	No	21.55	21.32	19.19	562.83	**Mostly sunny**
	Noon				25.71	29.69	28.05	874.34	
	Afternoon				25.84	26.50	24.53	694.14	
20-Sep	Morning	10	4	No	20.68	21.25	19.39	584.22	**Mostly sunny**
	Noon				25.12	29.08	28.00	911.65	
	Afternoon				25.75	26.63	24.82	716.30	
31-Aug	Morning	15	7	No	27.97	35.40	28.00	646.57	**Mostly sunny**
	Noon				31.68	42.20	35.63	891.72	
	Afternoon				34.41	34.86	27.73	493.53	

Conversely, when the flow rate was increased to 7 l/min, even with a higher inlet temperature of 15°C on 31 August and 1 September (Figure 14.), we observed a more substantial cooling effect. Here, the working temperature of the PVT-T system showed a reduction of 18.97% compared to the PV-T on 31 August and 17.46% on 1 September. These results highlight that, although a lower inlet temperature improves cooling, a higher flow rate has a more pronounced impact on reducing the working temperature of the modified PV panel, even with a higher inlet temperature and no insulation.

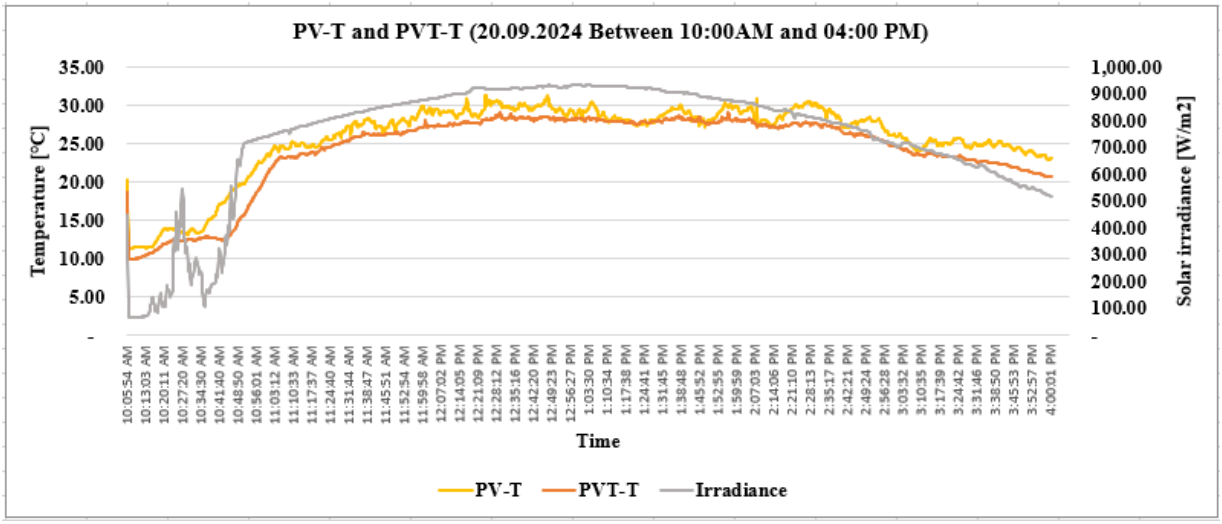

Figure 13. PV-T and PVT-T under flow rate of 4 *l*/min

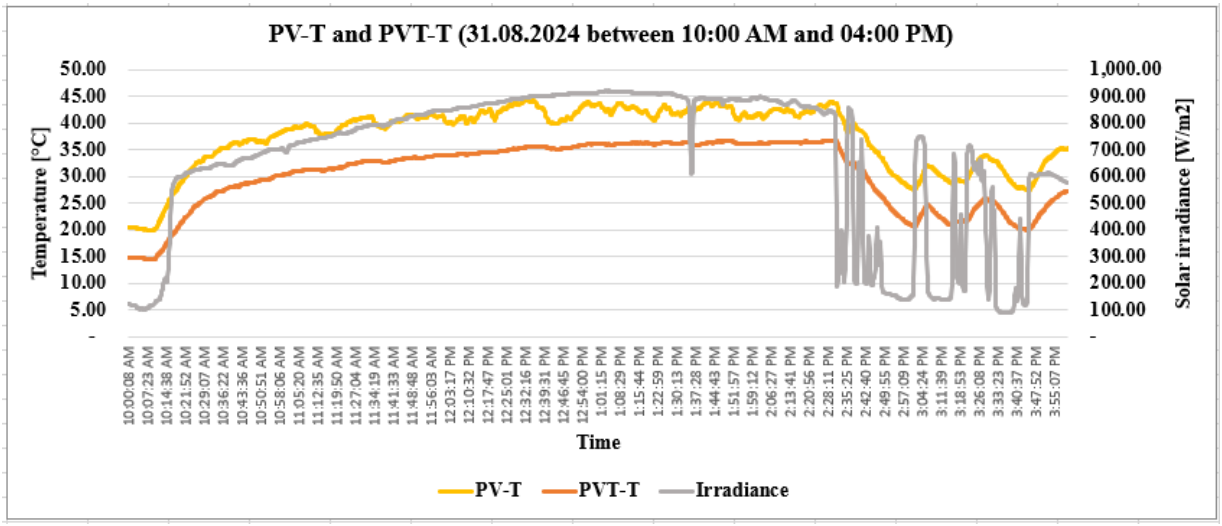

Figure 14. PV-T and PVT-T under flow rate of 7l/min

4. Conclusions

This study highlights how crucial thermal management is for photovoltaic panels. It shows that solar panels designed with better heat dissipation techniques can work more efficiently in high temperatures. Through careful experiments, researchers found that both insulation and cooling methods are key in controlling the temperatures and efficiency of solar systems. As previously has been investigated in other researches, heat capacity can be of great importance for solar energy systems, and in the present research we have focused on this area [14], [15].

Interestingly, while full insulation can help retain heat, it also leads to higher temperatures in the panels, which isn't ideal for performance. On the other hand, lowering the inlet temperature and increasing the flow rate proved to be effective in keeping temperatures down.

The results suggest that a balanced approach to thermal management, combining insulation and cooling, can significantly enhance the durability and efficiency of solar panels, especially in hot climates. The modified panels were able to maintain cooler operating temperatures, making them suitable for areas with strong sunlight.

This research not only adds valuable insights into how we manage heat in solar technology but also paves the way for more studies on improving heat dissipation techniques and materials for better solar panel

performance in various climates. Combined with the results of other research, optimal removal of recovered heat is found to be feasible even with the addition of heat pump systems [16], [17].

5. Acknowledgement

The research was supported by the project 'The feasibility of the circular economy during national defense activities' of 2021 Thematic Excellence Program of the National Research, Development and Innovation Office under grant no.: TKP2021-NVA-22, led by the Centre for Circular Economy Analysis.

The study was supported by the Stipendium Hungaricum Program and the Doctoral School of Mechanical Engineering, The Hungarian University of Agriculture and Life Sciences, Gödöllő, Hungary.

6. References

[1] **Natarajan, S., Mallick, T., Katz, M., and Weingaertner, S.** (2011): Numerical investigations of solar cell temperature for photovoltaic concentrator system with and without passive cooling arrangements. International Journal of Thermal Sciences, 50(12), 2514-2521. https://doi.org/10.1016/j.ijthermalsci.2011.06.014.

[2] **Al-Ghezi, M. K. S., Ahmed, R. T., and Chaichan, M. T.** (2022): The Influence of Temperature and Irradiance on Performance of the Photovoltaic Panel in the Middle of Iraq. International Journal of Renewable Energy Development, 11(2), 501–513. https://doi.org/10.14710/ijred.2022.43713.

[3] **Ale, T. O., Rotipin, K., and Makanju, T. D.** (2022): Temperature Effects on Optimal Performance of PV Module. Journal of Engineering Advancements, 162–165. https://doi.org/10.38032/jea.2022.04.004.

[4] **Tripathi, A. K., Ray, S., and Aruna, M.** (2021): Analysis on photovoltaic panel temperature under the influence of solar radiation and ambient temperature. Proceedings of the 2021 1st International Conference on Advances in Electrical, Computing, Communications and Sustainable Technologies, ICAECT 2021. https://doi.org/10.1109/ICAECT49130.2021.9392619.

[5] **Ghabour, R., Korzenszky, P.** (2022): Linear Model of DHW System Using Response Surface Method Approach, Tehnicki Vjesnik-Technical Gazette Vol. 29:1 66-72. p.

[6] **Ghabour, R., Korzenszky, P.** (2023): Dynamic Modelling and Experimental Analysis of Tankless Solar Heat Process System for Preheating Water in the Food Industry, Acta Polytechnica Hungarica 20 : 4 pp. 65-83. , 19 p.

[7] **Korzenszky, P., Géczi, G. (2012):** Heat pump application in food technology, Journal of Microbiology and Food Sciences Vol. 2, 493-500. p.

[8] **Han, Z., Liu, K., Li, G., Zhao, X., and Shittu, S.** (2021): Electrical and thermal performance comparison between PVT-ST and PV-ST systems. Energy, 237. https://doi.org/10.1016/j.energy.2021.121589.

[9] **Boumaaraf, B., Boumaaraf, H., Slimani, M. E. A., Tchoketch_Kebir, S., Ait-cheikh, M. S., and Touafek, K.** (2020): Performance evaluation of a locally modified PV module to a PV/T solar collector under climatic conditions of semi-arid region. Mathematics and Computers in *Simulation*, 167, 135–154. https://doi.org/10.1016/j.matcom.2019.09.013.

[10] **Boumaaraf, B., Touafek, K., Ait-cheikh, M. S., and Slimani, M. E. A.** (2020): Comparison of electrical and thermal performance evaluation of a classical PV generator and a water glazed hybrid photovoltaic–thermal collector. Mathematics and Computers in Simulation, 167, 176–193. https://doi.org/10.1016/j.matcom.2018.09.003.

[11] **Ghabour, R., Josimović, L., Korzenszky, P.** (2021): Two Analytical Methods for Optimising Solar Process Heat System Used in a Pasteurising Plant, Applied Engineering Letters 6 : 4 pp. 166-174. , 9 p.

[12] **Ghabour, R., Korzenszky, P.** (2021): Effect of in series and in parallel flow heater configuration of solar heat system for industrial processes, Science Technology and Innovation 14: 3 pp. 18-26., 9 p.

[13] **Ghabour, R., Korzenszky, P.** (2022): Optimal Design and Configuration for Pasteurising Heat Demand Supported by Solar Thermal System Using T*Sol Software, Annals of Faculty of Engineering Hunedoara: International Journal of Engineering 20: 2 pp. 105-110., 6 p.

[14] **Ghabour, R., Korzenszky, P.** (2020): Mathematical modelling and experimentation of soy wax PCM solar tank using response surface method, Analecta Technica Szegedinensia 14: 2 pp. 35-42., 8 p.

[15] **Tóth, L., Slihte, S., Ádám, B. Petróczki, K., Korzenszky, P., Gergely, Z.** (2011): Solar Assisted Ground Source Heat Pump System, Hungarian Agricultural Engineering Vol 23 57-61. p.

[16] **Géczi, G., Bense, L., Korzenszky, P.** (2043): Water tempering of Pools Using Air to Water Heat Pump Environmentally Friendly Solution, Rocznik Ochrona Srodowiska Vol. 16: 115-128. p.
[17] **Géczi, G., Korzenszky, P., Bense, L.** (2013): Ideális körülmények a levegő-víz hőszivattyú uszoda-technikai alkalmazása során, Magyar Épületgépészet Vol. 62: 7-10. p.